Cosmogenic ^{3}He in terrestrial rocks: a review

P.-H. Blard*

CRPG, CNRS, Université de Lorraine, 54000, Nancy, France

*Email: blard@crpg.cnrs-nancy.fr

Non-peer reviewed preprint posted on *EarthArXiv* on July 5th 2021.

Initial submission to *Chemical Geology* (Elsevier) on July 3rd 2021

Category: Invited Review Article

Editors:

Donald Porcelli, Email: donald.porcelli@earth.ox.ac.uk

Timothy Horscroft, Email: timothy.horscroft@elsevier.com

15,600 words

19 figures

1 Table

3 Supplementary Tables:

- Supp. Table 1: Magmatic ^{4}He concentrations database
- Supp. Table 2: Excel spreadsheet for computing radiogenic ^{4}He and nucleogenic ^{3}He
- Supp. Table 3: ^{3}He/^{10}Be cross-calibrated production rates database

Keywords: cosmogenic ^{3}He; exposure age; erosion; burial age; paleoaltimetry; magmatic ^{3}He; magmatic ^{4}He; radiogenic ^{4}He; nucleogenic ^{3}He; isochrons; helium closure age; production rates; ^{3}He/^{10}Be cross-calibration

Abstract

This review article summarizes the state of the art of cosmogenic ^{3}He (^3He_c), with a focus on the most efficient methods for measuring this cosmogenic noble gas in terrestrial samples. After briefly reviewing the scientific applications and production pathways of cosmogenic ^{3}He, I summarize the most important theoretical and practical aspects of ^{3}He analyses and describe the best strategies for correcting for non-cosmogenic ^{3}He components in minerals. I also review our knowledge of ^3He_c production rates and explore potential new applications for future studies.

Our ability to accurately and precisely measure cosmogenic ^{3}He is mainly constrained by the level of the non-cosmogenic ^{3}He background (i.e., magmatic, radiogenic, nucleogenic, and atmospheric ^{3}He), and thus by the geological characteristics of the samples. Constructing ^{3}He vs. ^{4}He isochrons by analyzing several aliquots from the same sample constitutes a useful and overlooked method that is advantageous because it obviates the often-complicated step of vacuum crushing. This method also allows the direct and joint determination of cosmogenic ^{3}He and the magmatic ^{3}He/^{4}He ratio. I perform numerical modeling to explore the impact of the non-cosmogenic ^{3}He components on the final uncertainties and detection limits of ^{3}He dating. Reducing the magmatic component by selecting phenocrysts in the 100–500 µm size fraction improves the precision of cosmogenic ^{3}He analyses. Moreover, it is important to measure U, Th, and Li concentrations in the analyzed minerals and their host rocks to ensure proper corrections for radiogenic ^{4}He and nucleogenic ^{3}He, improving both the accuracy and precision of the method.

After summarizing the most important aspects of ^{3}He analytical techniques, including the best ^3He_c extraction techniques and the key parameters of noble gas mass spectrometry that result in accurate and precise helium isotopic measurements, I also review ^3He_c production rates and their spatial variability. The global database of absolute calibration sites yields a world-wide average ^3He_c production rate in olivine and pyroxene of 124 ± 11 at g^{-1} yr^{-1} using the LSD scaling and the online CREp calculator (https://crep.otelo.univ-lorraine.fr/#/). Cross-calibrations against ^{10}Be indicate that the ratio of the production rate of ^3He_c in olivine/pyroxene to that of ^{10}Be in quartz is 33 ± 2 and increases by less than 7% between sea level and 5,000 m elevation. This important observation demonstrates that ^{3}He in olivine/pyroxene and ^{10}Be in quartz can be considered as synchronized chronometers. However, ^3He_c/^{10}Be cross-calibrations based on ^3He_c in accessory minerals (zircon, garnet, kyanite, apatite) yield unexpectedly high ^{3}He/^{10}Be production ratios of 40–60 above 3,000 m elevation. As the capture of cosmogenic

thermal neutrons by ^{6}Li is unlikely to explain this excess, I discuss other plausible mechanisms that should be explored, such as $^{3}He_c$ inherited from previous exposure episodes, unrecognized specific reaction pathways, or the impact of snow cover. New cross-calibration data obtained by measuring $^{3}He_c$ against other cosmogenic nuclides in different settings will advance our understanding of cosmogenic nuclide production rates and improve the accuracy and precision of applications relying on cosmogenic ^{3}He. Other improvements could extend the applicability of the ^{3}He geoscientific toolbox; for example, coupling ^{3}He with radioactive cosmogenic nuclides (^{10}Be, ^{36}Cl, ^{53}Mn) will allow paleoaltimetry or the determination of burial ages or paleo-depths in intermediate and mafic terrains.

1 - Introduction

In-situ cosmogenic nuclides are specific nuclides in rocks and minerals that are produced through nuclear reactions upon bombardment by high energy (>1 MeV) cosmic particles. Because cosmogenic nuclide concentrations in minerals depend on the amount of time the minerals were exposed at Earth's surface, they represent a powerful and wide array of geochronometric tools with applications in geomorphology, paleoclimatology and geohazard analysis (Fig. 1). Although a large body of literature is dedicated to radioactive cosmogenic nuclides (^{10}Be, ^{26}Al, and ^{36}Cl), less attention has been given to cosmogenic noble gases (^{21}Ne and ^{3}He): in 2020, articles relying on cosmogenic ^{3}He represented only 12% of the ~2,700 publications involving any type of in-situ cosmogenic nuclide (source: Web of Science). ^{3}He is nonetheless an interesting alternative to ^{10}Be for quartz-poor lithologies because it is present in measurable concentrations in minerals that are not suited to ^{10}Be or ^{26}Al analyses, such as those in mafic rocks (olivine, pyroxene). ^{3}He is also measurable in accessory minerals in silica-rich lithologies (zircon, apatite, iron oxides). Moreover, because of their nuclear stability, cosmogenic noble gases can, in theory, be used to analyze events that occurred beyond tens of millions of years ago (e.g. Sartégou et al., 2020) and are thus ideal complements to radioactive cosmogenic isotopes, which decay over shorter durations.

Since the discovery of terrestrial cosmogenic ^{3}He more than 30 years ago by Mark Kurz and others (Craig and Poreda 1986; M. D. Kurz 1986a), significant progress has developed cosmogenic ^{3}He into a pertinent geological probe (Fig. 1). Over the last decades, dozens of studies have used cosmogenic ^{3}He to date and quantify a large variety of Earth processes, such as the timing of volcanic eruptions (e.g., Heineke et al., 2016), fault kinetics (e.g., Medynski et al., 2016), denudation rates (e.g., Puchol et al., 2017), paleoclimatology (e.g., Martin et al., 2018), paleoaltimetry (e.g., Blard et al., 2006a), dating surfaces that are millions of years old (e.g., Margerison et al., 2005), or tsunami hazard analyses (e.g., Ramalho et al., 2015).

The measurement of cosmogenic ^{3}He requires specific facilities and apparatuses that are currently available in several noble gas laboratories worldwide (e.g., Caltech, Pasadena, USA; CRPG, Nancy, France; SUERC, Glasgow, UK; ETH, Zurich, Switzerland; GFZ, Potsdam, Germany; BGC, Berkeley, USA; LDO, Palisades, USA). However, because not all minerals are suitable for cosmogenic ^{3}He analysis, the reliability of cosmogenic ^{3}He data depends directly on the nature and geological history of the analyzed rocks. Because these methodological aspects have been disseminated in various specialized papers (Blard et al., 2008; Blard and Farley, 2008; Blard and Pik, 2008; Farley et al., 2006; Goehring et al., 2010; Kurz, 1986a, 1986b; Larsen et al., 2019, 2021; Martin et al., 2017; Protin et al., 2016; Shuster

et al., 2004; Trull et al., 1991), this review summarizes the most important theoretical and methodological aspects of cosmogenic ^{3}He analyses by reviewing the current state of the art and the best strategies for accurately and precisely measuring and interpreting cosmogenic ^{3}He concentrations.

I begin with a short history of the scientific breakthroughs that led to the discovery of terrestrial cosmogenic ^{3}He ($^{3}He_{c}$), then describe the different sources and production pathways of ^{3}He and ^{4}He in minerals. I then present methodological guidelines and suggestions about the most important theoretical and practical aspects of ^{3}He analyses in mafic minerals (olivine and pyroxene). These recipes are useful for attaining the best precision and accuracy during any ^{3}He measurement. For a given sample, our ability to detect cosmogenic ^{3}He is determined by its non-cosmogenic ^{3}He background, and then by its geological characteristics. I perform numerical modeling to explore the impact of the non-cosmogenic ^{3}He components on the obtained uncertainties and to assess the detection limits of ^{3}He dating. Then, I review and discuss our knowledge of the $^{3}He_{c}$ production rate and its spatial variability, relying on published calibration sites and cross-calibrations against other cosmogenic nuclides, notably ^{10}Be. Finally, I explore potential new applications based on the coupling of $^{3}He_{c}$ with radioactive cosmogenic nuclides (^{10}Be, ^{36}Cl, ^{53}Mn).

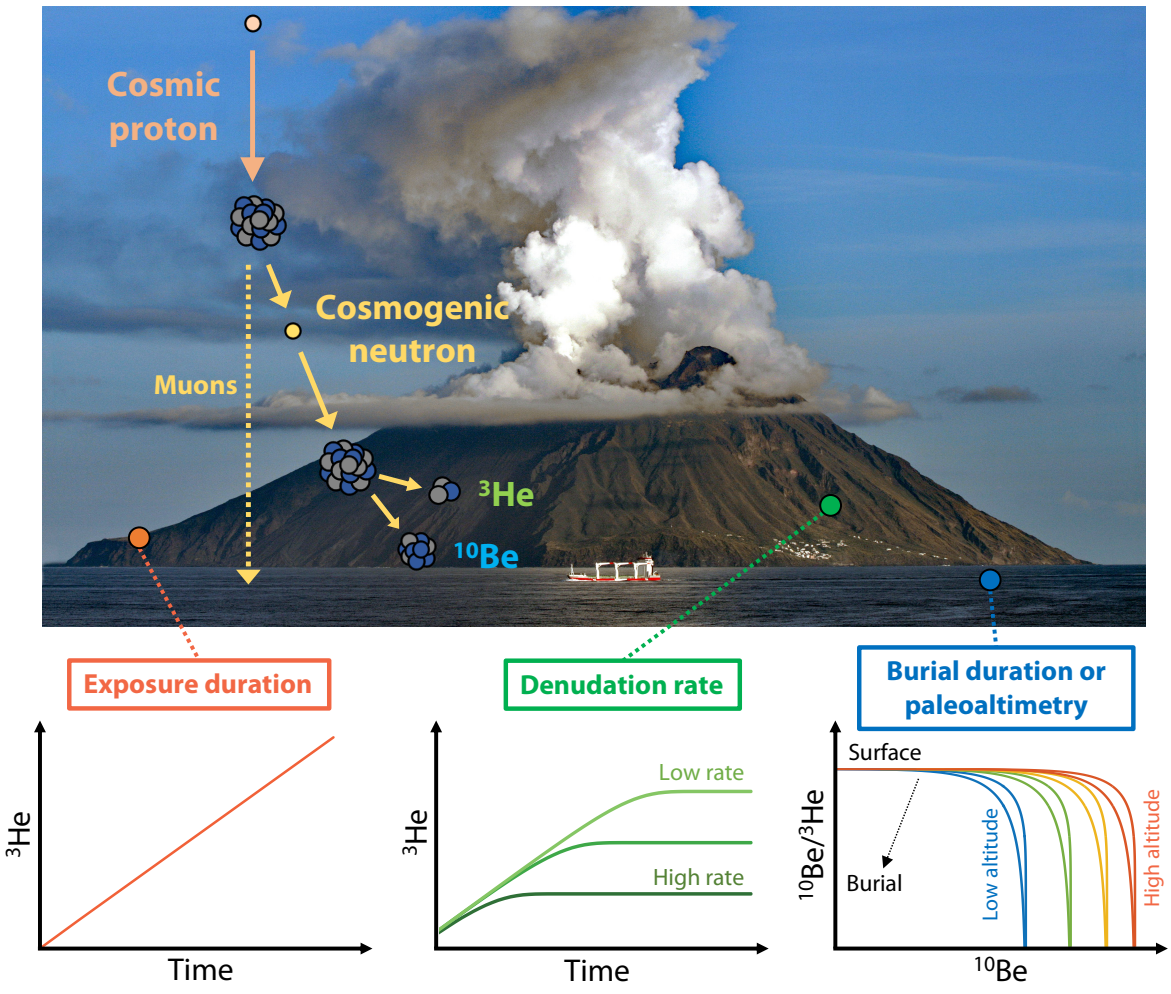

Figure 1. Principles of cosmogenic ^{3}He production and its main applications. ^3He_c is produced by spallation reactions induced by high-energy cosmogenic neutrons (> 10 MeV), low-energy cosmogenic neutrons (<1 keV) and muons. The three main applications of cosmogenic ^{3}He are determined by the geomorphological characteristics of the studied objects: 1) on non-eroded surfaces, cosmogenic ^{3}He concentrations measure exposure durations; 2) in eroding landscapes (active versants, rivers) that have reached steady-state ($t > \Lambda/(\rho\varepsilon)$), ^{3}He concentrations measure denudation rates; 3) when coupled with measurements of radioactive cosmogenic nuclides (e.g., ^{10}Be, $t_{1/2}$ = 1.4 Ma) in the same rock sample that is now buried beyond the penetration depth of cosmic particles, it is possible to determine paleoelevations, paleodepths, or measure burial durations. Picture of Stromboli volcano, Italy: © Jcb-caz-11, CC-BY-SA-4.0.

2. Basic concepts of in-situ terrestrial cosmogenic ^{3}He

2.1. Discovery of terrestrial cosmogenic ^{3}He

Until the mid-1980's, the presence of cosmogenic ^{3}He had only been documented in extraterrestrial materials such as lunar samples (e.g., Megrue, 1971) and meteorites (e.g., Fisher, 1972). These analyses were performed by melting samples under vacuum followed by He analyses in a static, high-vacuum Nier-source mass spectrometer (Aldrich and Nier 1946; Kurz 1986a). During the 1970's and 1980's, however, noble gas systems switched from glass to fully metal purification lines, lowering instrumental blanks and, hence, detection limits by 5 orders of magnitude, from 10^8 atoms (Megrue 1967) to $<10^3$ atoms on modern instruments (e.g., Zimmermann et al., 2018).

In 1986, Mark Kurz and others demonstrated that cosmogenic ^{3}He was also detectable in terrestrial rocks by analyzing olivines and pyroxenes from basalt samples exposed for about 500 kyr at the summit of Haleakalā volcano, Maui, Hawaii (Kurz, 1986a, 1986b; see also Craig and Poreda, 1986). The compelling evidence for the presence of cosmogenic ^{3}He resulted from their two-step analysis of He isotopes in olivine phenocrysts: first crushing the olivines in vacuo, then fusing the remaining powder. The fused olivine yielded a ^{3}He/^{4}He ratio of 2,000 Ra (where Ra = 1.384×10^{-6} is the atmospheric ^{3}He/^{4}He ratio; Kurz, 1986). Such a high value had never been documented on Earth, as it is far above the highest ^{3}He/^{4}He ratios measured by crushing mantle olivines, which preferentially release trapped mantellic helium (^{3}He/^{4}He = 8–30 Ra; e.g., Parman, 2007). The observed massive ^{3}He excess was thus interpreted as resulting from the build-up of cosmogenic ^{3}He in the mantle silicates after they had reached the Earth's surface. Additionally, relying on the fact that magmatic helium has a homogenous isotopic composition in phenocrysts of a few grams, Kurz (1986a, 1986b) proposed that the amount of ^{4}He released by melting can be used as a proxy for the concentration of magmatic ^{3}He:

$$^3\mathrm{He}_c = {}^3\mathrm{He}_{tot} - {}^4\mathrm{He}_{tot} \times (^3\mathrm{He}/^4\mathrm{He})_{mag}\,, \qquad (1)$$

where $^3\mathrm{He}_{tot}$ and $^4\mathrm{He}_{tot}$ are the total ^{3}He and ^{4}He concentrations, respectively, and $(^3\mathrm{He}/^4\mathrm{He})_{mag}$ is the magmatic ^{3}He/^{4}He ratio estimated from vacuum crushing.

For decades, this two-step crushing and fusion protocol was used with Equation (1) to correct for the magmatic ^{3}He component (e.g. Licciardi et al., 1999). However, several authors argued

that Equation (1) should be modified to account for the presence of radiogenic ^{4}He (Blard and Farley 2008; Dunai and Wijbrans 2000) to avoid overestimating the magmatic ^{3}He contribution (see section 3).

2.2. An ideal complementary companion to ^{10}Be

Also during the 1980's, progress in accelerator mass spectrometry (AMS) democratized the measurement of in-situ cosmogenic ^{10}Be in quartz samples (e.g., Klein et al., 1982; Litherland, 1980; Raisbeck et al., 1987). The nearly simultaneous discovery of cosmogenic ^{3}He in terrestrial samples thus ideally completed the spectrum of applications of these new geochronological tools because ^{3}He is suited to mafic minerals and volcanic environments, whereas ^{10}Be is suited to silicic, quartz-rich environments.

^{3}He has moreover several specific advantages compared to other cosmogenic nuclides:

i) Because ^{3}He is a light isotope, the cross section of spallation reactions producing cosmogenic ^{3}He are less sensitive to the masses of target elements compared to other nuclides (Dunai, 2010). Consequently, compared to ^{21}Ne, ^{36}Cl, and ^{10}Be, the rate of $^{3}He_c$ production by high-energy particles (>10 MeV) is less dependent on mineral chemical composition; indeed, empirical data show that olivine and pyroxene have the same $^{3}He_c$ production rates (Martin et al., 2017). That said, Fe-rich minerals have lower spallogenic production rates (Larsen et al., 2019; Shuster et al., 2012), whereas in Li-rich (> 10 ppm) minerals, ^{3}He production may be enhanced by the capture of cosmogenic thermal neutrons (Dunai et al., 2007).

ii) ^{3}He has one of the largest production rate to detection limit ratios, which theoretically enables the detection of exposure episodes shorter than 100 years in the most favorable conditions (Niedermann 2002).

iii) The nuclear stability of ^{3}He allows very old surfaces to be dated, whereas ^{10}Be and ^{36}Cl reach saturation after ~5 Myr and ~1 Myr of exposure, respectively. Moreover, ^{3}He may be used to document geological events that occurred in the deep past, such as ancient exposure episodes that occurred several million years ago.

Nonetheless, the stability of ^{3}He also somewhat limits its utility: any exposure episode may be recorded by cosmogenic ^{3}He, complicating the interpretation of scenarios with multiple

burial-exposure episodes. Moreover, the stability of ^{3}He implies that phenocrysts, especially ones that crystallized several million years ago, may also accumulate significant amounts of ^{3}He through other processes (e.g., Farley et al., 2006). These two properties may be considered the "Achilles' heel" of cosmogenic ^{3}He, and it is fundamental that users take into account the geological context of their samples, and notably the closure (U-Th-Sm)/^{4}He age of the analyzed phenocrysts (see section 3): as closure age increases, so does the detectable exposure age.

2.3. A useful geo-chronometer and probe for many applications in Earth surface science

Cosmogenic ^{3}He is now one of the most commonly used cosmogenic nuclides because it can date geological events and quantify numerous surface processes occurring in mafic volcanic environments. Indeed, $^{3}He_{c}$ covers a rather wide range of Earth science timescales, from dating historical lava flows (<1 ka; (Heineke et al. 2016) to the oldest known surface exposure ages on Earth's surface (>10 Ma; Margerison et al., 2005).

Thus, the questions addressed using cosmogenic ^{3}He have been numerous and intriguing (Fig. 2), ranging from dating volcanic eruptions (e.g. Kurz et al., 1990; Marchetti et al., 2020) reconstructing paleoglaciers dynamics (e.g. Blard et al., 2007; Bromley et al., 2011; Cerling, 1990; Martin et al., 2018), fault kinematics (e.g. Medynski et al. 2016; Ritz et al. 2016), determining fluvial erosion rates (e.g. Ferrier et al., 2013; Litty et al., 2021), and paleoaltimetry (e.g. Blard et al., 2005) to even more exotic and intriguing applications, such as identifying paleo-tsunami deposits (e.g. Ramalho et al., 2015) or dating ancient human footprints (Heineke et al. 2016).

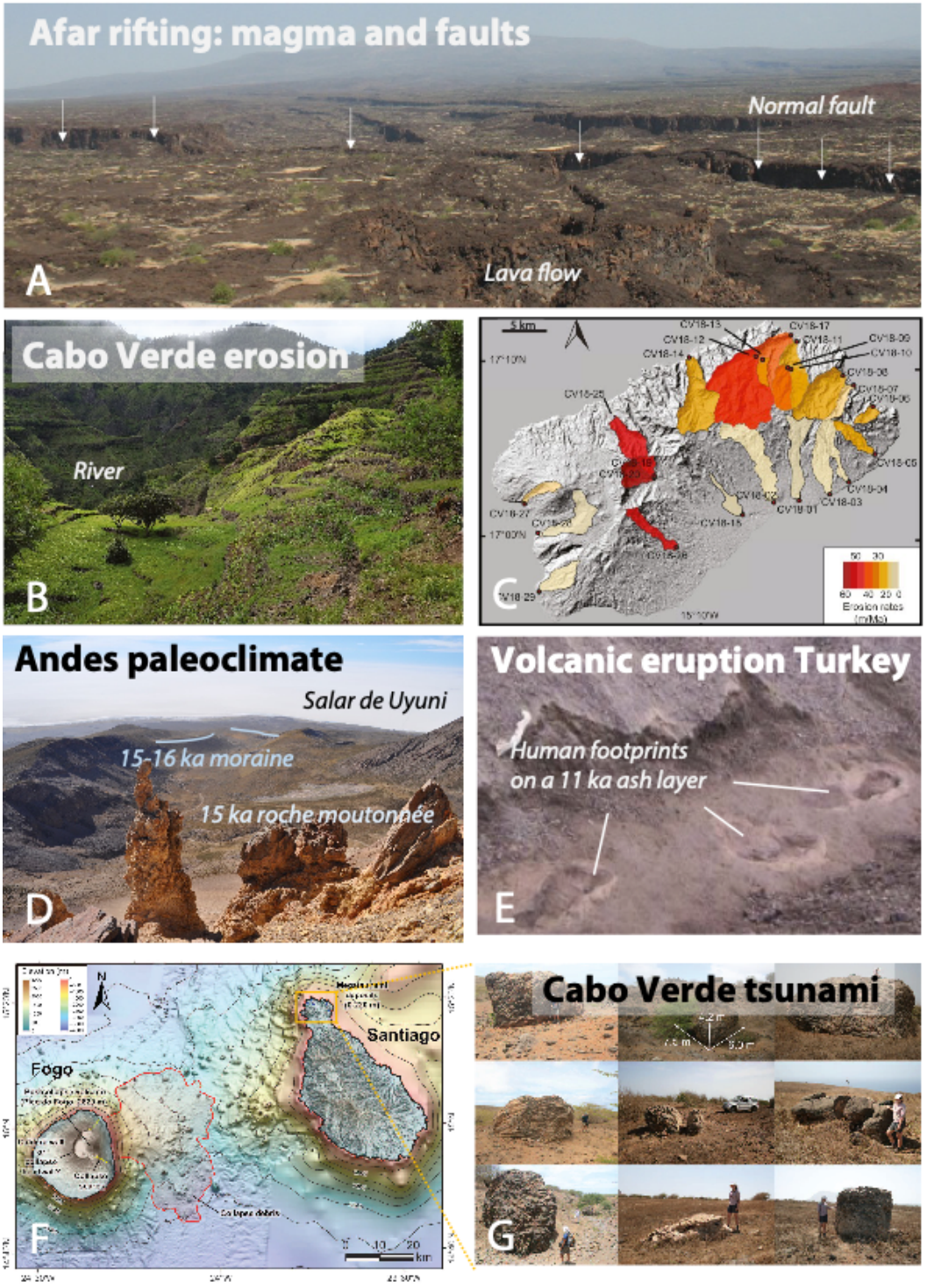

Figure 2. Geological questions addressed using cosmogenic ^{3}He: (A) dating lava infilling and fault scarps in the Afar rift (Medynski et al. 2016), (B, C) determining denudation rates in rivers of Santo Antao island, Cabo Verde (Litty et al. 2021), (D) moraine geochronology in the Tropical Andes (Martin et al. 2020), (E) dating 11-ka volcanic ash with preserved human footprints (Heineke et al. 2016), and (F, G) dating of a giant tsunami 73 ka due to flank collapse on the volcanic island of Fogo, Cabo Verde (Ramalho et al. 2015).

2.4. None like it hot: why cosmogenic ^{3}He is mainly measured in olivine, pyroxenes, iron oxides and accessory minerals?

To record a complete exposure history, cosmogenic nuclides must be quantitatively retained in the mineral of interest. Because of its small size (atomic radius = 31×10^{-12} m), helium has relatively high diffusion rates in silicates: at 15 °C, its diffusivity is ~10^{-14} to 10^{-13} cm^2 s^{-1} in quartz (Shuster et al. 2004; Tremblay et al. 2014) and ~10^{-22} to 10^{-21} cm^2 s^{-1} in olivine (Blard et al., 2008; Delon et al., 2020). Figure 3 shows the remaining fraction of cosmogenic ^{3}He in 100-µm to 1-cm olivine and quartz grains continuously exposed at Earth's surface. Even if a 1-cm quartz grain is sufficiently large to retain enough ^3H_e to record exposure durations up to 10^4 years, ^3He_c is not quantitatively retained in submillimetric quartz at typical surface temperatures on Earth (Fig. 3C). This is confirmed by measured cosmogenic ^{3}He concentrations in < 1 mm quartz that are systematically lower than expected from other age constraints (Brook and Kurz 1993; Cerling 1990; Trull et al. 1991). Nonetheless, this partial retentivity can be exploited to determine paleotemperatures (Tremblay et al. 2014).

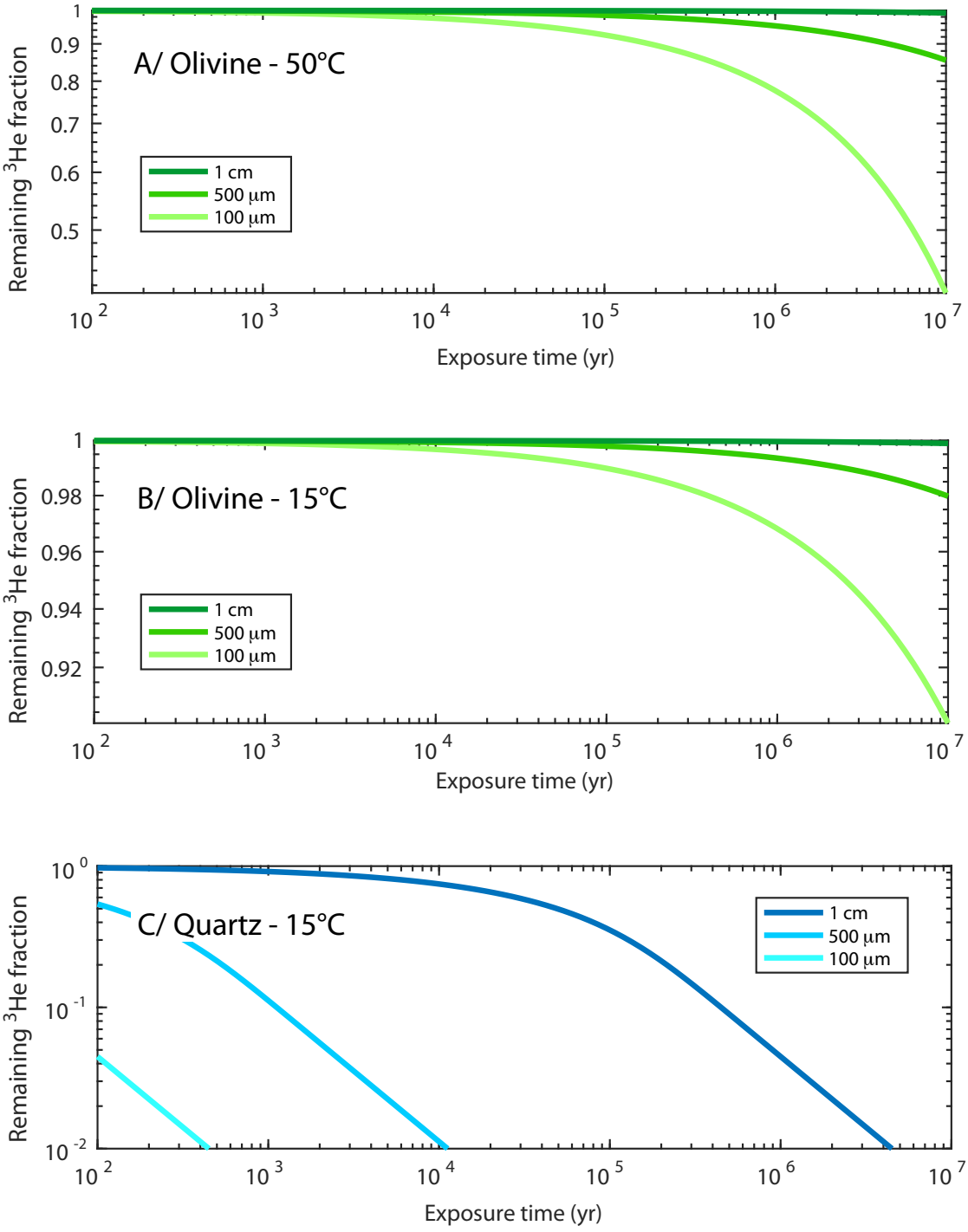

Figure 3. Modeled cosmogenic ^{3}He retention in minerals continuously exposed to cosmic rays: (A) olivine at 50 °C, (B) olivine at 15 °C, and (C) quartz at 15 °C. Note different *y*-axis scales in each plot. These curves were computed by solving the production-diffusion equation for spheres (Wolf, et al, 1998) of various diameters (100 µm, 500 µm, and 1 cm). ^{3}He diffusion parameters are from low-temperature (<200 °C) diffusion experiments on quartz (Tremblay et al, 2014) and olivine (Delon et al. 2020).

In contrast, olivine behaves as a nearly closed system for exposure durations up to 10^5 years (Fig. 3A, B): even 100-μm grains continuously exposed at 50 °C lose less than 10% of the ^{3}He produced. However, for exposure or paleoexposure ages older than 10^6 years, mineral sizes and thermal histories should be carefully evaluated to avoid bias due to thermal losses.

Other minerals with helium diffusivities low enough to evolve as closed systems over geological timescales at Earth's surface include pyroxene, hematite, magnetite, goethite, zircon, and apatite (Amidon et al., 2008; Blard et al., 2008; Farley, 2018; Kober et al., 2005; Shuster et al., 2012; Vasconcelos et al., 2019). In contrast, calcites demonstrated nearly open system behavior at Earth's surface temperatures at the 10 ka time scale (Amidon et al., 2015; Cherniak et al. 2015). The few available data moreover showed that helium diffusivity varies greatly from a one calcite to another (Amidon et al. 2015).

Because olivine and pyroxene have high helium retentivity and are rather abundant in intermediate and mafic rocks (generally 1–10% in andesites and basalts), they are considered to be the most convenient mineral phases for ^3He_c analyses, and are thus the most commonly used (e.g. Blard et al., 2006b; Bromley et al., 2014; Goehring et al., 2010; Martin et al., 2017). These phases are also relatively poor in U and Th (< 10 ppm, (Blard and Farley 2008)), and Li (< 10 ppm, (Amidon et al., 2009; Blard et al., 2013)), implying the limited production of radiogenic ^{4}He and nucleogenic ^{3}He, respectively.

3. ^{3}He sources and correcting for non-cosmogenic ^{3}He

Various natural processes control the incorporation and production of ^{3}He and ^{4}He in terrestrial minerals such as olivine and pyroxene (Fig. 4). It is thus fundamental to understand the budgets of these isotopes to ensure accurate and precise estimates of cosmogenic ^{3}He concentrations in minerals. Thus, in this section, I describe the different production pathways of He isotopes and the most suited strategies to correct for non-cosmogenic ^{3}He sources.

3.1. The global ^{3}He and ^{4}He budgets in terrestrial minerals

In terrestrial minerals, cosmogenic ^{3}He is mainly produced by spallation reactions involving high-energy (>1 MeV) cosmic particles (Lal 1987), but also by low-energy (<1 keV) thermal cosmogenic neutrons through $^6Li(n,\alpha)^3He$ reactions (Dunai et al. 2007) and muons (Larsen et al. 2021; Nesterenok and Yakubovich 2016). These processes produce equivalent amounts of ^{3}He and ^{3}H, but because ^{3}H decays into ^{3}He with a half-life of 12 years, this

intermediate step can be ignored at the geological timescale (Lal 1987). For simplicity, I hereafter assume that ^3He_c includes all these "cosmogenic" production pathways.

^3He_c is produced at a rate of about 120 at.g^{-1}.a^{-1} at sea level and high latitude (Martin et al. 2017) and this rate increases with elevation, reaching ~2,500 at^{-1}.g^{-1}.a^{-1} at 4,000 m elevation and high latitudes (Lal 1991; Stone 2000). Hence, geomorphological materials exposed at Earth's surface for 10^3 -10^6 years have ^3He_c concentrations in the range of 10^5 to 10^9 at.g^{-1}. Modern analytical systems connected to the most recent Nier-source mass spectrometers (see section 2.1) can measure such ^{3}He concentrations to an analytical precision of a few percent in mineral samples of ~10 mg to ~1 g. Nonetheless, the minimum detectable concentration of cosmogenic ^{3}He in a particular sample is determined by our ability to accurately and precisely determine the non-cosmogenic ^{3}He contributions in that sample, which become increasingly difficult as the He closre age of a mineral increases.

^{3}He has four known origins in minerals, each contributing variable ^{3}He concentrations (Fig. 4; Table 1):

i) Cosmogenic ^{3}He (^3He_c) is hosted in the matrix and its concentration increases with exposure age;

ii) Magmatic inherited ^{3}He ($^3He_{mag}$) is hosted in fluid/melt inclusions and the matrix, and its concentration is independent of time;

iii) Nucleogenic ^{3}He ($^3He_{nuc}$) is produced by neutron capture in ^{6}Li nuclei and their subsequent disintegration, is matrix-hosted, and its concentration increases with closure age (eruption age), and;

iv) Atmospheric ^{3}He ($^3He_{atm}$) is present as a contaminant on the surfaces of analyzed silicates and its concentration is time-independent.

In contrast, ^{4}He is 10^6 times more abundant than ^{3}He in the atmosphere and 10^5 times more abundant in the mantle (e.g., Marty and Jambon 1987). Hence, although cosmogenic ^{4}He is also produced in terrestrial rocks, the average non-cosmogenic ^{4}He concentrations in minerals are so large that they hamper the detection of any cosmogenic ^{4}He excess. It is thus reasonable to consider cosmogenic ^{4}He contributions as negligible. Thus, only three ^{4}He origins are relevant to the ^{4}He budget of terrestrial minerals that have been exposed at the Earth's surface (Fig. 4; Table 1):

i) Magmatic ^4He ($^4He_{mag}$) is fluid/melt inclusion- and matrix-hosted, and its concentration is time-independent;

ii) Radiogenic ^4He ($^4He^*$) is produced by the decay of ^{238}U, ^{235}U, and ^{232}Th, is matrix-hosted, and its concentration increases with closure age (eruption age), and;

iii) Atmospheric ^4He ($^4He_{atm}$) is present as a contaminant on the surfaces of analyzed silicates and its concentration is time-independent.

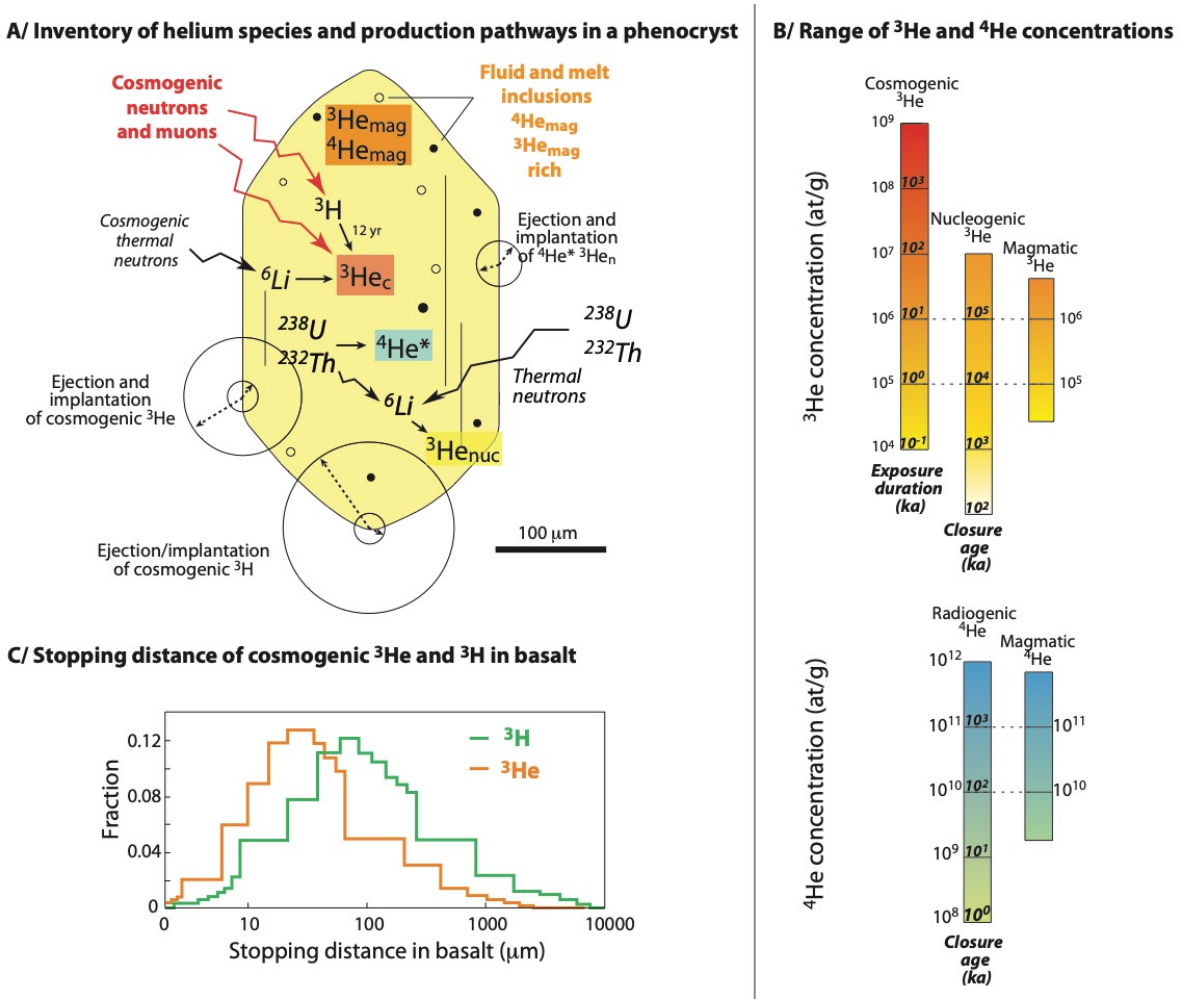

Figure 4. (A) Inventory of ^3He and ^4He species (^3He_c, cosmogenic ^3He; $^3He_{mag}$, magmatic ^3He; $^3He_{nuc}$, nucleogenic ^3He; $^4He_{mag}$, magmatic ^4He; $^4He^*$, radiogenic ^4He) and production pathways in an olivine phenocryst. (B) Ranges of ^3He and ^4He concentrations in phenocrysts, assuming cosmogenic ^3He production at sea level, a nucleogenic ^3He production rate of 0.01 at.g^{-1}.yr^{-1} and a radiogenic ^4He production rate of 10^5 at.g^{-1}.yr^{-1} (typical values for olivine phenocrysts in basalt) (C) Stopping distances of cosmogenic ^3He and ^3H in basalt (Larsen et al. 2019; Ziegler et al. 2010).

Table 1 – Characteristics of ^{3}He and ^{4}He varieties

Component	Magmatic	Atmospheric	Radiogenic	Nucleogenic	Cosmogenic
^{3}He	Hosted in fluid/melt inclusions and matrix. Time-independent concentration. Determination by vacuum crushing or isochrons. Less abundant in fractions finer than 500 µm.	Contaminant adsorbed at the grain surface. Time-independent concentration. Less abundant in fractions coarser than 100 µm.	Absent.	Produced by thermal neutron capture in ^{6}Li. Matrix-hosted. Concentration increases with eruption age.	Matrix-hosted. Concentration increases with exposure age.
^{4}He	Same as ^{3}He.	Same as ^{3}He.	Produced by decay of ^{238}U, ^{235}U, and ^{232}Th. Matrix-hosted. Concentration increases with eruption age.	Absent.	Negligible compared to other ^{4}He varieties.

When a geological sample is fused in vacuo, all ^{3}He species are released, whatever their location in the mineral, and the total ^{3}He budget is (modified from Farley et al., 2006; Blard and Farley, 2008):

$$^{3}\mathrm{He}_{\mathrm{tot}} = {}^{3}\mathrm{He}_{\mathrm{c}} + {}^{3}\mathrm{He}_{\mathrm{nuc}} + {}^{3}\mathrm{He}_{\mathrm{mag}} + {}^{3}\mathrm{He}_{\mathrm{atm}} . \quad (2)$$

Equation (2) is similar to:

$$^{3}\mathrm{He}_{\mathrm{tot}} = \int_0^{t_e} P_3 dt + \int_0^{t_c} P_{\mathrm{nuc}} dt + {}^{3}\mathrm{He}_{\mathrm{mag}} + {}^{3}\mathrm{He}_{\mathrm{atm}}, \quad (3)$$

where P_3 and P_{nuc} (at g^{-1} yr^{-1}) are the time-dependent local cosmogenic and nucleogenic ^{3}He production rates, respectively, and t_e and t_c (yr) are the exposure and closure ages of the sample, respectively.

The ^{4}He budget can be written as:

$$^{4}\mathrm{He}_{\mathrm{tot}} = {}^{4}\mathrm{He}^{*} + {}^{4}\mathrm{He}_{\mathrm{atm}} + {}^{4}\mathrm{He}_{\mathrm{mag}}, \quad (4)$$

or:

$$^{4}\mathrm{He}_{\mathrm{tot}} = \int_0^{t_c} P_4 dt + {}^{4}\mathrm{He}_{\mathrm{mag}} + {}^{4}\mathrm{He}_{\mathrm{atm}}, \quad (5)$$

where P_4 (at g^{-1} yr^{-1}) is the time-dependent ^{4}He* production rate and t_c (yr) is the closure age of the sample.

3.2. Magmatic ^{3}He

3.2.1. Impact of the $^3\mathrm{He}_{\mathrm{mag}}$ correction on the final cosmogenic ^{3}He uncertainty

Just as it is more difficult to find a golf ball in tall grass than on a well-maintained fairway, the uncertainty on the cosmogenic ^{3}He concentration increases with increasing contribution from magmatic ^{3}He (Figs. 4, 5). This is a signal-to-noise ratio issue: the higher the ratio, the lower the uncertainty arising from the magmatic ^{3}He correction. This relationship can be modeled by defining the uncertainty on the total cosmogenic ^{3}He concentration based on the uncertainties on the other variables as in Equation (6), which is obtained from the Taylor series approximation, assuming that all involved uncertainties are independent:

$$\sigma^2_{^3\mathrm{He}_c} = \sigma^2_{^3He_{tot}} + \left[\sigma_{^4\mathrm{He}_{\mathrm{mag}}} \cdot \left(\frac{^3\mathrm{He}}{^4\mathrm{He}}\right)_{\mathrm{mag}}\right]^2 + \left({}^{4}\mathrm{He}_{\mathrm{mag}} \cdot \sigma_{3/4}\right)^2, \quad (6)$$

where $\sigma_{^3\mathrm{He}_c}$, $\sigma_{^3\mathrm{He}_{\mathrm{tot}}}$, $\sigma_{^4\mathrm{He}_{\mathrm{mag}}}$, and $\sigma_{3/4}$ are the uncertainties on the cosmogenic ^{3}He concentration, the total ^{3}He amount extracted by fusion, the magmatic ^{4}He concentration, and the magmatic ^{3}He/^{4}He ratio, respectively.

Figure 5 shows the impact of the $^3He_{mag}$ correction on the final uncertainty of the measured ^3He_c concentration under different exposure scenarios using Equation (6). This calculation illustrates the importance of the $^3He_c/^3He_{mag}$ ratio on the final uncertainty on ^3He_c: the larger the ratio, the lower the uncertainty.

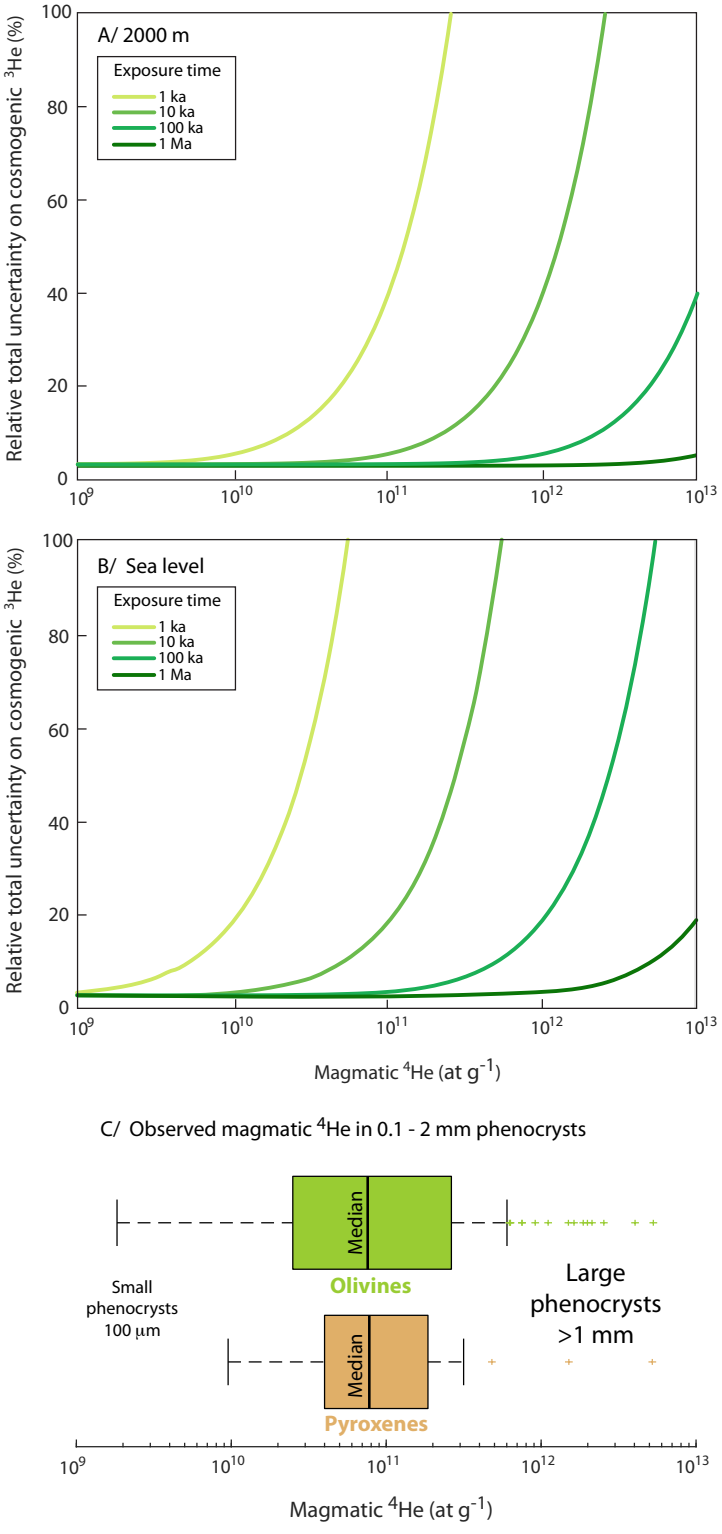

Figure 5. (A, B) Modeling the impact of the magmatic ^{4}He concentration on the total relative uncertainty (1σ) on the measured cosmogenic ^{3}He concentration for variable exposure durations. Because the ^3He_c production rate changes with elevation, this simulation considers a mineral at (A) 2,000 m elevation and (B) sea level. This calculation applies Equation (6) assuming a magmatic ^{3}He/^{4}He ratio of 8 Ra with an uncertainty of 20%, an uncertainty of 3% on the total amount of ^{3}He extracted by fusion, an uncertainty of 1% on the total amount of ^{4}He extracted by fusion, and a negligible contribution from radiogenic ^{4}He. (C) The distribution of the total magmatic ^{4}He concentrations observed in olivine and pyroxene phenocrysts (Ackert et al. 2003; Blard et al. 2006; Cerling and Craig 1994; Dunai and Wijbrans 2000; Eaves et al. 2015; Fenton and Niedermann 2014; Foeken et al. 2012; Goehring et al. 2010; Licciardi et al. 2006; Licciardi et al. 1999). This dataset includes only lavas that are young enough (<200 ka) to ensure that the radiogenic ^{4}He correction does not represent a significant systematic uncertainty.

A recent compilation of magmatic helium concentrations measured in olivine and pyroxene phenocrysts in basalts (Puchol et al. 2017) indicates that the total magmatic helium concentrations in these phenocrysts are largely variable, both at the scale of a single lava flow and among minerals in a single sample (Fig. 5, Table S1). On average, magmatic ^{4}He concentrations measured in 132 olivine and 32 pyroxene phenocrysts (ranging in size from 0.2 to 2 mm and from basalts in different geological settings) display mean ^{4}He concentrations of 3×10^{11} at g^{-1} (median of 8×10^{10} at g^{-1}) for both olivine and pyroxene and a significant intersample variability (standard deviation > 6×10^{10} at g^{-1}; Fig. 5, Table S1). This dataset also indicates that magmatic helium concentrations vary between aliquots of hundreds of grains, even when the measured aliquots originate from the same sample.

Assuming that these phenocrysts have ^{3}He/^{4}He ratios of 8 Ra, an average ^{4}He concentration of 3×10^{11} at g^{-1} represents ~3.3×10^6 at g^{-1} magmatic ^{3}He. In the case of a sample exposed at high latitude and sea level (production rate ~125 at g^{-1} yr^{-1}), and assuming a 10% uncertainty on the magmatic ^{3}He concentration, the total error on the exposure age will be ~3 kyr (Fig. 5). Note, however, that some samples may be very rich in ^{4}He, reaching concentrations above 10^{12} at g^{-1}. The amounts and heterogeneities of magmatic helium in phenocrysts are controlled by a significant nugget effect and by the abundance and repartitioning of fluid and melt inclusions, for which geological context plays a main role (Puchol et al., 2017). However, this dataset is not large enough to establish a systematic or to understand why some volcanic fields present phenocrysts with higher magmatic helium contents than others (Table S1). In any case, an efficient means of minimizing the uncertainty from the magmatic He correction is to select phenocrysts with low magmatic helium concentrations, or to find methods for reducing this initial concentration.

3.2.2. Using grains sized 100–500 µm reduces the magmatic helium contribution

Observations show that phenocryst size is a first-order control on helium concentrations, all other things being equal (Puchol et al. 2017). Furthermore, progressive phenocryst crushing experiments have demonstrated that laboratory (Williams et al. 2005) or natural crushing (e.g., by erosion; Puchol et al., 2007) may reduce the magmatic He content by releasing the magmatic component that is preferentially hosted in melt and fluid inclusions. Hence, crushing grains and then fusing the finest fraction may appear to be a good strategy because it purges magmatic helium and thus reduces the uncertainty on the computed cosmogenic ^{3}He concentration. Although it is sometimes misleading to propose a universal grain size cutoff, experiments have shown that analyzing phenocrysts smaller than 500 µm is generally efficient in significantly reducing the magmatic helium component and intergrain variability (Puchol et al. 2017; Williams et al. 2005).

However, reducing the granulometry of the analyzed phenocrysts should be performed with caution: several studies have reported the suspected loss of matrix-hosted ^{3}He during in-vacuo crushing (Blard et al. 2006; Hilton et al. 1993; Yokochi et al. 2005) and, more worrisome, Protin et al. (2016) recently demonstrated that significant amounts of atmospheric helium may be adsorbed onto the newly created surfaces when crushing silicates in atmospheric conditions. This effect must be considered seriously because experimental data indicate that the high adsorption energy of atmospheric helium requires heating above 1000 °C to release the contamination, which affects cosmogenic ^{3}He (Protin et al. 2016). Because atmospheric helium is adsorbed on surfaces, the magnitude of the contamination is inversely proportional to grain size. Experimental data from olivines show that contamination remains insignificant (compared to matrix-hosted helium varieties) for grains larger than 100 µm (Protin et al. 2016). As both the loss of matrix-hosted cosmogenic ^{3}He and unexpected atmospheric contamination result in underestimated cosmogenic ^{3}He concentrations, grains smaller than 100 µm should be avoided in cosmogenic ^{3}He analyses. Consequently, combining the need to reduce the magmatic helium component while avoiding any atmospheric helium contamination defines the ideal granulometric window for cosmogenic ^{3}He analyses: the fusion of minerals ranging in size ***from 100 to 500 µm*** should be favored (Fig. 5).

Another promising and innovative technique recently tested by (Hofmann et al. 2021) is to use X-ray micro-computed tomography (µCT) to identify grains that are free of melt/fluid inclusions and thus have much lower magmatic ^{3}He concentrations. Finally, an alternative to crushing is to melt several aliquots from the same sample and build ^{3}He vs. ^{4}He isochrons

(section 3.5.3). Using this method, one can distinguish the cosmogenic and magmatic ^{3}He components without vacuum crushing, avoiding all the above-mentioned potential issues.

3.3. Radiogenic ^{4}He

Radiogenic ^{4}He is produced by the radioactive decay of U and Th present in the mineral. In many geological settings, radiogenic ^{4}He concentrations are non-negligible and may indeed be of the same order of magnitude as the magmatic ^{4}He component. In such samples, it is important to properly estimate the ^{4}He* concentration to accurately estimate the magmatic ^{4}He and ^{3}He contributions (Blard and Farley 2008). In some cases, the radiogenic ^{4}He concentration may even be several orders of magnitude greater than the magmatic ^{4}He concentration, requiring specific approaches to estimate the magmatic ^{3}He component (Martin et al. 2018).

The radiogenic ^{4}He concentration, which is determined by a mineral's closure age t_c, can be used to determine the most suitable method and analytical strategies for performing non-cosmogenic ^{3}He corrections (see section 3.5).

3.3.1. The production of radiogenic ^{4}He: general principles and equations

Radiogenic ^{4}He is produced by the α-decay of ^{235}U, ^{238}U, and ^{232}Th when these elements are present in a studied mineral and its host lithology. ^{147}Sm and ^{148}Sm also release alpha particles through radioactive decay, but this contribution is generally negligible in silicates. ^{4}He* production through time is described as:

$$^{4}\mathrm{He}^{*} = \int_{0}^{t_c} P_4 dt \,, \qquad (7)$$

where t_c is the helium closure age (i.e., the eruption age in the case of volcanic rocks) and P_4 is the production rate. If t_c is long enough to have reached secular equilibrium, Equation (7) simplifies to:

$$^{4}\mathrm{He}^{*} = P_4 \times t_c \,. \qquad (8)$$

Note that, in the case of rocks with young crystallization ages (<500 ka), the assumption of secular equilibrium may not be valid, and disequilibrium must be considered when calculating P_4 (Aciego et al. 2007; Farley et al. 2002). That said, even for lavas younger than 500 ka and when using the maximum ^{230}Th/^{238}U fractionation reported for pyroxenes and

olivines (Aciego et al. 2007; Wood et al. 1999), the obtained value of P_4 differs from that obtained under the secular equilibrium assumption by <5% (Farley et al. 2002)

To avoid circular reasoning and the difficulty of estimating the magmatic ^{4}He contribution, t_c should be estimated using a different radiochronometer than (U-Th)/^{4}He*, such as K-Ar or ^{40}Ar/^{39}Ar; this is often feasible for lavas because the crystallization age equals the helium closure age. However, in the case of plutonic or metamorphic rocks, in which minerals generally have helium closure ages younger than the crystallization age, (U-Th)/^{4}He* dating is a necessary alternative. In those cases, this should be done using minerals with large (U-Th)/^{4}He$_{mag}$ ratios to avoid bias and uncertainties in estimating ^{4}He* that result from the magmatic ^{4}He component.

Since the ejection distance of alpha particles is ~20 μm in rocks (Ziegler 1977), some radiogenic ^{4}He produced in the surrounding matrix is also implanted in minerals (Lal 1989). Conversely, a fraction of the in-situ ^{4}He* may also be ejected from minerals. Thus, one must consider both ejection and implantation when computing P_4. Based on a series development formula, P_4 can be calculated as (Farley et al. 2006):

$$P_4 = I_4 \left[1 - 1.5(S/D) + 0.5(S/D)^3\right] + M_4 \left[1.5(S/D) - 0.5(S/D)^3\right], \quad (9)$$

where I_4 and M_4 are the ^{4}He* production rates in the mineral of interest and in the surrounding lava, respectively, S (μm) is the stopping distance of alpha particles (~20 μm). D (μm) is the crystal diameter, and Equation (9) is thus only valid for minerals having a spherical geometry; for non-spherical phenocrysts, it is necessary to compute an equivalent sphere diameter (Farley and Stockli 2002).

If secular equilibrium is reached, I_4 and M_4 follow (e.g., Wolf et al., 1998):

$$I_4 \text{ (or } M_4) = 8\lambda_{238}[^{238}\text{U}] + 7\lambda_{235}[^{235}\text{U}] + 6\lambda_{232}[^{232}\text{Th}], \quad (10)$$

where [^{238}U], [^{235}U], and [^{232}Th] are the isotopic concentrations measured in the mineral (for I_4) or the lava (for M_4) and λ_{238}, λ_{235}, and λ_{232} are their respective decay constants.

3.3.2. Removing the implanted ^{4}He* component

The proportion of in-situ relative to implanted ^{4}He* production is controlled by phenocryst size and by the relative U and Th concentrations in the phenocrysts and their host, i.e., the effective mineral/melt partition coefficients for these elements. These partition coefficients vary greatly across lithologies and geological settings (Blard and Farley 2008) and are strongly dependent on the abundance of U-Th-rich melt inclusions, and should thus be called "apparent partition coefficients". The presence of U-Th-rich melt inclusions may also induce significant spatial heterogeneities in the mineral of interest, implying that spot analyses by secondary ion mass spectrometry should be avoided. Bulk U-Th analyses after mineral dissolution are thus preferable because they represent the mean U-Th concentration.

Correcting for implantation and ejection may also be complicated by several issues, and thus be a source of significant uncertainties. This is particularly true for detrital minerals in river sediments: because these minerals may have been fragmented, their initial sizes are generally unknown, as well as the exact U and Th concentrations of their source rocks. Moreover, in the case of non-spherical grains, shape estimates and the conversion to equivalent sphere diameter may also induce significant uncertainties.

Removing the external portion (at least 20 μm) of phenocrysts should therefore be a systematic sample preparation step because it obviates the need to correct for implanted and ejected components (Aciego et al. 2007; Blackburn et al. 2007; Bromley et al. 2014; Gayer et al. 2008; Min et al. 2006). Using this method, geometric corrections are unnecessary and the radiogenic ^{4}He production rate equals the in-situ ^{4}He* production rate, simplifying Equation (9) to $P_4 = I_4$; this has the potential to reduce the uncertainties associated with calculating the ^{4}He* component. For olivine and pyroxene, Bromley et al. (2014) proposed a chemical treatment in which minerals are leached for 2 hours in a 3% HF:10% HCl acid solution in an ultrasonic bath at 40 °C (see Fig. 7). Physical techniques, such as over-pressurized air abrasion in closed chambers, also efficiently remove the external ^{4}He*-enriched rim (Aleinikoff et al. 1990).

If it is not possible to remove the external rim affected by alpha particle mobility, it is of primary importance to measure the U and Th concentrations in both the phenocrysts and their host rock, especially in samples with large closure/exposure age ratios.

3.3.3. Uncertainty arising from the radiogenic ^{4}He correction

To show the importance of accurately and precisely correcting for radiogenic ^{4}He, I modelled the total uncertainty on the cosmogenic ^{3}He concentration for different exposure ages, closure age scenarios (10 ka to 1 Ga), and different elevations in Figure 6. In this model, the total uncertainty on cosmogenic ^{3}He is computed from a Taylor series expansion as:

$$\sigma^2_{^3\mathrm{He_c}} = \sigma^2_{^3\mathrm{He_f}} + \left[\sigma_{^4\mathrm{He_{mag}}} \cdot \left(\frac{^3\mathrm{He}}{^4\mathrm{He}}\right)_{\mathrm{mag}}\right]^2 + \left[\sigma_{^4\mathrm{He^*}} \cdot \left(\frac{^3\mathrm{He}}{^4\mathrm{He}}\right)_{\mathrm{mag}}\right]^2 + \left[\left(^4\mathrm{He_{tot}} - {}^4\mathrm{He^*}\right) \cdot \sigma_{3/4}\right]^2 . \quad (11)$$

The model results demonstrate that the radiogenic ^{4}He correction may induce a significant uncertainty on the final estimated cosmogenic ^{3}He concentration, with the error increasing with increasing closure/exposure age ratio and magmatic ^{4}He concentration. Thus, precision can be increased by selecting samples with the youngest possible (U-Th)/^{4}He closure age, when possible, and by reducing the magmatic He component by preferentially selecting grains in the 100–500 μm size range or by identifying inclusion free minerals by μCT (Hofmann et al. 2021).

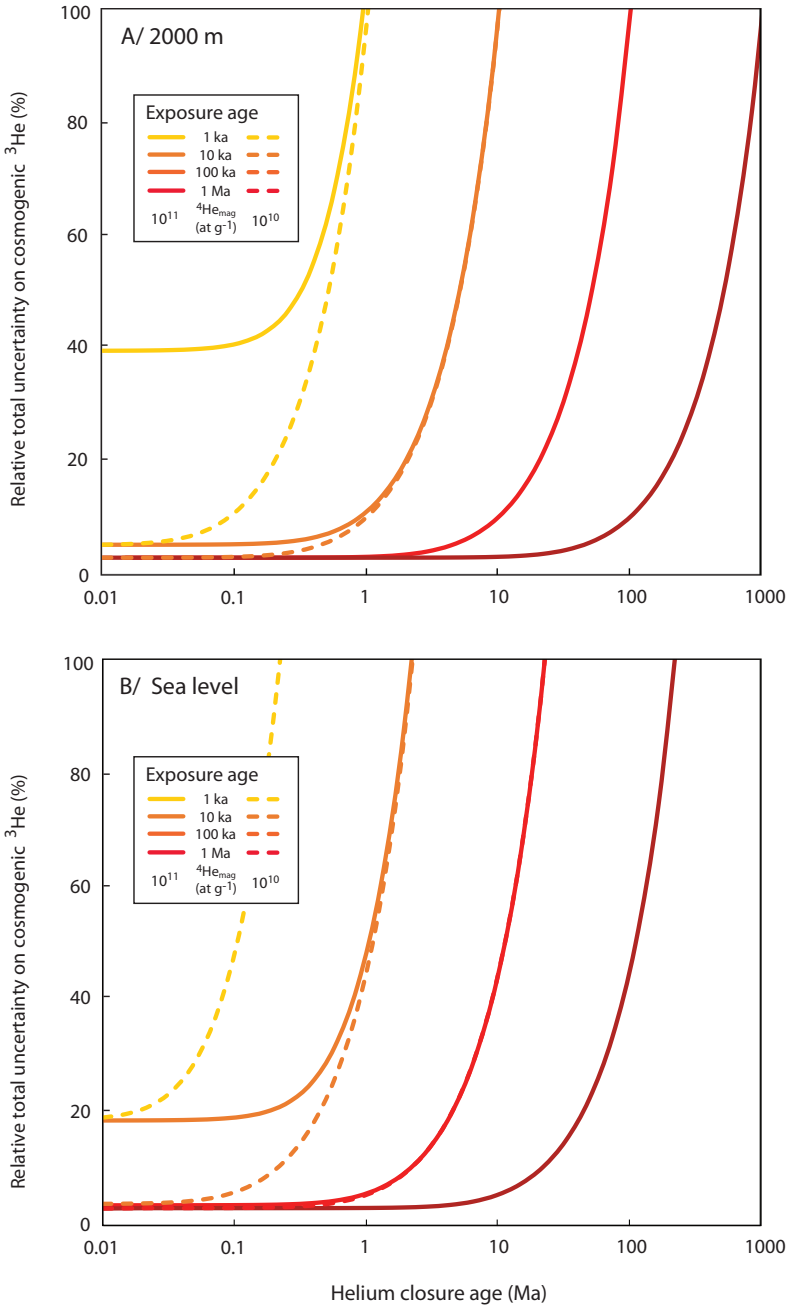

610

611

612 **Figure 6. Modeling the impact of the radiogenic ^{4}He correction—described by the (U-Th)/^{4}He***
613 **cooling age—on the total relative uncertainty (1σ) on the measured cosmogenic ^{3}He**
614 **concentration for variable exposure durations. Two magmatic ^{4}He concentrations are**
615 **considered: 10^{10} and 10^{11} at g^{-1} (dashed and solid curves, respectively). Because the ^3He_c**
616 **production rate changes with elevation, this simulation considers samples exposed at (A) 2,000 m**
617 **elevation and (B) sea level. This calculation applies Equation (11) assuming a magmatic ^{3}He/^{4}He**
618 **ratio of 8 Ra with 20% uncertainty, an uncertainty of 3% on the total amount of ^{3}He extracted**
619 **by fusion, an uncertainty of 1% on the magmatic ^{4}He concentration, and an uncertainty of 10%**
620 **on the estimated radiogenic ^{4}He concentration.**

621

622

623 **3.4. Nucleogenic ^{3}He**

624

625 **3.4.1. The production of nucleogenic ^{3}He: general principles and equation**

626 In minerals, nucleogenic ^{3}He is produced by the capture of low-energy neutrons by ^{6}Li
627 through the reaction (Andrews 1985; Andrews and Kay 1982; Dunai et al. 2007):

628

629 $$^6Li(n,\alpha)\ ^3H \xrightarrow[\beta\ decay]{} {}^3He \quad . \qquad (12)$$

630

631 Neutrons involved in this reaction are "thermal", "epithermal", and "slow" neutrons
632 with energies ranging between 0.025 and 300 eV, far below those of the cosmogenic "fast"
633 neutrons (>1 MeV) involved in the main cosmogenic ^{3}He production pathway (Dunai 2010;
634 Gosse and Phillips 2001). Some of this low-energy neutron flux into rocks originates from
635 nuclear reactions between cosmic rays and the terrestrial environment (Lal 1987). However,
636 ^{3}He production through the capture of cosmogenic thermal neutrons is significantly lower than
637 that by cosmogenic spallation, at least in the case of minerals with typical Li concentrations of
638 2–50 ppm (Dunai et al. 2007).

639 Low-energy neutrons involved in the production of ^{3}He through capture by ^{6}Li are also
640 produced by (α,n) reactions (Andrews 1985; Andrews and Kay 1982) involving elements
641 within rocks and alpha particles emitted by the natural decay of U and T. The total production
642 rate P_{nuc} of nucleogenic ^{3}He thus depends on the Li concentration in the mineral of interest and
643 the bulk U and Th concentrations and chemical composition of the rock within ~1 m of the
644 mineral. In a given mineral, P_{nuc} can be calculated as (modified from Andrews, 1985):

645

646 $$P_{\mathrm{nuc}} = f_{\mathrm{n}} \frac{[\sigma_{\mathrm{Li}} C_{\mathrm{Li}}]_{\mathrm{mineral}}}{[\sum_i^k \sigma_i C_i]_{\mathrm{rock}}} \quad . \qquad (13)$$

647 where f_n is the average thermal neutron flux originating from the bulk rock, σ_i is the neutron
648 capture cross section specific to element i, and C_i is the concentration of element i (in mol g^{-1}
649 or atomic percent). According to Andrews and Kay (1982), 17 elements (k = 17) are needed to
650 accurately compute P_{nuc}: nine major elements (Si, Al, Fe, Mn, Mg, Ca, Na, K, Ti) and eight
651 trace elements with cross sections larger than 1 barn (Li, B, Co, Cr, Ni, Gd, Sm, Cl).

652 The (α,n) reactions occurring in the bulk rock determine f_n, which is computed as
653 (Andrews and Kay 1982):

654

$$f_n = \frac{U}{100} \cdot (13.8 \cdot Na + 5.4 \cdot Mg + 5.0 \cdot Al + 1.31 \cdot Si + 0.6 \cdot Ca) + \frac{Th}{100} \cdot (6 \cdot Na + 2.45 \cdot Mg + 2.55 \cdot Al + 0.56 \cdot Si + 0.25 \cdot Ca) + 0.4764 \cdot U \,, \quad (14)$$

where U and Th concentrations are in ppm (10^{-6} g g^{-1}) and the concentrations of the other elements are in atomic percent (%). Importantly, all these elemental concentrations must be measured in a rock sample that is representative of the bulk rock. Indeed, the absorption paths of low-energy neutrons produced through (α,n) reactions in rocks typically range between 50 and 80 cm, implying that the radiogenic thermal neutron flux is spatially averaged and rather homogenous within a monolithological geological unit (Dunai et al. 2007; Lal 1987). An Excel spreadsheet is available in the Supplementary Information (Table S2) to compute P_{nuc} and the total $^3He_{nuc}$ concentration when the closure age is known; it requires the 17 major and trace element concentrations involved in Equation (13) as inputs.

3.4.2. Uncertainty arising from the nucleogenic ^{3}He correction

The total nucleogenic ^{3}He concentration in a mineral is controlled by the mineral's Li concentration, the bulk chemical composition of its host rock, and the helium closure age (Fig. 7A). To assess the impact of correcting for $^3He_{nuc}$ on the precision of the measured cosmogenic ^{3}He concentration, I modeled the uncertainty arising from the nucleogenic ^{3}He correction as a function of helium closure age for variable exposure durations (1 ka, 10 ka, 100 ka, 1 Ma), at 2,000 m elevation or sea level (Fig. 7B, C). Similar to the radiogenic ^{4}He correction, the exposure/closure age ratio impacts the detection limit and final uncertainty arising from the nucleogenic ^{3}He correction. Whenever possible, it is thus important to select rock samples with the largest possible exposure/closure age ratio to improve the precision on the measured cosmogenic ^{3}He concentration.

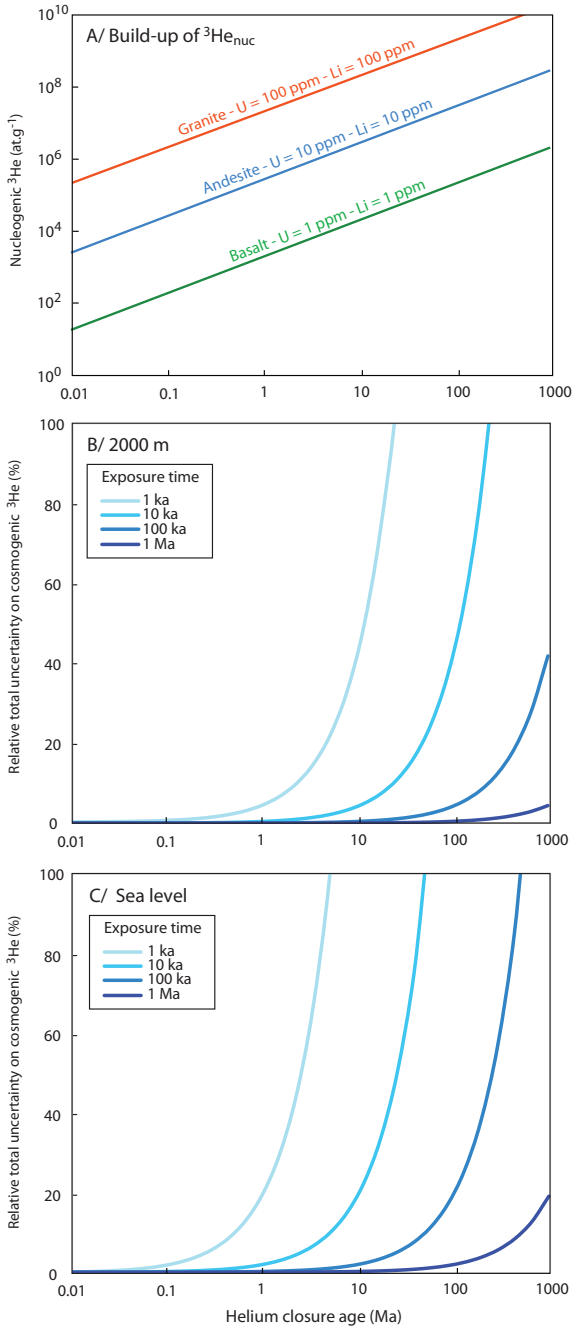

Figure 7. (A) Nucleogenic ^{3}He concentrations for various Li contents typical of different lithologies. (B, C) Uncertainty on the cosmogenic ^{3}He concentration due to the nucleogenic ^{3}He correction, at 2,000 m elevation, and sea level, respectively. This modeling assumes a mineral containing 10 ppm Li in a rock of average andesitic composition with a bulk U content of 10 ppm, corresponding to P_n = 0.25 at g^{-1} yr^{-1} (shown in blue in (A). This model assumes that the nucleogenic production rate is known with a relative uncertainty of 10%.

3.5. Strategies to estimate the non-cosmogenic ^{3}He components

Correcting for non-cosmogenic ^{3}He components is key to achieving low detection limits and final uncertainties on cosmogenic ^{3}He concentrations. Several characteristics of a rock's geological history must be carefully evaluated for each sample, notably the helium closure age, the amount of magmatic helium in the minerals, and the concentrations of U, Th, and Li in the minerals and their host rocks. The minimum measurable surface exposure age may thus vary by several orders of magnitude, from 10^2 to $>10^6$ years.

Different analytical strategies and procedures can be used to correct for the non-cosmogenic ^{3}He components, and the choice of the best strategy mainly depends on the specific characteristics of a given sample. Figure 8 is an easy-to-use flowchart that summarizes the analytical protocol, from bulk sample crushing to final cosmogenic ^{3}He calculation, for various sample cases.

Flowchart for cosmogenic ^{3}He measurements

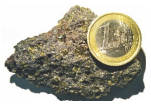

$$^3He_{tot} = {}^3He_c + {}^3He_{mag} + {}^3He_{nuc}$$
$$^3He_{tot} = {}^3He_c + {}^4He_{mag} \times \left(\frac{^3He}{^4He}\right)_{mag} + f(U_{rock}, Th_{rock}, Li_{min}, t_c)$$
$$^4He_{tot} = {}^4He_{mag} + {}^4He^* = {}^4He_{mag} + f(U_{min}, Th_{min}, t_c)$$

Measurement

Calculation

1 – Isolation of minerals (olivines, pyroxenes)

Save a 3 cm x 3 cm piece
Crush bulk rock
Sieve: 100-500 µm and 500-1000 µm
Density and magnetic separation
Quality check: handpicking under a microscope to remove grains with adhering lava, oxides, clays

Thin section: petrographic characteristics (optional)

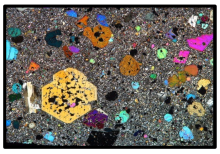

~1 g bulk rock aliquot → **Major and trace elements in rock Li, U-Th-Sm**

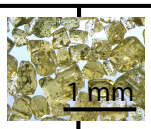

2 – Removal of 20 µm external rim

to remove the implanted ^{4}He*

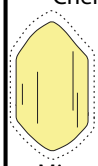

Chemical: HF 3% - HCl 5% for 2 hours (20 mL/g) at 40 °C
HCl 40% rinsing ×3 - H_2O rinsing ×3 - Drying

or

Physical: abrasion with compressed air

Microscope quality check: remove newly formed fluorides

~1 g mineral aliquot → **Major and trace elements in the mineral U-Th-Sm, Li**

Thermal neutron flux in the rock

^{4}He* and ^{3}He$_{nuc}$ × closure age t_c [&] → P_4 and P_{nuc}

^{4}He* >> ^{4}He$_{mag}$?

YES

1a – 10 min vacuum crushing: ^{3}He$_{mag}$
or
1b – Fusion of a shielded sample: ^{3}He$_{mag}$ + ^{3}He$_{nuc}$

2 - Fusion of 100-500 µm minerals: ^{3}He$_{tot}$ ^{4}He $_{tot}$

$^3He_c = {}^3He_{tot} - {}^3He_{mag} - {}^3He_{nuc}$

Hypothesis: $^3He_{mag}$ homogeneous

NO

or

Standard method

1 - Crushing in vacuuo ~ 0.5 g aliquot of 0.5-1 mm minerals
$(^3He/^4He)_{mag}$

2 – Fusion [#] of ~0.05 g to 1 g aliquot of 100-500 µm minerals
^{3}He$_{tot}$ ^{4}He $_{total}$

$$^3He_c = {}^3He_{tot} - ({}^4He_{tot} - {}^4He^*) \times \left(\frac{^3He}{^4He}\right)_{mag} - {}^3He_{nuc}$$

[#] *Before any He extraction in a furnace, weigh the samples and wrap in metal foil.*

Isochrons

Fusion[#] of several aliquots of ~ 0.5 g of 0.1 to 1 mm minerals
^{3}He$_{total}$ ^{4}He $_{total}$

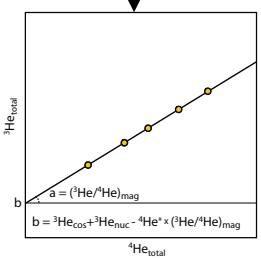

$$^3He_c = b + {}^4He^* \times a - {}^3He_{nuc}$$

[&] **Particular case of uneroded lava flow: t_c is unnecessary**

Standard method

$$^3He_c = \frac{1}{R}\left[{}^3He_{tot} - {}^4He_{tot} \times \left(\frac{^3He}{^4He}\right)_{mag}\right]$$

Isochrons

$$^3He_c = \frac{b}{R}$$

with:

$$R = 1 - \frac{P_4}{P_3} \times \left(\frac{^3He}{^4He}\right)_{mag}$$

Figure 8. Flowchart presenting up-to-date protocols for measuring cosmogenic ^{3}He, including the estimation of radiogenic ^{4}He and nucleogenic ^{3}He, which requires independent knowledge of the helium closure age of a rock, t_c, except in the special case of uneroded lava flows. See text for detailed equations, notably those for calculating the radiogenic ^{4}He production rate, P_4 (Equations 9-10) and the nucleogenic ^{3}He production rate, P_{nuc} (Equations 13-14).

3.5.1. The general case: He closure age > exposure age, but ^{4}He* is not significantly larger than $^4He_{mag}$

For typical U and Th concentrations, the common case in which ^{4}He* and magmatic ^{4}He concentrations are of comparable orders of magnitudes (i.e., $0 < {}^4He^*/{}^4He_{tot} < 1$) is encountered in minerals with helium closure ages younger than a few tens of millions of years (Blard and Farley 2008). In such cases, an efficient strategy is to compute ^{4}He* using Equations (7)–(10); the magmatic He correction can then be performed accurately using a modified version of Equation (1) (Blard and Farley 2008):

$$^3He_c = {}^3He_{tot} - ({}^4He_{tot} - {}^4He^*) \times ({}^3He/{}^4He)_{mag} - {}^3He_{nuc} . \quad (15)$$

In this case, the total uncertainty on cosmogenic ^{3}He can be computed applying Equation (11).

3.5.2. Samples with similar closure and exposure ages

Although rare, the condition that $t_c = t_e$ applies to the case of uneroded lava flows. In such cases, the accumulation of radiogenic ^{4}He and cosmogenic ^{3}He in the minerals of interest (olivine, pyroxenes) starts synchronously when a lava flow cools at the Earth's surface (Blard and Farley 2008). Because $t_c = t_e$:

$$^4He^* = \frac{P_4}{P_3} \times {}^3He_c . \quad (16)$$

Then, using Equation (16) to substitute ^{4}He* into Equation (15), and making the reasonable assumption that $^3He_{nuc}$ is negligible in this case, isolating ^3He_c on the left-hand side gives:

$$^3He_c = \frac{{}^3He_{tot} - {}^4He_{tot} \times \left(\frac{{}^3He}{{}^4He}\right)_{mag}}{R}, \quad (17)$$

where

$$R = 1 - \frac{P_4}{P_3} \times \left(\frac{^3\mathrm{He}}{^4\mathrm{He}}\right)_{\mathrm{mag}} . \quad (18)$$

Equation (18) defines the so-called *R*-factor ("*R*" for radiogenic; Blard and Farley, 2008; Blard and Pik, 2008). This approach has the advantage of including the full impact of the radiogenic ^{4}He correction on the calculation of the cosmogenic ^{3}He concentration without requiring any independent estimate on the helium closure age of the rock.

Calculating *R* requires only the local time-integrated production rate P_3, the ^{4}He* production rate P_4, and the magmatic ^{3}He/^{4}He ratio. The lower the value of *R*, the greater the correction arising from radiogenic ^{4}He. When $R \approx 1$, the radiogenic correction is negligible compared to the production of cosmogenic ^{3}He, i.e., $\frac{P_4}{P_3} \cdot \left(\frac{^3\mathrm{He}}{^4\mathrm{He}}\right)_{\mathrm{mag}} \ll 1$, and the magmatic correction simplifies to Equation (15). However, this situation is rare in nature; modelling *R* for different exposure altitudes and U and Th concentrations shows that *R* is generally < 1 (Fig. 9). Importantly, in the case of lava flows used to calibrate the cosmogenic ^{3}He production rate, most actual *R*-factors are between 0.80 and 0.95 (Blard and Farley 2008), meaning that neglecting the radiogenic ^{4}He correction would translate to underestimating $^3\mathrm{He}_c$ by 5–20%. Because some earlier studies did not perform this radiogenic ^{4}He correction, we have recomputed all reported *R*-factors in the updated online production rate database ICE-D (http://calibration.ice-d.org/), which is used as a reference by the CREp calculator (https://crep.otelo.univ-lorraine.fr/#/) to compute cosmogenic ^{3}He exposure ages (Martin et al. 2017).

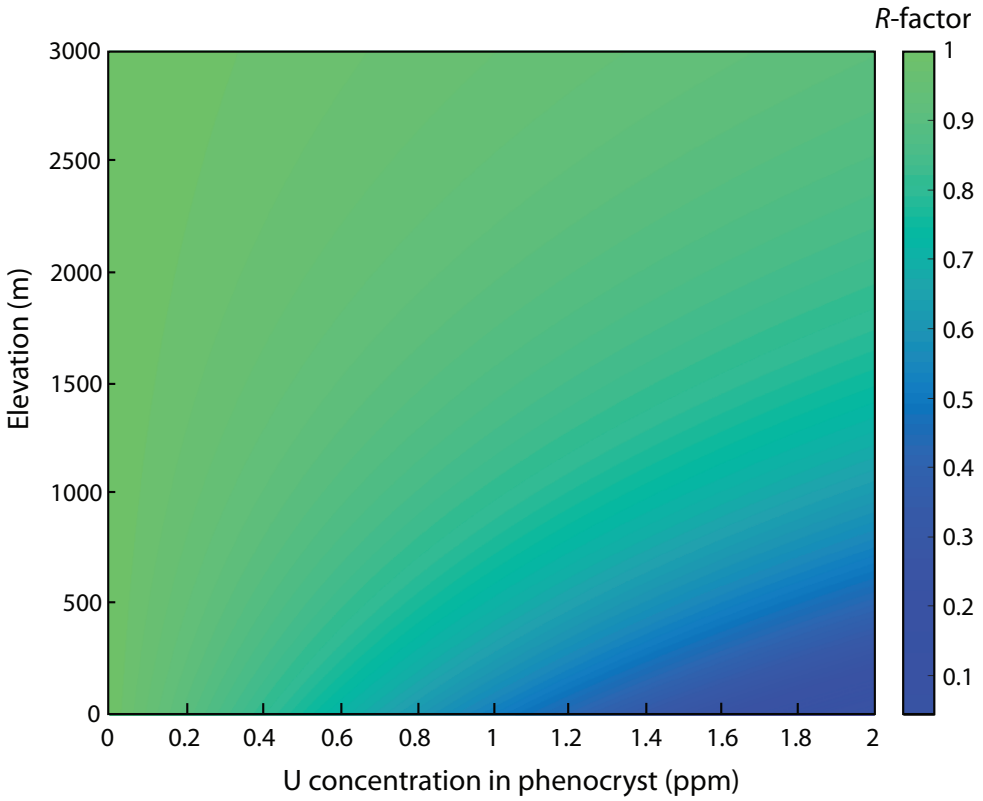

Figure 9. Modeled values of *R*-factor for uneroded lava flows as a function of U concentration in the phenocrysts and exposure elevation. Here, *R* is computed for a Th/U ratio of 3 and a magmatic $^{3}He/^{4}He$ ratio of 8 Ra. Implantation of $^{4}He^{*}$ from surrounding lava is neglected. The equations of Stone (2000) were used to scale the sea-level $^{3}He_{c}$ production rate of 124 at g^{-1} yr^{-1} (Martin et al., 2017). This simulation shows that *R* is strongly dependent on the altitude at which a lava flow is emplaced.

3.5.3. Isochrons

An alternative method of estimating non-cosmogenic ^{3}He components is to fuse several aliquots of the same mineral sample. Measured ^{3}He and ^{4}He concentrations obtained by melting different aliquots with variable magmatic helium concentrations define straight lines in $^{3}He_{melt}$ vs. $^{4}He_{melt}$ space (Cerling and Craig 1994) or $(^{3}He/^{4}He)_{melt}$ vs. $1/^{4}He_{melt}$ space (Blard and Pik 2008) (Fig. 10); these 'melt' concentrations represent total concentrations. The main advantage of building cosmogenic helium isochrons is to avoid the vacuum crushing step; the magmatic $^{3}He/^{4}He$ ratio is directly defined by the linear regression of an isochron. Even though the isochron method is powerful for estimating the magmatic ^{3}He contribution, note that this technique still requires the determination of potential contributions from radiogenic ^{4}He (by measuring U and Th concentrations and the helium closure age; see section 3.3) and

781 nucleogenic ^{3}He components (by measuring bulk-rock major and trace elements and mineral
782 Li concentrations; see section 3.4).
783 Below, I detail the basic equations and outcomes that can be derived from the isochron approach.
784
785 **3.5.3.1. ^{3}He vs. ^{4}He "Cerling" isochrons (Cerling and Craig 1994).** The general
786 "Cerling-isochron" equation is:
787
788 $$^3\mathrm{He}_{\mathrm{tot}} = {}^4\mathrm{He}_{\mathrm{tot}} \times \left(\frac{^3\mathrm{He}}{^4\mathrm{He}}\right)_{\mathrm{mag}} + \left[{}^3\mathrm{He}_{\mathrm{c}} + {}^3\mathrm{He}_{\mathrm{nuc}} - {}^4\mathrm{He}^* \times \left(\frac{^3\mathrm{He}}{^4\mathrm{He}}\right)_{\mathrm{mag}} \right]. \quad (19)$$

789
790 This corresponds to the equation of a line, $y = ax + b$, in which the slope a is $(^3\mathrm{He}/^4\mathrm{He})_{\mathrm{mag}}$
791 and the y-intercept b is the sum of all components that are independent of the magmatic
792 component, including cosmogenic ^{3}He (Fig. 10A). $^3\mathrm{He}_{\mathrm{c}}$ can then be estimated after correcting
793 for the nucleogenic ^{3}He and radiogenic ^{4}He components as:
794
795 $$^3\mathrm{He}_{\mathrm{c}} = b + {}^4\mathrm{He}^* \times a - {}^3\mathrm{He}_{\mathrm{nuc}} . \quad (20)$$

796
797 In the specific case of uneroded lava flows, the radiogenic ^{4}He correction may be simplified
798 using the R-factor (Eq. 18) to:
799
800 $$^3\mathrm{He}_{\mathrm{c}} = \frac{b}{R}. \quad (21)$$

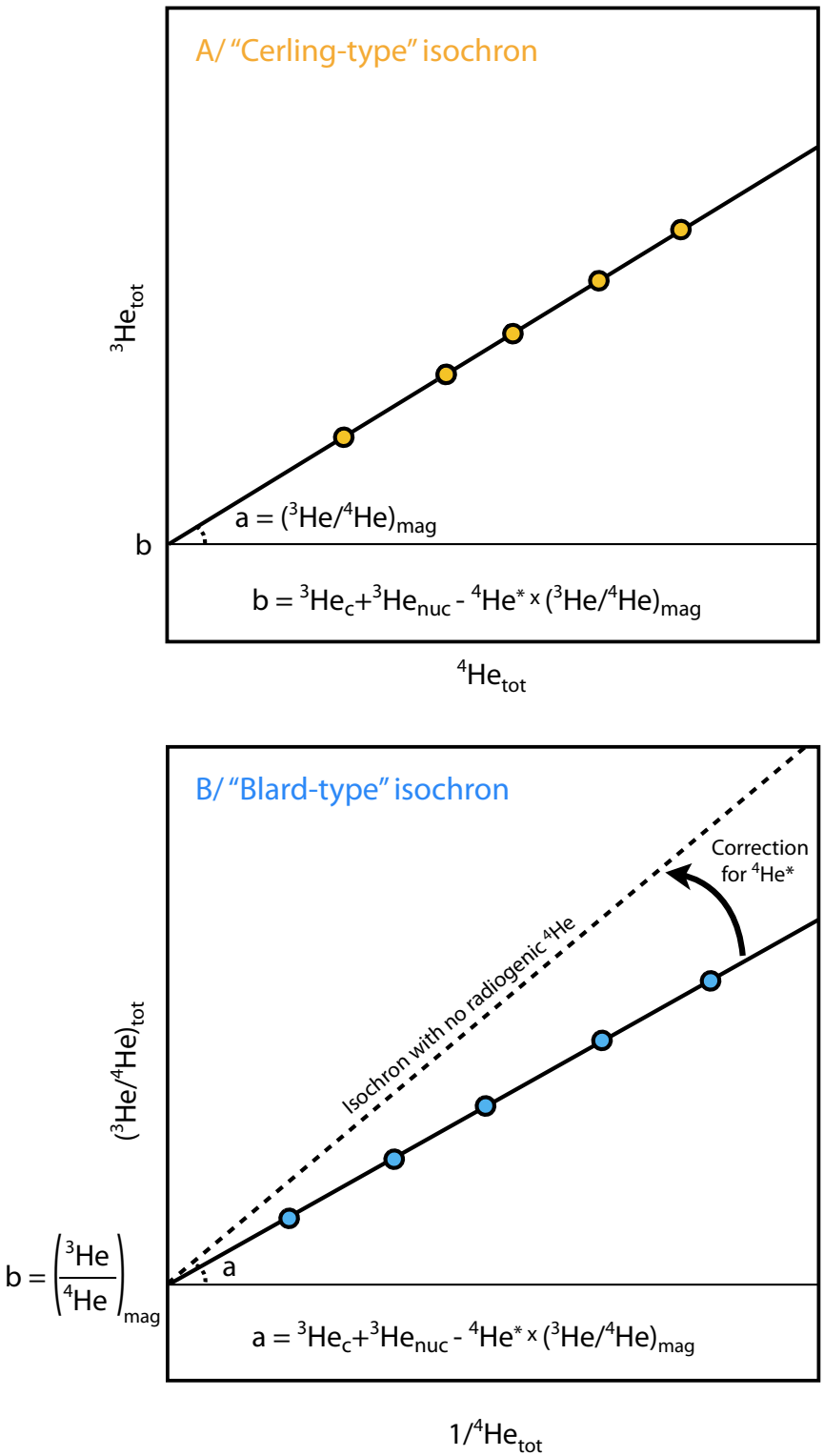

Figure 10. (A) Cerling-type (Cerling 1990) and (B) Blard-type (Blard and Pik 2008) cosmogenic ^{3}He isochrons.

807 **3.5.3.2. ^{3}He/^{4}He vs. 1/^{4}He "Blard" isochrons (Blard and Pik 2008).** The general
808 "Blard-isochron" equation is:
809
810 $$\left(\frac{^3\mathrm{He}}{^4\mathrm{He}}\right)_{\mathrm{tot}} = \left[{}^3\mathrm{He}_{\mathrm{c}} + {}^3\mathrm{He}_{\mathrm{nuc}} - {}^4\mathrm{He}^* \times \left(\frac{^3\mathrm{He}}{^4\mathrm{He}}\right)_{\mathrm{mag}} \right] \times \frac{1}{^4\mathrm{He}_{\mathrm{tot}}} + \left(\frac{^3\mathrm{He}}{^4\mathrm{He}}\right)_{\mathrm{mag}} . \qquad (22)$$
811
812 Again, this corresponds to the equation of a line, but in this case the *y*-intercept is (^{3}He/^{4}He)$_{mag}$
813 and the slope is the sum of "magmatic-independent" components, including cosmogenic ^{3}He
814 (Fig. 10B). ^{3}He$_c$ can then be estimated after correcting for the nucleogenic ^{3}He and radiogenic
815 ^{4}He components as:
816
817 $$^3\mathrm{He}_{\mathrm{c}} = a + {}^4\mathrm{He}^* \times b - {}^3\mathrm{He}_{\mathrm{nuc}} . \qquad (23)$$
818
819 Using the R-factor in the specific case of uneroded lava flows, the radiogenic ^{4}He correction
820 may be simplified to:
821
822 $$^3\mathrm{He}_{\mathrm{c}} = \frac{a}{R} . \qquad (24)$$
823
824 Note that the mathematical regression of Blard-type iscochrons requires computing the
825 correlation factor ρ_{err} between the (^{3}He/^{4}He)$_{tot}$ and 1/^{4}He$_{tot}$ uncertainties:
826
827 $$\rho_{\mathrm{err}} = \frac{\sigma_4 / {}^4He}{\sqrt{\left(\sigma_3 / {}^3He\right)^2 + \left(\sigma_4 / {}^4He\right)^2}} . \qquad (25)$$
828
829 To achieve the best isochron regression, statistical parameters (MSWD, York, 1966)
830 should be calculated using modern numerical tools, such as the online version of IsoplotR
831 (http://isoplotr.es.ucl.ac.uk/; Vermeesch, 2018). Although, in its current version, IsoplotR does
832 not include a specific tool for computing cosmogenic ^{3}He, this is easily done using the generic
833 functions of "other *x vs y* regressions" in this online software.
834
835
836
837

3.5.4. Samples with large amounts of radiogenic $^4He^*$ ($^4He^* >> ^4He_{mag}$)

In this case, the amount of ^4He extracted by fusion is similar to, and indistinguishable from, the radiogenic $^4He^*$ concentration within analytical uncertainties. In other words, the magmatic ^4He component is below the detection limit. This occurs for long closure ages (typically $>10^6$ yr) or in minerals with particularly high U-Th concentrations (>>10 ppm), such as zircons. In such a situation, using the total amount of ^4He extracted by fusion to estimate the concentrations of magmatic ^4He and ^3He is misleading, even when applying Equation (15). This may induce major uncertainties, and indeed potential inaccuracies, on the final cosmogenic ^3He concentrations (Fig. 6). However, it is not always straightforward to diagnose this extreme case, notably because, in practice, there exists a continuum between situations where $^4He^* \approx ^4He_{mag}$ and those where $^4He^* >> ^4He_{mag}$. If the closure age and the U-Th concentrations of the mineral of interest are well known, one can determine if $^4He^* >> ^4He_{mag}$ by calculating the amount of $^4He^*$ and comparing it with the total amount of ^4He extracted by fusion. Another way to pose this diagnostic is the impossibility of building isochrons: fused aliquots will present significant scatter in $^3He_{tot}$ vs. $^4He_{tot}$ space and will not align on a straight line, displaying errorchrons.

However it is established that $^4He^* >> ^4He_{mag}$, an alternative strategy must be employed to estimate the magmatic ^3He correction. The most efficient alternatives are:

1) Find and fuse a sample of the same lithology that has been shielded from cosmic rays to estimate the magmatic and nucleogenic ^3He components (e.g., Amidon et al., 2009). This assumes that the magmatic ^3He component is homogeneous.

2) Prolonged in vacuo crushing (10 min, 100 strokes) of an aliquot of the same sample that has been dated by cosmogenic ^3He. This allows the extraction of the majority of the magmatic ^3He, which can be used to perform the magmatic ^3He correction (Blard et al. 2009; Martin et al. 2018).

Note that these strategies may be sources of undetected inaccuracies, for example due to unrecognized magmatic or nucleogenic ^3He components. Thus, when it is determined that $^4He^* >> ^4He_{mag}$, it is key to minimize the contribution of magmatic helium by selecting samples in the 100–500 µm size fraction (Puchol et al. 2017; Williams et al. 2005) or use prescreening methods to select inclusion free minerals (Hofmann et al. 2021).

4. Analytical methods for measuring ^{3}He and ^{4}He in minerals

4.1. Extraction procedure

As detailed in section 2.1, different extraction techniques must be used to selectively release the different helium components: measuring magmatic helium requires crushing in vacuo, whereas the complete extraction of cosmogenic ^{3}He generally requires that minerals be completely melted, often using a high-vacuum, high-temperature furnace or a laser:

1) ***In-vacuo crushing.*** This method is suited to selectively releasing the magmatic component (Kurz, 1986a, 1986b). The several types and sizes of available crushers can accommodate different sample sizes with variable crushing efficiency (Blard et al., 2008; Scarsi, 2000). Typical crushers comprise ~50–100-g stainless steel cylinders that are moved in vacuo by external solenoids (Kurz 1986a; Yokochi et al. 2005). The associated ^{3}He and ^{4}He blanks of ~5×10^3 and 5×10^8 atoms per minute of crushing, respectively (Blard et al., 2008). Typical sample sizes are 0.5–1 g of solid materials; larger samples require a larger crusher to ensure crushing efficiency. If samples are too poor in magmatic helium to yield high signal/blank ratios, the isochron approach may be a useful alternative because it obviates the magmatic crushing step (e.g., Marchetti et al., 2020).
2) ***Heating furnace systems.*** High-temperature heating (>1300 °C, depending on the mineral) is necessary to extract the entire cosmogenic ^{3}He component present in samples, either by achieving total diffusion or melting. Double-vacuum resistance furnaces are ideal because they can be used to heat sample sizes ranging from 100 mg to 2 g (e.g., Amidon et al., 2009; Kurz, 1986b; Margerison et al., 2005). These apparatuses have typical ^{4}He blanks of 10^{-15}–10^{-14} mol when heating at 1500 °C for 15 minutes (see review by Zimmermann et al., 2018). For most analyzed concentrations, such amounts of phenocrysts (0.1–2 g) are necessary to ensure sufficiently high signal/blank ratios. Recently, Zimmermann et al. (2018) developed and patented a new all-metal single-vacuum furnace whose crucible is heated by induction (Fig. 11). Compared to classical double-vacuum resistance furnaces, this design ensures better blanks (^{4}He = $(8 \pm 3) \times 10^{-16}$ mol for 15 min at 1500 °C), faster heating and cooling rates (400 °C min^{-1}), improved robustness, lower functional costs, and, for models equipped with a thermocouple or thermal camera, improved temperature control.

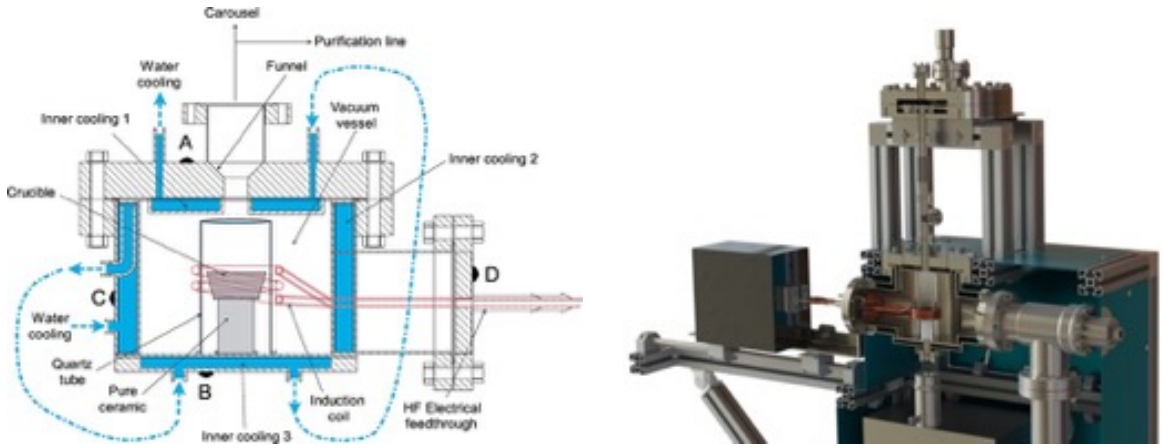

Figure 11. Newly patented all-metal single-vacuum induction furnace (Zimmermann et al. 2018) allowing 1-g samples to be heated to 2000 °C in less than 5 minutes. Photo credit: ©Cryoscan/CNRS/Satt-Sayens

3) ***Lasers.*** Depending on their wavelength, lasers may either be used for ablation or heating. Although this extraction system is best suited for ^{3}He-rich extraterrestrial materials (e.g., Megrue, 1971), the utility of lasers is limited for terrestrial cosmogenic ^{3}He. These extraction devices can only heat a maximum of 10 mg of material (less in the case of ablation), but have ^{4}He blanks on the order of 10^{-15}–10^{-14} mol, implying lower signal/blank ratios compared to furnaces (Zimmermann et al. 2018).

4.2. Mass spectrometry

Mass spectrometers operated in static mode remain the most precise, accurate, and sensitive instruments for measuring helium isotopes in solid minerals. Since the invention of Nier-type sources (Fig. 12; De Laeter and Kurz, 2006), the main improvements have been in the design, materials, and detector sensitivity. State-of-the-art analytical instruments for measuring ^{3}He and ^{4}He abundances are stainless steel mass spectrometers with Nier-type sources, such as the Noblesse AN37 or the ThermoFisher SFT ("Split Flight Tube"; Fig. 12). The geometry of the SFT flight tube is designed to minimize the analytical volume (1400 cc) while simultaneously collecting ^{4}He on a Faraday cup (with 10^{10}–10^{12} Ω amplifiers) and ^{3}He on an electron multiplier. Whereas mono-collection mass spectrometers require peak jumping, this bi-collection of helium isotopes improves analytical stability and speed. The resolution on the electron multiplier is 700, ensuring the complete separation of $^{3}He^{+}$ from the isobars HD^{+}

941 and HHH^+. Sensitivities of the Thermo SFT and the Noblesse AN37 are comparable, in the
942 range of 0.1-0.2 A/bar.
943

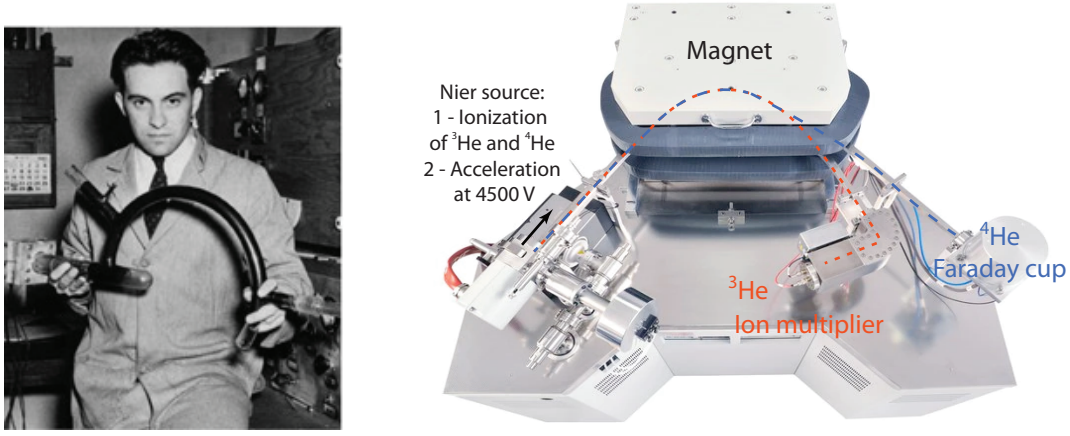

944
945 **Figure 12. (Left) A photograph taken in 1940 of Alfred O. C. Nier (1911–1994) showing the glass**
946 **mass spectrometer that he developed and which was used to measure ^{4}He (De Laeter and Kurz**
947 **2006). (Right) A modern all-metal ©ThermoFisher SFT spectrometer.**
948

949 The most promising recent development in noble gas mass spectrometry is the creation
950 of the compressed ion source, which can increase instrumental sensitivity for helium and neon
951 by one to two orders of magnitude (Baur 1999; Matsumoto et al. 2010). For now, however, this
952 advancement remains theoretical because, in practice, measurements are limited by the blank
953 levels of the extraction system and, more importantly, by the presence of non-cosmogenic
954 helium in samples. To fully exploit this progress in the sensitivity of noble gas mass
955 spectrometers, parallel analytical developments must focus on reducing blanks and selecting
956 minerals with the lowest possible non-cosmogenic ^{3}He concentrations.
957

958 **4.3. Interlaboratory comparisons**

959 To identify potential sources of systematic and random uncertainties, interlaboratory
960 comparisons performed by analyzing splits of the same standard material provide useful
961 insights (Blard et al. 2015; Vermeesch et al. 2015). Recently, six international laboratories
962 (GFZ, Potsdam; Caltech, Pasadena; CRPG, Nancy; SUERC, Glasgow; BGC, Berkeley; Lamont
963 Doherty Earth Observatory, New York) participated in an intercomparison experiment (Blard
964 et al. 2015), analyzing 5–22 aliquots of the CRONUS-P pyroxene standard, which is known to
965 be homogeneous (Schaefer et al. 2016). The interlaboratory dataset (totaling 66 determinations
966 from the six laboratories; Fig. 13) is characterized by a global weighted mean of (5.02 ± 0.06)

$\times 10^9$ at ^{3}He g^{-1} with an overdispersion of 2.8% (at 1σ). ^{4}He is characterized by a larger variability than ^{3}He, with a global weighted mean of $(3.60 \pm 0.09) \times 10^{13}$ at ^{4}He g^{-1} (1σ) with an overdispersion of 5.2% (1σ; Blard et al., 2015). This probably reflects systematic differences between the six laboratories, since the interlaboratory over-dispersion is, by definition, larger than the analytical uncertainties. To further evaluate this and homogenize datasets, thereby improving the accuracy of cosmogenic ^{3}He dating, all future studies presenting cosmogenic ^{3}He results should also report the ^{3}He concentration measured in the CRONUS-P material under the same analytical conditions.

Potential sources of systematic uncertainties that may explain these previously overlooked interlaboratory offsets are discussed in the next subsection.

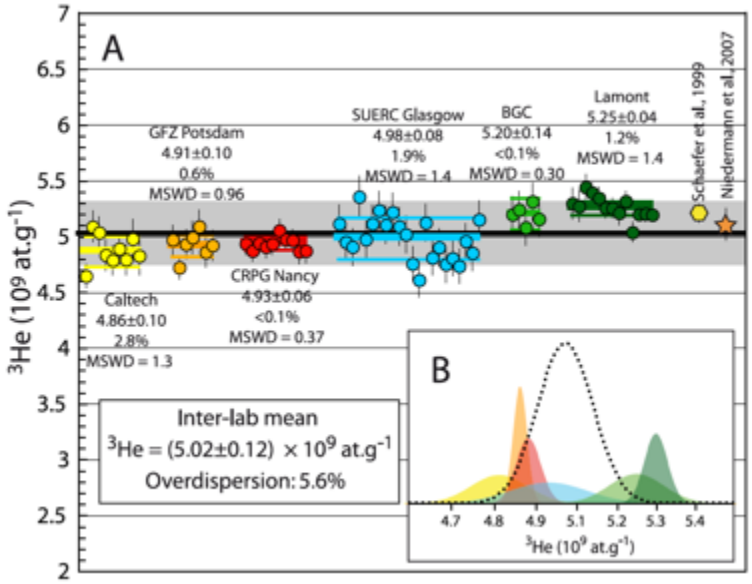

Figure 13. Interlaboratory comparison of ^{3}He concentrations measured in the CRONUS-P pyroxene standard (Blard et al. 2015). Plotted individual analytical uncertainties are at 1σ. For each lab are also given the weighted mean (2σ), the standard error of the mean (2σ), the intra-lab overdispersion and MSWD. The standard error of the global weighted mean and the inter-lab overdispersion are given at 2σ. Overdispersion describes the interlaboratory variance that is not included in the analytical uncertainties.

4.4. Potential sources of systematic uncertainties in ^{3}He and ^{4}He measurements

Various analytical issues may contribute to the systematic differences in the ^{3}He and ^{4}He concentrations measured in different laboratories. Indeed, the measurement of helium isotopic abundances may be subject to potentially overlooked biases. Nonetheless, as some such biases have been recognized in some laboratories, discussing them openly and suggesting possible control benchmarks is a first step toward improving analytical precision and accuracy.

Estimate of the initial pressure in gas standard tanks. Nearly all laboratories use a gas standard as a primary reference to calibrate the sensitivities of their mass spectrometers. For this, it is vital to properly estimate the initial helium pressure (i.e., the number of ^{3}He and ^{4}He atoms) in the gas tank. This determination must be as accurate as possible, but depends on the non-linear behavior of capacitance manometers or the use of poorly calibrated volumes during dilution of the calibration gas in the reservoir. When a new gas standard is prepared, a useful experiment is to cross-check the measured initial pressure against a measurement of a solid standard material, such as CRONUS-P.

Tank depletion after several standard iterations. For daily calibration procedures, laboratories generally extract a small aliquot (<1 cc) from a large bottle of the gas standard (typically 2 L). Although the aliquot/standard reservoir ratio is small ($\sim 10^{-4}$), it is essential to know the volumes of both the aliquot and the standard bottle to correctly calculate the amount of standard gas remaining in the bottle over time. See Fleck and Calvert (2014) for a complete discussion of the most accurate depletion equation. Modern automated extraction systems can use $>10^{3}$ standard aliquots per year; hence, a small initial bias on the aliquot/bottle volume ratio may be significantly amplified over several years of standard use. Thus, even if the gas standard remains the most convenient for daily calibrations, regularly cross-checking against a solid standard material is again a useful and important control routine.

Volumetric calibration of the extraction and purification line. Since pressure may reach high values ($>10^{-5}$ mbar) in furnaces operating at >1000 °C, it is often necessary to split the extracted gas to remove the gas fraction in the "dirty" part of the purification line. Depending on the line configuration, this may imply that dilution routines differ between samples and gas standards. Correcting for this dilution requires precise and accurate knowledge of the volumes involved. Extraction line volumes are generally determined with capacitance manometers at pressures between a few millibars and 1 bar. This measurement may be biased by adsorption onto the internal surfaces and thus overestimate the true volume. It is therefore particularly complicated to estimate volumes in which chemical and physical traps are present. Hence, when possible, splitting and dilution should be avoided or limited to a small fraction of the gas to reduce potential inaccuracies. Ideally, cryofocusing is useful for avoiding this issue and applying the same dilution to samples and standards.

Overly efficient and unknown He cryotrapping in the presence of heavier noble (Ne) or other gases. In most laboratories, helium is cryofocused in a cryopump sorber head that is cooled to <10 K before being released into the last part of the line at 35 K, the empirically established vacuum-release temperature for helium in most cryopump systems. This cryotrapping step is useful because it optimizes He purification and separation from other noble gases. Because the cryopump is generally placed in the ultimate section of the purification line, cryofocusing also maximizes the gas pressure before the inlet to the mass spectrometer, improving the sensitivity of the entire analytical system. At the CRPG, we tested the impact of the release temperature by measuring the helium signal obtained at various temperatures between 35 and 100 K (unpublished data): when analyzing pure helium gas, 35 K is sufficient to release 100% of the helium that was previously trapped on the cryopump sorber head. However, when analyzing helium extracted from silicates, 5% of the total helium remained trapped at 35 K, and heating to 70 K was necessary to release the totality of the sample helium. Hence, it is possible that the release temperature of helium from the cryopump sorbing step depends on the He/Ne ratio, or to the presence of other gases that were not removed in the upstream part of the purification line. These observations are not sufficient to define a clear relationship between the helium trapping and release temperatures and the ratio of He to other gases, and more attention should be given to this issue. New experimental data with variable He/(other gas) ratios would be useful for improving the accuracy of He isotopic measurements.

Pressure effects on the linearity of mass spectrometer sensitivity. Empirical observations have shown that the amount of helium present in the mass spectrometer may modify instrumental sensitivity when measuring ^{3}He and ^{4}He (Fig. 14; Burnard and Farley, 2000; Mabry et al., 2013; Sano et al., 2008). This effect is more pronounced at low helium pressures ($<10^{-9}$ mbar) and may reach 20% in the worse situations (Sano et al., 2008; Zimmermann and Bekaert 2020). The mechanisms producing this pressure dependence are not well constrained, but such instrumental fractionation could occur in a Nier-type source due to a space-charge effect on the ionization efficiency (Burnard and Farley 2000). Other possible mechanisms might involve the flight tube or the detectors (Sano et al., 2008). Importantly, this pressure effect varies significantly from one mass spectrometer to another (Sano et al., 2008) and is sensitive to the source settings, notably the trap current (Burnard and Farley, 2000; Mabry et al., 2013).

To minimize the potential bias arising from this pressure effect, source settings should be optimized to define the largest possible zone of stability (Fig. 14). Lower trap currents (50–

200 μA) minimize this non-linearity. If it is not possible to suppress this instrumental fractionation, it is important to analyze similar amounts of gas standard and sample. Because the presence of other gases may also affect this instrumental bias (see above), it may be useful to ensure that samples and standards are of similar helium purity, notably He/Ne ratios. Since this procedure often requires splitting gas standards, the volume of the preparation line must be accurately calibrated. Alternatively, this issue could be overcome by using He-poor gas standards: if a single pipette delivers a low-pressure helium signal in the range 10^{-11}–10^{-10} mbar, the dilution step will be unnecessary.

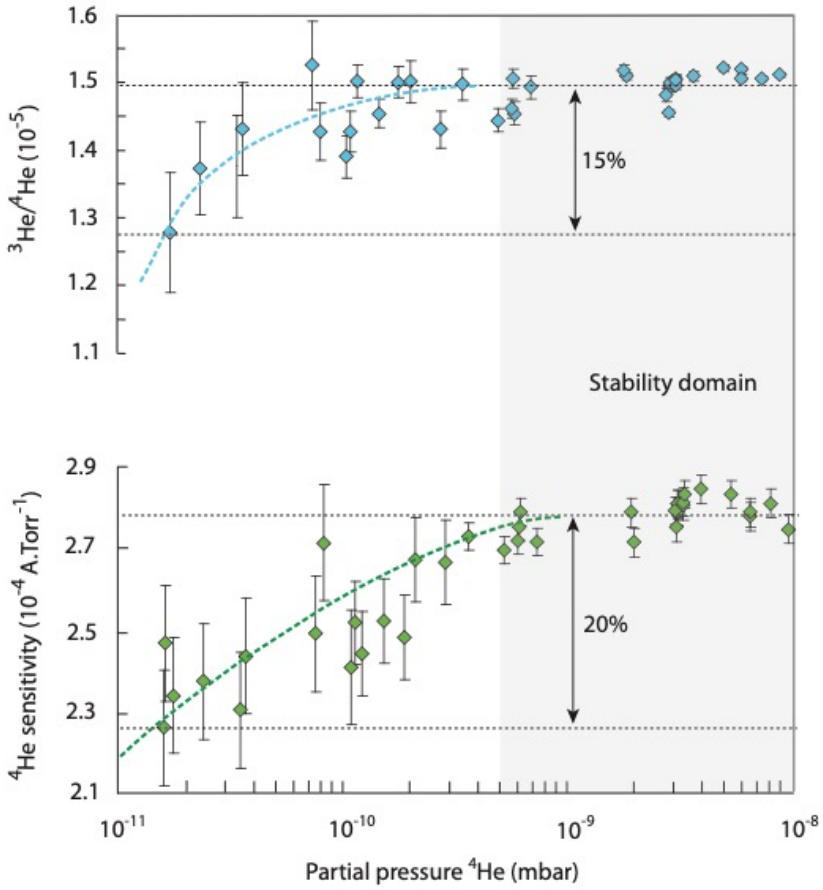

Figure 14. (Top) Measured $^3He/^4He$ ratios and (bottom) instrumental sensitivity (A Torr^{-1}) as a function of the true helium pressure in the mass spectrometer. These data were obtained for a VG5400 with a source-trap current of 400 μA (Zimmermann and Bekaert 2020); this effect is less pronounced on the Helix SFT (Sano et al. 2008). Note that source settings may affect this relationship because lower trap currents (<300 μA) reduce the impact of helium pressure on instrumental sensitivity.

Variations of the absolute $^3He/^4He$ atmospheric ratio. Many gas standards are prepared using atmospheric helium that is artificially enriched in ^3He. Other standards are natural magmatic gases with $^3He/^4He$ ratios greater than that of the atmosphere. In either case, standards must be cross-calibrated against a gas of known composition to determine their absolute He contents and $^3He/^4He$ ratios. This is often performed against atmospheric helium, because the $^3He/^4He$ ratio in this reservoir is spatially homogeneous with a variability lower than 2‰ (95% confidence interval; Boucher et al., 2018). However, for absolute determinations of ^3He, it is vital to know with accuracy the absolute value of the atmospheric $^3He/^4He$ ratio. The few studies that have attempted to measure the absolute $^3He/^4He$ ratio in air (Clarke et al. 1976; Hoffman and Nier 1993; Lupton and Graham 1991; Mamyrin et al. 1970) yield a weighted average of $(1.386 \pm 0.010) \times 10^{-6}$ (2σ; Boucher et al., 2018). However, a few studies have reported values beyond this range; notably, Sano et al. (2008) analyzed air collected in the center of Tokyo (Japan) and obtained a ratio of 1.34×10^{-6}, ~3.5% lower than the world average, suggestive of a potential ^4He enrichment by a local anthropogenic source. Moreover, temporal variations of the atmospheric $^3He/^4He$ ratio are possible (Sano et al. 2010), but this effect is probably smaller than 1% in the Northern Hemisphere over the past 40 years (Mabry et al. 2015).

All these sources of systematic uncertainties may accumulate, leading in the worst cases to under-/over-estimates and interlaboratory discrepancies larger than 5%. To reduce these potential inaccuracies and improve interlaboratory comparisons, it is highly recommended that future studies analyze solid standard materials such as the CRONUS-P pyroxene (Schaefer et al. 2016) and report the measured ^3He and ^4He concentrations (Blard et al. 2015).

5. Discussion: ^{3}He cosmogenic production rates, the accuracy of spatial scaling, cross-calibration with other cosmogenic nuclides, online calculators and new frontiers

5.1. Production rates

Knowing cosmogenic ^{3}He production rates accurately and precisely is important because this parameter is involved in all applications of cosmogenic ^{3}He, notably in calculating surface exposure ages. Production rates are spatially variable (Gosse and Phillips 2001; Lal 1991; Lal and Peters 1967) because the Earth's magnetic field controls the flux and repartition of incoming primary charged cosmic particles (Dunai 2001; Lal 1991; Lal and Peters 1967), and because atmospheric shielding results in elevation-dependent production rates (Hess 1912; Lal 1991; Lal and Peters 1967; Pacini et al. 1911; Stone 2000). Hence, scaling models are necessary to calculate the production rate at a given sampling location by accounting for spatial characteristics (altitude, latitude, longitude) and exposure duration. Such scaling models were initially established from empirical relationships linking production rate to latitude, longitude, and altitude based on physical observations of the reactions triggered by cosmic particles (Balco et al. 2008). Recent scaling models based on ab-initio physical modeling efficiently describe the spatial variability of production rates (Argento et al. 2013; Lifton et al. 2014). However, geological calibration sites for cosmogenic nuclide production rates are necessary to check and refine these models (Borchers et al. 2016; Martin et al. 2017). A production rate calibration site is a continuously exposed geomorphological surface that has gone uneroded since its emplacement at the surface, and whose exposure age can be determined independently (e.g., by ^{14}C, K-Ar, or luminescence dating). If a scaling model is accurate, all calibration sites should yield the same normalized production rate, within uncertainties, after the dataset is scaled to sea level and high latitude (>60°; SLHL).

5.2. The global $^{3}He_{c}$ production rate calibration database

Figure 15A shows the locations of the 24 production rate calibration sites available in the literature (Ackert et al., 2003; Amidon and Farley, 2011; Blard et al., 2013; Blard et al., 2006b; Borchers et al., 2016; Cerling and Craig, 1994; Delunel et al., 2016; Dunai and Wijbrans, 2000; Eaves et al., 2016; Fenton et al., 2019; Foeken et al., 2012; Goehring et al., 2010; Licciardi et al., 2006, 1999). The SLHL ^{3}He production rates presented in Figure 15B–E were computed from this empirical dataset using the CREp calculator (https://crep.otelo.univ-lorraine.fr/#/).Whereas the compilation of Borchers et al. (2016) only considers a limited sub-dataset, this up-to-date synthesis integrates all published raw calibration data from the 24

calibration sites, which are available in the ICE-D online database (http://calibration.ice-d.org/). This new dataset also ensures that all $^{3}He_{c}$ concentrations are corrected for radiogenic ^{4}He, which amounts to a 1–5% correction at a few sites (Blard and Farley 2008). SLHL and time corrections were performed here with the Lifton-Sato-Dunai (LSD) scaling scheme (Lifton et al. 2014), the ERA-40 atmospheric model, and the Virtual Dipole Moment (VDM) dataset, derived from atmospheric ^{10}Be (Muscheler et al. 2005). This analysis shows that there is no clear correlation between SLHL P_3 and the latitudes, altitudes, or exposure durations of these calibration surfaces, suggesting that this time-dependent scaling model is accurate for the majority of the calibrated production rates (Balco et al. 2008). This dataset defines a worldwide average weighted mean of 124 ± 11 at g^{-1} yr^{-1} with MSWD = 5 (Fig. 15B). For comparison, the Lal-Stone time-dependent scheme (Balco et al. 2008) yields a larger dispersion (MSWD = 7), suggesting that the LSD model performs slightly better, at least for ^{3}He (Borchers et al. 2016; Martin et al. 2017). When plotted against exposure duration, SLHL P_3 values scaled with the Lal-Stone model present a slight negative correlation (i.e., lower P_3 values for longer exposure times >100 ka); this is not the case with the LSD scaling.

Tests of the different atmospheric models have shown that the spatially distributed ERA-40 atmospheric grid (Uppala et al. 2005) performs better than the standard atmosphere model (Stone 2000) in reducing the scatter on SLHL P_3 (Martin et al. 2017). Similarly, the VDM database (Muscheler et al. 2005) yields the lowest dispersion (Martin et al. 2017). However, local inaccuracies persist and require further investigation and additional data and calibration sites: 4 of the 24 calibration sites yield SLHL P_3 values beyond 2σ from the weighted mean. For example, in Western Africa, a calibration site on Fogo Island (Cabo Verde) yielded a SLHL P_3 value that is particularly low, 2σ below the weighted average (Foeken et al. 2012). Future calibration studies in these regions will indicate whether this outlier is due to an improper independent K-Ar date or unrecognized erosion, or whether it results from an as yet unrecognized local anomaly such as high atmospheric pressure or a specific magnetic field anomaly (Lifton et al. 2014). In contrast, the Hawaiian calibration site yields a SLHL P_3 more than 2σ above the global average, suggesting either inaccuracy in the independent dating or in the atmospheric or temporal correction.

To reduce potential inaccuracies in the spatial scaling, local calibration sites should generally be favored over the use of a global average, particularly in low-latitude, high-altitude sites such as the Tropical Andes, where two consistent calibration sites are present (Blard et al., 2013; Delunel et al., 2016). In the High Tropics, the altitude and magnetic field corrections are

extreme, and the use of a global averaged production rate there may yield large discrepancies between the different scaling schemes. However, many regions do not have any ^{3}He calibration sites (Fig. 15A), hindering the use of a local calibration to compute exposure ages. Future calibration studies could focus on Eurasia, Oceania, Africa, Central America, Greenland, and Antarctica, where calibration sites are scarce or absent. High-elevation, high-latitude calibration sites are also scarce.

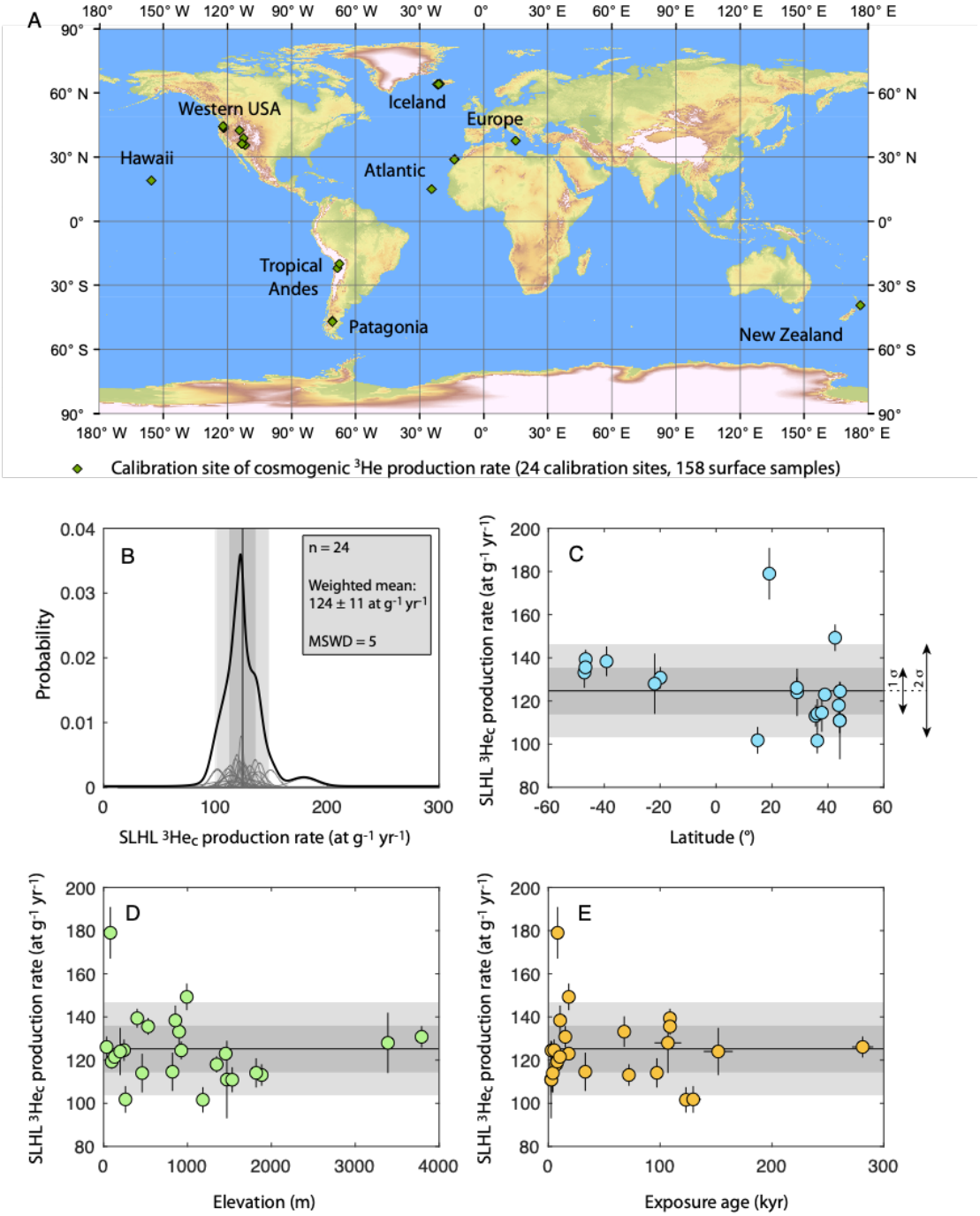

Figure 15. (A) Calibration sites for cosmogenic ^{3}He production rates available in the ICE-D calibration database (24 calibration sites, 158 surface samples). (B) The distribution of production rates and (C–E) production rate variations with latitude, elevation, and exposure age, respectively, were computed and plotted using the online CREp calculator (https://crep.otelo.univ-lorraine.fr/). SLHL and time corrections were performed here with the LSD scaling scheme (Lifton, Sato, and Dunai 2014) using the ERA-40 atmospheric model and the VDM dataset derived from atmospheric ^{10}Be (Muscheler et al. 2005). Source articles of the ^{3}He calibration site dataset: (Ackert et al., 2003; Amidon and Farley, 2011; Blard et al., 2013; Blard et al., 2006b; Borchers et al., 2016; Cerling and Craig, 1994; Delunel et al., 2016; Dunai and Wijbrans, 2000; Eaves et al., 2016; Fenton et al., 2019; Foeken et al., 2012; Goehring et al., 2010; Licciardi et al., 2006, 1999).

5.3. Online calculators

Three main calculators are available online to compute ^{3}He exposure ages from ^{3}He data: (i) the CRONUS calculator (http://cronus.cosmogenicnuclides.rocks/2.1/; Marrero et al., 2016), (ii) the BGC-WU calculator, formerly the initial CRONUS calculator (https://hess.ess.washington.edu/; Balco et al., 2008) and (iii) the CREp calculator (https://crep.otelo.univ-lorraine.fr/#/; Martin et al., 2017).

Each calculator requires particular characteristics (spatial position, thickness, topographic mask) as inputs to compute production rates specific to the collected samples. This scaling is performed using the most accurate available models, i.e., the Lal-Stone time-dependent model (Balco et al. 2008) and/or the LSD model (Lifton et al., 2014). Note that, in each calculator, the input cosmogenic ^{3}He concentration data must already be corrected for other ^{3}He sources.

The CRONUS calculator uses a unique and non-modifiable $^{3}He_{c}$ production rate and VDM correction. In contrast, the CREp and BGC-WU calculators allow users to choose from among several production rates: world average, regional mean, and local production rates. In CREp, these production rates can easily be selected from a clickable map. Moreover, CREp connects to the ICE-D calibration database daily, which is regularly updated to incorporate the newest literature data. The CREp and BGC-WU calculators also offer the possibility of using different atmopsheric models and geomagnetic databases.

5.4. Production of cosmogenic ^{3}He by muons

Numerical modeling based on experimental cross sections suggests that both fast muons and negative-muon capture reactions may produce cosmogenic ^{3}He (Lal 1987; Nesterenok and Yakubovich 2016). However, geological evidence of such reactions has been scarce, which has

precluded the precise calibration of the muogenic production of ^{3}He (M. D. Kurz 1986a; Shuster et al. 2012). Larsen et al. (2021) recently presented a vertical profile of ^{3}He concentrations measured in pyroxenes and ilmenites along a 300-m-long drill core in the Columbia River basalts, which were emplaced by successive massive eruptions 16 Ma (Kasbohm and Schoene 2018). After correcting for non-cosmogenic ^{3}He components, this dataset displays a clear attenuation profile that precisely defines the muogenic production of ^{3}He: assuming a single exponential attenuation model (Braucher et al. 2011), the surficial SLHL muogenic ^{3}He production rate is 0.3 ± 0.1 at g^{-1} yr^{-1} and the attenuation length is 8,780 g cm^{-2} (Fig. 16; Larsen et al., 2021). Hence, in a massif having an average density of 2.7 g cm^{-3}, the muogenic production rate decreases by an exponential factor each 30 m.

At Earth's surface, the contribution of this muogenic component represents only 3‰ of the spallogenic ^{3}He production (Martin et al. 2017), which can be safely neglected when determining cosmogenic ^{3}He exposure ages. However, these production parameters imply that muogenic ^{3}He becomes dominant at depths >5 m and may represent 10^{5}–10^{6} at g^{-1} in the case of exposures longer than 1 Myr. The attenuation length of muogenic ^{3}He is much longer than that of ^{10}Be (Braucher et al. 2011), which complicates finding cosmogenically shielded samples. Shielded samples are useful for determining the non-cosmogenic ^{3}He correction for surficial samples (e.g., Amidon and Farley, 2011), analyzing the pristine $^{3}He/^{4}He$ magmatic component (Dodson et al., 1997), and ensuring the preservation of paleo-exposure signals and computing accurate burial ages (Blard et al. 2006). Given the muogenic ^{3}He production parameters obtained by Larsen et al. (2021), several tens of meters of shielding are required to ensure the absence of cosmogenic ^{3}He for these applications.

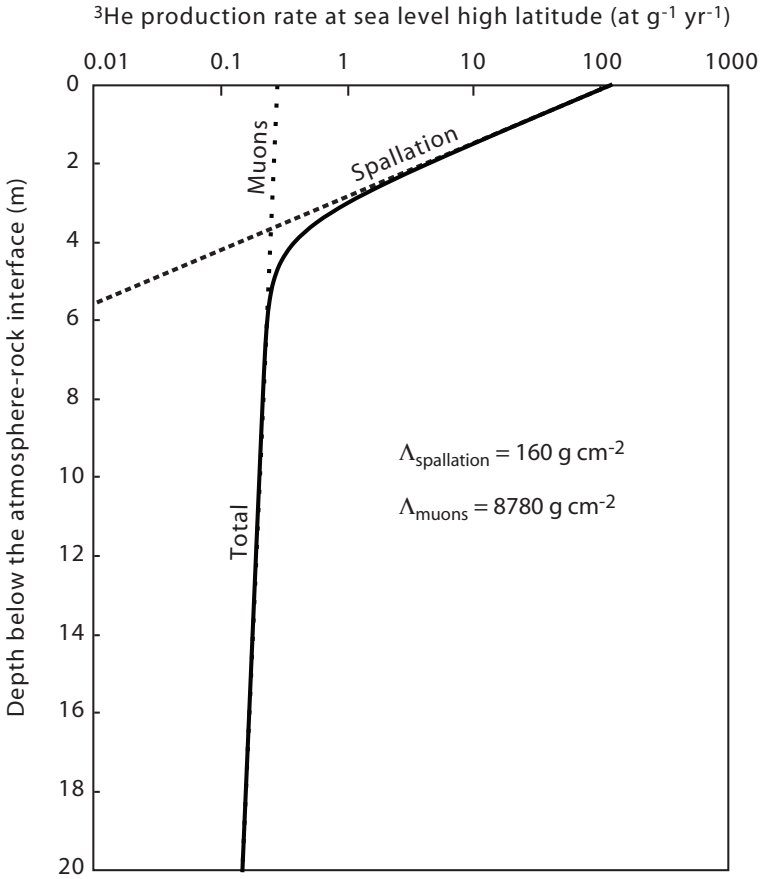

Figure 16. Vertical attenuation of spallogenic and muogenic ^{3}He production rates below the atmosphere-rock interface at SLHL. This model assumes surficial spallogenic and muogenic ^{3}He production rates of 124 at g^{-1} yr^{-1} (Martin et al. 2017) and 0.3 at g^{-1} yr^{-1} (Larsen et al. 2021), respectively, with respective attenuation lengths of 160 g cm^{-2} (Gosse and Phillips 2001) and 8,780 g cm^{-2} (Larsen et al. 2021). In this calculation, rock density is assumed to be 2.7 g cm^{-3}.

These muogenic production parameters affect the calculation of denudation rates from cosmogenic ^{3}He measurements in basin-wide eroded sediments (e.g., Ferrier et al., 2013; Puchol et al., 2017). Because ^{3}He is not radioactive, all muogenic ^{3}He nuclides produced at depth will be preserved until they reach the rock surface. Therefore, muon parameters must be included in the equation used to compute the denudation rate (ε) from cosmogenic ^{3}He concentrations:

$$\varepsilon = \frac{\Lambda_n \bar{P}_n + \Lambda_\mu \bar{P}_\mu}{\rho\ {}^3\mathrm{He}_c}, \qquad (26)$$

where $\bar{P}_n$ and $\bar{P}_\mu$ are the basin-averaged spallogenic and muogenic production rates (at g^{-1} yr^{-1}), respectively, Λ_n and Λ_μ are their respective attenuation lengths (g cm^{-2}; Charreau et al., 2019), and ρ is density of the rock (g cm^{-3}).

Previous articles by Ferrier et al. (2013), Litty et al. (2021), and Puchol et al. (2017) calculated denudation rates considering only the spallation parameters. Ideally, these published denudation rates should thus be recomputed with Equation (26), employing the new, well-defined muogenic parameters of Larsen et al. (2021). This revision would increase denudation rates by 5% for basins at an average elevation of 2,000 m, whereas denudation rates at sea level, where the contribution of muogenic production is the largest, would increase by 13%. In the case of ^{10}Be in quartz, incorporating muogenic production may increase calculated denudation rates by 20% at sea level (Lupker et al. 2012).

5.5. Cross-calibration of ^{3}He against ^{10}Be and other cosmogenic nuclides

The most commonly used empirical scaling models that were published in the 1990's and 2000's (Dunai and Wijbrans 2000; Lal 1991; Stone 2000) consider the impact of elevation to be similar for all cosmogenic nuclides, including ^{3}He and ^{10}Be. However, ab-initio physical models have recently revisited the use of different spatial scaling factors for each nuclide (Argento et al. 2013; Lifton et al. 2014), after D. Lal initially proposed the idea in his PhD thesis (Lal 1958). These models predict that the ^{3}He/^{10}Be production ratio increases with increasing elevation, with the computed production of ^{3}He exceeding that of ^{10}Be by 4% at 3,000 m elevation and up to 7% at 5,000 m (Fig. 17). Empirical benchmarks are necessary to test the validity of these theoretical models and better constrain the spatial variations of each nuclide's production rate. This can be done by measuring the ^{3}He/^{10}Be production ratios in rocks that have recently been exposed at the surface: if the possibility of an inherited cosmogenic ^{3}He component produced during an earlier exposure episode can be discarded, such cross-calibrations are key because they integrate the same exposure history for both nuclides. Only a handful of studies have produced such cross-calibration data: three articles reported cosmogenic ^{3}He concentrations in pyroxenes and ^{10}Be concentrations in coexisting quartz (Amidon et al., 2009; Blard et al., 2013; Luna et al., 2018), three others documented ^{3}He in accessory minerals (apatites, zircons, kyanites, garnets, iron oxides) and ^{10}Be in coexisting quartz (Amidon et al. 2008; Gayer et al. 2004; Kober et al. 2007), and another few articles reported cosmogenic ^{3}He concentrations in olivines/pyroxenes and ^{10}Be in coexisting feldspars (Blard et al., 2013; Zerathe et al., 2017) or olivines/pyroxenes (Blard et al., 2008;

Nishiizumi et al., 1990). For this review, I updated and homogenized these $^{3}He/^{10}Be$ cross-calibration datasets by recalculating the $^{3}He/^{10}Be$ production ratios ($R_{3/10}$) using Equation (3) in Blard et al. (2013); the updated data are available in Table S3 and are plotted in Figures 17–19. Note that all ^{3}He concentrations in this dataset were corrected for both magmatic and nucleogenic ^{3}He, and thus include all cosmogenic production pathways: spallation, thermal neutron capture, and muogenic production. In the following, I use this updated dataset to test correlations and review potential causes of the spatial and rock-specific variabilities of the $^{3}He/^{10}Be$ production ratio.

The cross-calibration studies based on cosmogenic ^{3}He in pyroxenes and ^{10}Be in coexisting quartz (Amidon et al., 2009; Blard et al., 2013; Luna et al., 2018) provide important observations (Fig. 17A). This nuclide-mineral pair is among the most commonly used, and its absolute production rates are the best documented (http://calibration.ice-d.org). Using this dataset, the CREp calculator (Martin et al., 2017), and the Lal-Stone time-dependent scaling (Balco et al. 2008) provides a theoretical SLHL $R_{3/10}$ value of 30.1 ± 3.1 (Fig. 17). Then, comparing ^{3}He in pyroxene-^{10}Be in quartz cross-calibrations measured at 1,333, 4,530, and 4,827 m elevation indicates a slight impact of elevation on the measured $R_{3/10}$ value (Fig. 17A). These data are in agreement, within 1σ uncertainties, with the theoretical models of Argento et al. (2013) and Lifton et al. (2014) that predict a 7–8% increase of $R_{3/10}$ at 5,000 m compared to the sea-level value. Although this observation supports the use of nuclide-specific scaling, further new cross-calibration and absolute calibration datasets at variable elevations and latitudes will be useful for confirming and refining this relationship. I stress that the use of classical, non-nuclide-specific scaling factors, such as the Lal-Stone (Balco et al. 2008) or LSD scaling (Lifton et al. 2014), do not yield inaccuracies if using locally calibrated production rates, i.e., from calibration sites at similar elevations as the dated objects (Blard et al., 2013; Kelly et al., 2015; Martin et al., 2015).

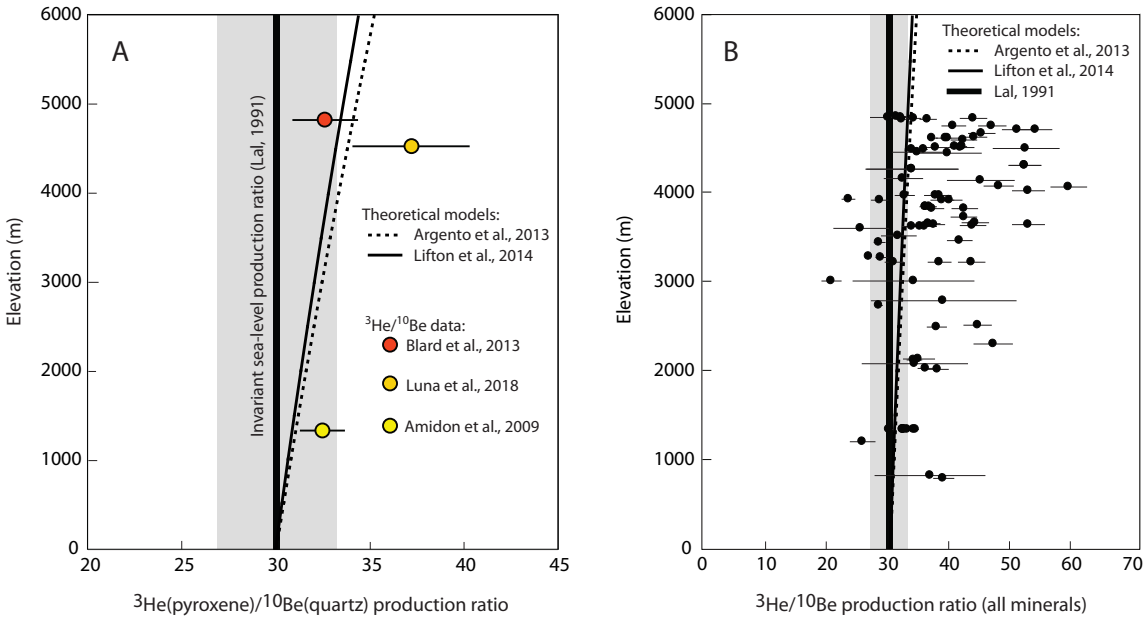

Figure 17. Comparison of modeled (Argento et al., 2013; Lifton et al., 2014; Lal, 1991) and observed $^{3}He/^{10}Be$ production ratios vs. elevation. Cross-calibrations are from (A) ^{3}He in pyroxenes and ^{10}Be in quartz (Amidon et al., 2009; Blard et al., 2013; Luna et al., 2018) and (B) $^{3}He/^{10}Be$ in any mineral pair (Amidon et al., 2008, 2009; Blard et al., 2008, 2013; Gayer et al., 2004; Kober et al., 2007; Luna et al., 2018; Nishiizumi et al., 1990; Zerathe et al., 2017). The vertical line shows the $^{3}He/^{10}Be$ production ratio at SLHL calculated using ^{3}He in pyroxene-^{10}Be in quartz data (http://calibration.ice-d.org), the CREp calculator (https://crep.otelo.univ-lorraine.fr/#/; Martin et al., 2017), and the Lal-Stone time-dependent scaling (Balco et al. 2008); the gray shaded bar indicates 1σ uncertainty.

However, considering the entire $^{3}He/^{10}Be$ cross-calibration dataset, reported $R_{3/10}$ values deviate markedly from SLHL production ratio, and even from the theoretical production modeleds of Argento et al. (2013) and Lifton et al. (2014). These high $R_{3/10}$ values reach ~50 above 4,000 m, which is mainly explained by the fact that the cross-calibration data are based on ^{3}He concentrations measured in accessory minerals (garnet, apatite, zircon; Amidon et al., 2008; Gayer et al., 2004). By determining the ^{3}He in garnet/^{10}Be in quartz production ratio from Himalayan glacial rocks at 3,000–4,500 m elevation, Gayer et al. (2004) identified the overproduction of cosmogenic ^{3}He compared to the standard scaling model that assumes an elevation-independent $^{3}He/^{10}Be$ production ratio (Fig. 17; Lal, 1991). Dunai et al. (2007) attributed this high-elevation ^{3}He production excess to the unrecognized impact of cosmogenic thermal neutrons through the $^{6}Li(n,\alpha)^{3}H$ reaction. According to Dunai et al. (2007), this reaction could account for a 50% increase of cosmogenic ^{3}He production in the Li-rich garnets (20–100 ppm Li) analyzed by Gayer et al. (2004). However, Amidon et al. (2008) later reported

^{3}He and ^{10}Be cross-calibration data on Li-poor (<10 ppm) minerals (zircons, kyanites) from the high Himalayas, which yielded ^{3}He/^{10}Be production ratios in the same range as those determined in garnet by Gayer et al. (2004) (Fig. 17). This empirical evidence indicates that Li is not the main driver of this "anomalously" high cosmogenic ^{3}He production rate. Furthermore, when ^{3}He/^{10}Be cross-calibration data across all mineral pairs (n = 88) are plotted against Li concentration (Fig. 18), no correlation is observed (R^2 = 0.19, n = 78). Hence, other mechanisms are required to explain the high $R_{3/10}$ values above 3,000 m. Interestingly, the highest anomalous ^{3}He production rates are reported for metamorphic or plutonic lithologies (Gayer et al., 2004; Amidon et al., 2008), whereas materials from recent (<10 Ma) volcanic terrains yield much lower ^{3}He/^{10}Be production ratios (Amidon et al., 2009; Blard et al., 2013; Luna et al., 2018).

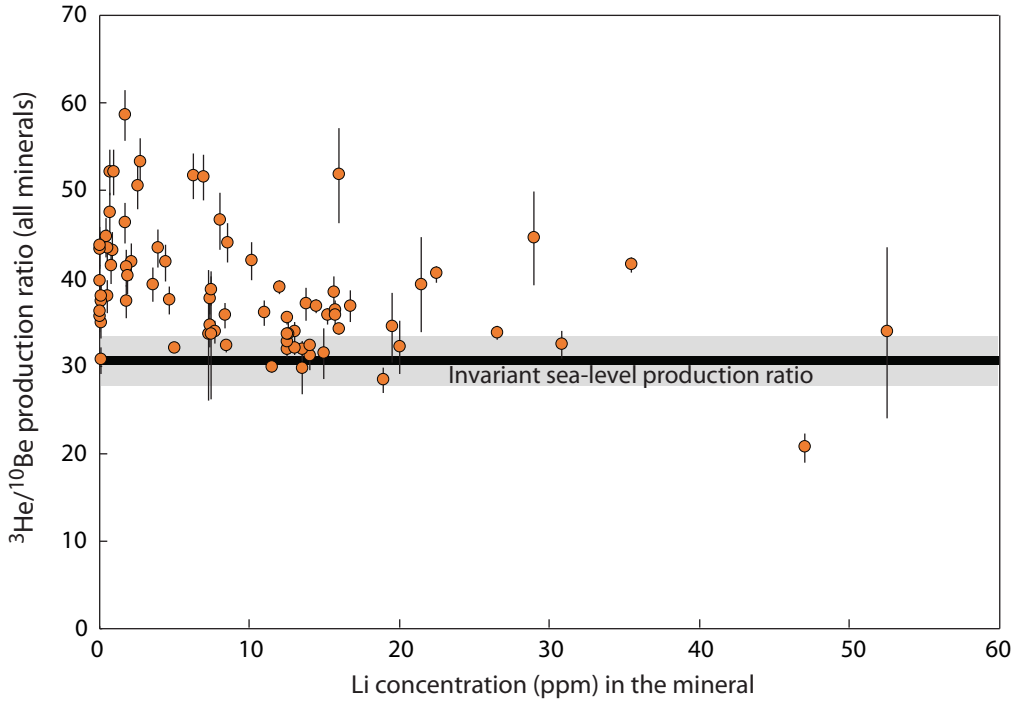

Figure 18. ^{3}He/^{10}Be production ratio plotted against Li concentration (ppm) in the cosmogenic ^{3}He-hosting mineral (data sources: Amidon et al., 2008, 2009; Blard et al., 2008, 2013; Gayer et al., 2004; Kober et al., 2007; Luna et al., 2018; Nishiizumi et al., 1990; Zerathe et al., 2017).

Although further evidence is required to reach definitive conclusions, several mechanisms might explain these observations:

i) Because ^{3}He is a stable nuclide, it is more prone to be affected by inheritance from previous exposure episodes that might have occurred several million years ago. Hence, after the radioactive decay of ^{10}Be during subsequent burial

episodes, such inherited ^{3}He concentrations will appear to be in excess compared to the actual $R_{3/10}$ value. This mechanism was proposed by Zerathe et al. (2017) to identify two outliers among a dataset of eight samples from a ^{3}He/^{10}Be cross-calibration based on andesitic boulders. Another observation supporting this explanation is the relationship between observed $R_{3/10}$ values and ^{10}Be-derived exposure ages for the whole dataset (Fig. 19). I used ^{10}Be to compute these exposure ages because it is less susceptible than ^{3}He to be biased by inheritance and because its production rate is better constrained. Interestingly, the scatter among observed $R_{3/10}$ values is much greater for younger exposure ages (<50 ka), and the maximum values of $R_{3/10}$ (>50) are only observed in that population. Moreover, exposure ages older than 100 ka (n = 10 of 88) systematically yield $R_{3/10}$ < 40. If true, the interpretation of ^{3}He inheritance implies that the anomalously large ^{3}He/^{10}Be production ratios are not real, but a geomorphological artifact. However, the Himalayan samples (Gayer et al., 2004; Amidon et al., 2008) are from a region characterized by quite efficient exhumation (1–10 km/Ma; Amidon et al., 2008), a context that, in theory, favors the rapid turnover and rejuvenation of the subsurface, which should preclude significant inheritance.

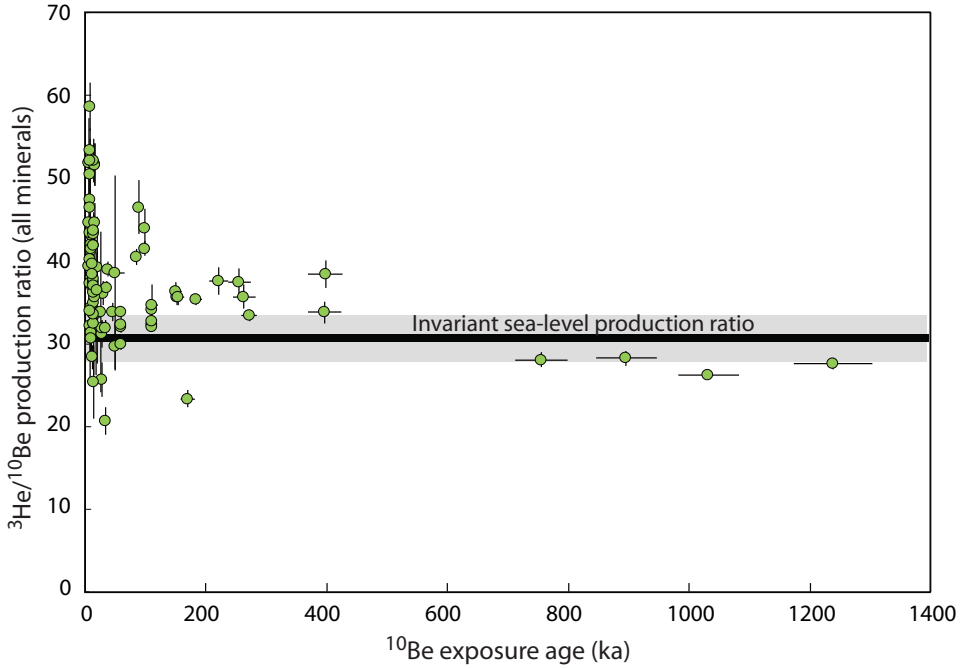

Figure 19. ^{3}He/^{10}Be production ratios plotted against ^{10}Be exposure ages (data sources: Amidon et al., 2008, 2009; Blard et al., 2008, 2013; Gayer et al., 2004; Kober et al., 2007; Luna et al., 2018; Nishiizumi et al., 1990; Zerathe et al., 2017).

(ii) Larsen et al. (2019) recently underscored that the composition of the whole rock may play a major role in the ^{3}He production rate, and that this bulk chemistry could be more important that the mineral composition itself because of the long-distance (20–100 μm) ejection of cosmogenic ^{3}He and ^{3}H (Fig. 4; Nesterenok and Yakubovich, 2016). The impact of this ^{3}He redistribution is larger for smaller grains (Larsen et al. 2019). This explanation may be compatible with the fact that the greatest observed ^{3}He overproduction (i.e., $R_{3/10} > 40$) at high elevation has so far only been documented in silicic lithologies (Amidon et al. 2008; Gayer et al. 2004), and not in intermediate rocks such as dacite or andesite (Blard et al., 2013; Luna et al., 2018). Although potential production pathways may be evoked (e.g., Lal, 1987) to explain this bulk compositional effect, the exact reaction(s) and element(s) that may have induced this unrecognized ^{3}He production remain elusive and should be explored with additional data.

(iii) Liquid water, ice, or snow enhance thermal neutron capture and may modify the balance between spallation and thermal neutron production in the first few meters below the air-rock interface. This may affect the ^{3}He/^{10}Be production ratio because ^{10}Be is not produced by thermal neutron capture (Delunel et al. 2014; Dunai et al. 2014). Indeed, the largest anomalous ^{3}He/^{10}Be production ratios above 3,000 m have only been documented in wet regions of the Himalayas (Amidon et al. 2008; Gayer et al. 2004), and not in the dry Andes (Blard et al., 2013; Luna et al., 2018; Zerathe et al., 2017). However, the global dataset clearly indicates that $R_{3/10}$ is not correlated with Li content, which contradicts the potential involvement of a ^{6}Li(n,α)^{3}H reaction. If future data confirm the role of water or snow in inducing high ^{3}He/^{10}Be production ratios, the existence of an unknown production pathway involving thermal neutrons and an element other than Li should be explored. ^{2}H(n)^{3}H and ^{10}B(n,^{8}Be)^{3}H reactions are potential candidates (Lal 1987). They could be tested with ad hoc experimental data.

New ^{3}He/^{10}Be cross-calibration data and measuring cosmogenic ^{3}He in different minerals (with variable compositions and grain sizes) from different lithologies (andesite,

dacite, granite-like composition) exposed at variable elevations and in different climatic contexts with variable snow cover will be useful in addressing these questions.

Cross-calibrations of ^{3}He against cosmogenic nuclides other than ^{10}Be are rare; few studies have provided intercomparison data with cosmogenic ^{21}Ne, ^{26}Al, and ^{36}Cl measured in the same samples as ^{3}He (Licciardi et al. 2008; Luna et al. 2018; Schimmelpfennig et al. 2011). The ^{36}Cl production rate is extremely sensitive to mineral composition, notably the K, Ca, and Cl contents of the target minerals (Schimmelpfennig et al. 2009). The ^{3}He/^{36}Cl production ratios reported by Licciardi et al. (2008), Luna et al. (2018), and Schimmelpfennig et al. (2011) were obtained by measuring ^{36}Cl concentrations in enstatites and feldspars or whole rocks with variable chemical compositions, notably their Cl contents. As these studies are based on different localities at variable latitudes and altitudes, there are too many unknowns to draw definitive conclusions about ^{3}He/^{36}Cl production ratios from these datasets.

That said, Schimmelpfennig et al. (2011) documented the variability of ^{3}He/^{36}Cl production ratios by measuring ^{3}He, ^{36}Cl, and ^{21}Ne in low-Ca pyroxenes (15% Ca) of homogenous composition sampled along a vertical transect between 1,000 and 4,300 m elevation at Kilimanjaro volcano (3°S, Tanzania). This dataset suggests that the ^{3}He/^{21}Ne and ^{3}He/^{36}Cl production ratios in low-Ca pyroxenes (average values of 5.4 ± 0.2 and 17.2 ± 1.8, respectively) are not elevation-dependent. Luna et al. (2018) also measured ^{3}He/^{21}Ne in low-Ca pyroxenes ($En_{88–94}$) from moraines of the Altiplano-Puna plateau (24°S, Argentina) at 4,500 m elevation; they reported a ^{3}He/^{21}Ne production ratio of 4.06 ± 0.12. The contrast with the ^{3}He/^{21}Ne production ratio determined by Luna et al. (2018) probably results from distinct absolute ^{21}Ne production rates resulting from different pyroxene compositions.

Although many uncertainties remain on the element-specific production pathways of other nuclides, these cross-calibrations against ^{21}Ne and ^{36}Cl support the hypothesis that ^{3}He in olivines and pyroxenes is probably not characterized by an unrecognized overproduction at high elevation (>2,000 m; Blard et al., 2013), in contrast to accessory minerals such as garnet (Gayer et al. 2004), kyanite, or zircon (Amidon et al. 2008). New cross-calibrations varying mineralogy, elevation, latitude, and snow cover will be useful for confirming this conclusion.

5.6. New directions of cosmogenic ^{3}He coupled with cosmogenic radioactive nuclides (^{14}C, ^{10}Be, ^{36}Cl, and ^{53}Mn)

Measuring two (or more) cosmogenic nuclides with different half lives in the same minerals has great potential for many geoscience applications, including i) burial dating (Lebatard et al. 2014), ii) measuring paleo-depths of exposure (Hidy et al. 2018) or the thickness

of snow cover (Hippe et al. 2014), iii) determining paleo-elevations (Blard et al. 2019a, 2019b), or iv) detecting complex exposure histories such as the dynamics of sediment transfer (Wittmann and von Blanckenburg 2009). The most commonly used nuclide pair for these applications is $^{26}Al/^{10}Be$ in quartz (Granger 2006), although $^{10}Be/^{21}Ne$ in quartz has the potential to probe longer timescales (5–20 Ma, compared to 0.5–6 Ma for $^{26}Al/^{10}Be$) (Balco and Shuster 2009; Sartégou et al. 2020).

Despite their intriguing potential, these nuclide pairs remain to be tested in quartz-free environments, such as andesitic or mafic terrains. Although measuring ^{3}He is often possible in such geological settings, measuring radioactive cosmogenic nuclides in the same rock sample remains challenging; only a few studies have reported joint measurements of ^{3}He and a radioactive cosmogenic nuclide in the same mineral (Blard et al., 2008; Licciardi et al., 2008; Nishiizumi et al., 1990).

Because the measurement of ^{36}Cl in Ca- and K-rich minerals (feldspars, pyroxene) is quite well established (Schimmelpfennig et al. 2009), the ^{3}He-^{36}Cl pair is, for now, the most accessible nuclide pair for multi-isotopic analyses in mafic terrains (Licciardi et al. 2008). However, given the half-life of ^{36}Cl ($t_{1/2}$ = 301 kyr), this pair can only be used to probe the last few million years in the best cases. Measuring ^{10}Be in olivine and pyroxene might prove useful in extending this temporal range, although removing atmospheric ^{10}Be contamination from mafic minerals has long been considered an unsolvable problem (Ivy-Ochs et al. 1998). A new chemical procedure employing a preliminary crushing step has allowed the accurate measurement of ^{10}Be in olivine and pyroxene (Blard et al., 2008; Eaves et al., 2018). Using these data and the Lal-Stone time-dependent model, Eaves et al. (2018) determined the SLHL ^{10}Be production rate to be 3.2 ± 0.8 at g^{-1} yr^{-1} in olivine and pyroxene, extending the utility of ^{10}Be burial age or paleoaltimetry measurements in intermediate and mafic rocks to 5 Ma. Recent developments in accelerator mass spectrometry offer the possibility to measure ^{53}Mn in Fe-rich minerals, such as iron-oxides (Schiffer et al. 2020). With a half-life of 3.74 Myr, ^{53}Mn is an interesting complement to ^{3}He; this nuclide pair could extend the dating range to 25 Ma. The ability to measure short-lived in-situ cosmogenic ^{14}C ($t_{1/2}$ = 5,730 yr; Pigati et al., 2010) in the same mineral as ^{3}He is also an interesting development because this pair could be used to determine paleo-depths of exposure, snow cover thicknesses, landslide volumes, and burial ages from 1 to 40 ka.

All such applications involving exposures below the rock-atmosphere interface, i.e., burial episodes, should carefully integrate the impact of the muogenic contribution using the most recently determined parameters (currently, those of Larsen et al., 2021).

6. Concluding remarks

In this review article, I have summarized and different strategies that can be applied to accurately and precisely measure cosmogenic ^{3}He concentrations. Even using the most accurate and precise mass spectrometer, non-cosmogenic ^{3}He concentrations are the main aspect determining the detection limit and the precision of the method; correcting for other sources of ^{3}He in the mineral of interest thus requires particular attention. The choice of the best correction strategy is determined by the respective concentrations of radiogenic and magmatic ^{4}He:

Case 1: Magmatic and radiogenic ^{4}He concentrations are of the same order of magnitude. Measure U, Th, and Li and independently determine the He closure age to compute ^{4}He*.

Strategy 1a – Crush and fuse minerals, use Equation (15).

Strategy 1b – Fuse multiple aliquots and build isochrons (see section 3.5.3).

Case 2: Uneroded lavas (a particularity of Case 1). In this case, it is not necessary to calculate the He closure age. However, U, Th, and Li measurements remain necessary to correct for radiogenic He by calculating the *R*-factor.

Strategy 2a – Crush and fuse minerals, use Equations (17-18).

Strategy 2b – Fuse multiple aliquots and build isochrons (see section 3.5.3).

Case 3: ^{4}He* >> ^{4}He$_{mag}$. This is the case for samples with very long closure ages (>>1 Myr) and/or U-Th-rich minerals (>> 1 ppm). In this situation, the correction for magmatic ^{3}He is not easy and may hinder the precision on cosmogenic ^{3}He, particularly for short exposure ages (<10 ka). Prolonged crushing or the fusion of cosmogenically shielded samples from the same lithology are ways to estimate the magmatic ^{3}He component.

Future improvements will be to i) improve our knowledge of the spatial and temporal variability of production rates, ii) develop the measurement of cosmogenic ^{3}He in new minerals, iii) better document the impacts of the chemical compositions of minerals and their host rocks on production rates, and iv) better understand exotic ^{3}He production pathways, notably those involving muons and thermal neutrons. These future directions have the potential to improve the accuracy and precision of the ^{3}He geoscientific toolbox and open the door to new applications (burial dating, paleoaltimetry, paleo-depths, durations of volcanic eruptions) and lithologies.

Acknowledgment

I thank Chemical Geology and notably D. Hilton, D. Porcelli and T. Horscroft who invited me to write this review article. I am grateful to them for their tremendous patience. Indeed, I started writing this article about five years ago, meaning that I spent 1,000 nights near the cosmic camel Alexandrin during the entire writing process. I am grateful to Robert Dennen (rd-editing.com) for English language editing. This review greatly benefited from numerous previous works and discussions with my colleagues who use cosmogenic nuclides in geoscience (J. Charreau, J.-F. Ritz, C. Litty, S. Zerathe, P. Valla) and the cosmogenic ^{3}He experts: K.A. Farley, R. Pik, T.J. Dunai, B.M. Goehring, G. Balco, F.M. Stuart, W.H. Amidon, I.J. Larsen, P.G. Burnard, P. Vermeesch, J.M. Licciardi, E. Gayer, R. Delunel, C.R. Fenton, D.W. Marchetti, D.L. Shuster, G. Bromley, N.A. Lifton, J.M. Schaefer, G. Winkler, R.P. Ackert, S. Niedermann, M. Tremblay, P.M. Vasconcelos, R. Yokochi, S. Mukhopadhyay, B. Marty, H. Baur, I. Leya, R. Wieler, J. Masarik, and many others. Finally, I of course send a special "thank you" to the helium pioneers, whose fundamental discoveries and principal publications opened new paths and fields of research: G.H. Megrue, M.D. Kurz, T.E. Cerling, D. Lal, H. Craig. "*Nani gigantum humeris insidentes – We are dwarfs standing on the shoulders of giants*" Bernard de Chartres, 12th century.

References

Aciego, Sarah M., Donald J. DePaolo, B.M. Kennedy, Michael P. Lamb, Kenneth W.W. Sims, and William E. Dietrich. 2007. "Combining [3He] Cosmogenic Dating with U–Th/He Eruption Ages Using Olivine in Basalt." *Earth and Planetary Science Letters* 254 (3–4): 288–302. https://doi.org/10.1016/j.epsl.2006.11.039.

Ackert, Robert P., Brad S. Singer, Hervé Guillou, Mike R. Kaplan, and Mark D. Kurz. 2003. "Long-Term Cosmogenic 3He Production Rates from 40Ar/39Ar and K–Ar Dated Patagonian Lava Flows at 47°S." *Earth and Planetary Science Letters* 210 (1–2): 119–36. https://doi.org/10.1016/S0012-821X(03)00134-1.

Aldrich, LT, and AOC Nier. 1946. "The Abundance of He3 in Atmospheric and Well Helium." *Physical Review* 70 (11–12): 983.

Aleinikoff, John N., Donald L. Winegarden, and Marianne Walter. 1990. "U-Pb Ages of Zircon Rims: A New Analytical Method Using the Air-Abrasion Technique." *Chemical Geology: Isotope Geoscience Section* 80 (4): 351–63. https://doi.org/10.1016/0168-9622(90)90015-5.

Amidon, W H, and K A Farley. 2011. "Cosmogenic 3He Production Rates in Apatite, Zircon and Pyroxene Inferred from Bonneville Flood Erosional Surfaces." *Quaternary Geochronology* 6: 10–21.

Amidon, W H, K A Farley, D W Burbank, and B Pratt-Sitaula. 2008. "Anomalous Cosmogenic 3He Production and Elevation Scaling in the High Himalaya." *Earth and Planetary Science Letters* 265 (1–2): 287–301.

Amidon, W H, D H Rood, and K A Farley. 2009. "Cosmogenic 3He and 21Ne Production Rates Calibrated against 10Be in Minerals from the Coso Volcanic Field." *Earth and Planetary Science Letters* 280 (1–4): 194–204.

Amidon, William H., Daniel Hobbs, and Scott A. Hynek. 2015. "Retention of Cosmogenic 3He in Calcite." *Quaternary Geochronology* 27 (April): 172–84. https://doi.org/10.1016/j.quageo.2015.03.004.

Andrews, J. N., and R. L. F. Kay. 1982. "Natural Production of Tritium in Permeable Rocks." *Nature* 298 (5872): 361–63. https://doi.org/10.1038/298361a0.

Andrews, J.N. 1985. "The Isotopic Composition of Radiogenic Helium and Its Use to Study Groundwater Movement in Confined Aquifers." *Chemical Geology* 49 (1–3): 339–51. https://doi.org/10.1016/0009-2541(85)90166-4.

Argento, David C., Robert C. Reedy, and John O. Stone. 2013. "Modeling the Earth's Cosmic Radiation." *Nuclear Instruments and Methods in Physics Research Section B: Beam Interactions with Materials and Atoms* 294 (January): 464–69. https://doi.org/10.1016/j.nimb.2012.05.022.

Balco, Greg, and David L. Shuster. 2009. "26Al-10Be-21Ne Burial Dating." *Earth and Planetary Science Letters* 286 (3–4): 570–75. https://doi.org/10.1016/j.epsl.2009.07.025.

Balco, Greg, John O. Stone, Nathaniel A. Lifton, and Tibor J. Dunai. 2008. "A Complete and Easily Accessible Means of Calculating Surface Exposure Ages or Erosion Rates from 10Be and 26Al Measurements." *Quaternary Geochronology* 3 (3): 174–95. https://doi.org/10.1016/j.quageo.2007.12.001.

Baur, H. 1999. "A Noble Gas Mass Spectrometer Compressor Source with Two Orders of Magnitude Improvement in Sensitivity." *EOS, Trans. Am. Geophys. Union* 46: F1118.

Blackburn, Terrence J., Daniel F. Stockli, and J. Douglas Walker. 2007. "Magnetite (U–Th)/He Dating and Its Application to the Geochronology of Intermediate to Mafic Volcanic Rocks." *Earth and Planetary Science Letters* 259 (3–4): 360–71. https://doi.org/10.1016/j.epsl.2007.04.044.

Blard, P. H., J. Lavé, K. A. Farley, M. Fornari, N. Jiménez, and V. Ramirez. 2009. "Late Local Glacial Maximum in the Central Altiplano Triggered by Cold and Locally-Wet Conditions during the Paleolake Tauca Episode (17-15 Ka, Heinrich 1)." *Quaternary Science Reviews* 28 (27–28): 3414–27. https://doi.org/10.1016/j.quascirev.2009.09.025.

Blard, P.-H., G. Balco, P. G. Burnard, K. A. Farley, C. R. Fenton, R. Friedrich, A. J T Jull, et al. 2015. "An Inter-Laboratory Comparison of Cosmogenic 3He and Radiogenic 4He in the CRONUS-P Pyroxene Standard." *Quaternary Geochronology* 26: 11–19. https://doi.org/10.1016/j.quageo.2014.08.004.

Blard, P.-H., D. Bourlès, J. Lavé, and R. Pik. 2006. "Applications of Ancient Cosmic-Ray Exposures: Theory, Techniques and Limitations." *Quaternary Geochronology* 1 (1): 59–73. https://doi.org/10.1016/j.quageo.2006.06.003.

Blard, P-H, D Bourles, R Pik, and J Lave. 2008. "In Situ Cosmogenic 10Be in Olivines and Pyroxenes." *Quaternary Geochronology* 3 (3): 196–205. https://doi.org/10.1016/j.quageo.2007.11.006.

Blard, P.-H., R. Braucher, J. Lavé, and D. Bourlès. 2013. "Cosmogenic 10Be Production Rate Calibrated against 3He in the High Tropical Andes (3800-4900 m, 20-22° S)." *Earth and Planetary Science Letters* 382: 140–49. https://doi.org/10.1016/j.epsl.2013.09.010.

Blard, P-H, and K Farley. 2008. "The Influence of Radiogenic 4He on Cosmogenic 3He Determinations in Volcanic Olivine and Pyroxene." *Earth and Planetary Science Letters* 276 (1–2): 20–29.

https://doi.org/10.1016/j.epsl.2008.09.003.
Blard, P.-H., J. Lave, R. Pik, X. Quidelleur, D.L. Bourles, and G. Kieffer. 2005. "Fossil Cosmogenic 3He Record from K–Ar Dated Basaltic Flows of Mount Etna Volcano (Sicily, 38°N): Evaluation of a New Paleoaltimeter." *Earth and Planetary Science Letters* 236 (3–4): 613–31. https://doi.org/10.1016/j.epsl.2005.05.028.
Blard, P.-H., J. Lavé, R. Pik, P. Wagnon, and D. Bourlès. 2007. "Persistence of Full Glacial Conditions in the Central Pacific until 15,000 Years Ago." *Nature* 449 (7162): 591–94. https://doi.org/10.1038/nature06142.
Blard, PH, J Lavé, F Sylvestre, CJ Placzek, C Claude, V Galy, T Condom, and B Tibari. 2013. "Cosmogenic 3He Production Rate in the High Tropical Andes (3800 m, 20 S): Implications for the Local Last Glacial Maximum." *Earth and Planetary Science Letters* 377: 260–75.
Blard, P.-H., M. Lupker, and M. Rousseau. 2019. "Paired-Cosmogenic Nuclide Paleoaltimetry." *Earth and Planetary Science Letters* 515 (June): 271–82. https://doi.org/10.1016/j.epsl.2019.03.005.
Blard, P.-H., Maarten Lupker, Moïse Rousseau, and Jim Tesson. 2019. "Two MATLAB Programs for Computing Paleo-Elevations and Burial Ages from Paired-Cosmogenic Nuclides." *MethodsX* 6: 1547–56. https://doi.org/10.1016/j.mex.2019.05.017.
Blard, P.-H., and R. Pik. 2008. "An Alternative Isochron Method for Measuring Cosmogenic 3He in Lava Flows." *Chemical Geology* 251 (1–4): 20–32. https://doi.org/10.1016/j.chemgeo.2008.02.004.
Blard, P.-H., R. Pik, J. Lave, D. Bourles, P.G. Burnard, R. Yokochi, B. Marty, and F. Trusdell. 2006. "Cosmogenic 3He Production Rates Revisited from Evidences of Grain Size Dependent Release of Matrix-Sited Helium." *Earth and Planetary Science Letters* 247 (3–4): 222–34. https://doi.org/10.1016/j.epsl.2006.05.012.
Blard, P.-H., N. Puchol, and K.A. Farley. 2008. "Constraints on the Loss of Matrix-Sited Helium during Vacuum Crushing of Mafic Phenocrysts." *Geochimica et Cosmochimica Acta* 72 (15): 3788–3803. https://doi.org/10.1016/j.gca.2008.05.044.
Borchers, Brian, Shasta Marrero, Greg Balco, Marc Caffee, Brent Goehring, Nathaniel Lifton, Kunihiko Nishiizumi, Fred Phillips, Joerg Schaefer, and John Stone. 2016. "Geological Calibration of Spallation Production Rates in the CRONUS-Earth Project." *Quaternary Geochronology* 31: 188–98. https://doi.org/10.1016/j.quageo.2015.01.009.
Boucher, Christine, Tefang Lan, Jennifer Mabry, David V. Bekaert, Peter G. Burnard, and Bernard Marty. 2018. "Spatial Analysis of the Atmospheric Helium Isotopic Composition: Geochemical and Environmental Implications." *Geochimica et Cosmochimica Acta* 237 (September): 120–30. https://doi.org/10.1016/j.gca.2018.06.010.
Braucher, R., S. Merchel, J. Borgomano, and D. L. Bourlès. 2011. "Production of Cosmogenic Radionuclides at Great Depth: A Multi Element Approach." *Earth and Planetary Science Letters* 309 (1–2): 1–9. https://doi.org/10.1016/j.epsl.2011.06.036.
Bromley, Gordon R.M., Brenda L. Hall, Joerg M. Schaefer, Gisela Winckler, Claire E. Todd, and Kurt M. Rademaker. 2011. "Glacier Fluctuations in the Southern Peruvian Andes during the Late-Glacial Period, Constrained with Cosmogenic3He." *Journal of Quaternary Science* 26 (1): 37–43. https://doi.org/10.1002/jqs.1424.
Bromley, Gordon R.M., Gisela Winckler, Joerg M. Schaefer, Michael R. Kaplan, Kathy J. Licht, and Brenda L. Hall. 2014. "Pyroxene Separation by HF Leaching and Its Impact on Helium Surface-Exposure Dating." *Quaternary Geochronology* 23 (October): 1–8. https://doi.org/10.1016/j.quageo.2014.04.003.
Brook, Edward J., and Mark D. Kurz. 1993. "Surface-Exposure Chronology Using *in Situ* Cosmogenic ^{3}He in Antarctic Quartz Sandstone Boulders." *Quaternary Research* 39 (1): 1–10. https://doi.org/10.1006/qres.1993.1001.
Burnard, P. G., and K. A. Farley. 2000. "Calibration of Pressure-Dependent Sensitivity and Discrimination in Nier-Type Noble Gas Ion Sources: TECHNICAL BRIEF." *Geochemistry, Geophysics, Geosystems* 1 (7): n/a-n/a. https://doi.org/10.1029/2000GC000038.
Cerling, T. E. 1990. "Dating Geomorphologic Surfaces Using Cosmogenic 3He." *Quaternary Research* 33 (2): 148–56. https://doi.org/10.1016/0033-5894(90)90015-D.
Cerling, Thure E., and Harmon Craig. 1994. "Cosmogenic 3He Production Rates from 39°N to 46°N Latitude, Western USA and France." *Geochimica et Cosmochimica Acta* 58 (1): 249–55. https://doi.org/10.1016/0016-7037(94)90462-6.
Charreau, Julien, Pierre-Henri Blard, Jéna Zumaque, Léo C.P. Martin, Tony Delobel, and Lucas Szafran. 2019. "Basinga: A Cell-by-cell GIS Toolbox for Computing Basin Average Scaling Factors, Cosmogenic Production Rates and Denudation Rates." *Earth Surface Processes and Landforms* 44 (12): 2349–65. https://doi.org/10.1002/esp.4649.
Cherniak, D.J., W. Amidon, D. Hobbs, and E.B. Watson. 2015. "Diffusion of Helium in Carbonates: Effects of Mineral Structure and Composition." *Geochimica et Cosmochimica Acta* 165 (September): 449–65.

https://doi.org/10.1016/j.gca.2015.06.033.
Clarke, W.B., W.J. Jenkins, and Z. Top. 1976. "Determination of Tritium by Mass Spectrometric Measurement of 3He." *The International Journal of Applied Radiation and Isotopes* 27 (9): 515–22. https://doi.org/10.1016/0020-708X(76)90082-X.
Craig, H., and R. J. Poreda. 1986. "Cosmogenic 3He in Terrestrial Rocks: The Summit Lavas of Maui." *Proceedings of the National Academy of Sciences* 83 (7): 1970–74. https://doi.org/10.1073/pnas.83.7.1970.
De Laeter, John, and Mark D. Kurz. 2006. "Alfred Nier and the Sector Field Mass Spectrometer." *Journal of Mass Spectrometry* 41 (7): 847–54. https://doi.org/10.1002/jms.1057.
Delon, Rémi, Sylvie Demouchy, Yves Marrocchi, Mohamed Ali Bouhifd, Julien Gasc, Patrick Cordier, Sanae Koizumi, and Pete G. Burnard. 2020. "Effect of Deformation on Helium Storage and Diffusion in Polycrystalline Forsterite." *Geochimica et Cosmochimica Acta* 273 (March): 226–43. https://doi.org/10.1016/j.gca.2020.01.018.
Delunel, Romain, Pierre-Henri Blard, Léo C.P. Martin, Sébastien Nomade, and Fritz Schlunegger. 2016. "Long Term Low Latitude and High Elevation Cosmogenic 3He Production Rate Inferred from a 107ka-Old Lava Flow in Northern Chile; 22°S-3400ma.s.l." *Geochimica et Cosmochimica Acta* 184: 71–87. https://doi.org/10.1016/j.gca.2016.04.023.
Delunel, Romain, Didier L. Bourlès, Peter A. van der Beek, Fritz Schlunegger, Ingo Leya, Jozef Masarik, and Emmanuel Paquet. 2014. "Snow Shielding Factors for Cosmogenic Nuclide Dating Inferred from Long-Term Neutron Detector Monitoring." *Quaternary Geochronology* 24 (December): 16–26. https://doi.org/10.1016/j.quageo.2014.07.003.
Dodson, Allen, B. Mack Kennedy, and Donald J. DePaolo. 1997. "Helium and Neon Isotopes in the Imnaha Basalt, Columbia River Basalt Group: Evidence for a Yellowstone Plume Source." *Earth and Planetary Science Letters* 150 (3–4): 443–51. https://doi.org/10.1016/S0012-821X(97)00090-3.
Dunai, Tibor J. 2010. *Cosmogenic Nuclides: Principles, Concepts and Applications in the Earth Surface Sciences*. Cambridge: Cambridge University Press. https://doi.org/10.1017/CBO9780511804519.
Dunai, Tibor J., Finlay M. Stuart, Raphaël Pik, Pete Burnard, and Eric Gayer. 2007. "Production of 3He in Crustal Rocks by Cosmogenic Thermal Neutrons." *Earth and Planetary Science Letters* 258 (1–2): 228–36. https://doi.org/10.1016/j.epsl.2007.03.031.
Dunai, Tibor J., and Jan R. Wijbrans. 2000. "Long-Term Cosmogenic 3He Production Rates (152 Ka–1.35 Ma) from 40Ar/39Ar Dated Basalt Flows at 29°N Latitude." *Earth and Planetary Science Letters* 176 (1): 147–56. https://doi.org/10.1016/S0012-821X(99)00308-8.
Dunai, T.J. 2001. "Influence of Secular Variation of the Geomagnetic Field on Production Rates of in Situ Produced Cosmogenic Nuclides." *Earth and Planetary Science Letters* 193 (1–2): 197–212. https://doi.org/10.1016/S0012-821X(01)00503-9.
Dunai, T.J., S.A. Binnie, A.S. Hein, and S.M. Paling. 2014. "The Effects of a Hydrogen-Rich Ground Cover on Cosmogenic Thermal Neutrons: Implications for Exposure Dating." *Quaternary Geochronology* 22 (August): 183–91. https://doi.org/10.1016/j.quageo.2013.01.001.
Eaves, Shaun R., Julia A. Collins, R. Selwyn Jones, Kevin P. Norton, Stephen G. Tims, and Andrew N. Mackintosh. 2018. "Further Constraint of the in Situ Cosmogenic 10Be Production Rate in Pyroxene and a Viability Test for Late Quaternary Exposure Dating." *Quaternary Geochronology* 48 (October): 121–32. https://doi.org/10.1016/j.quageo.2018.09.006.
Eaves, Shaun R., Andrew N. Mackintosh, Gisela Winckler, Joerg M. Schaefer, Brent V. Alloway, and Dougal B. Townsend. 2016. "A Cosmogenic He-3 Chronology of Late Quaternary Glacier Fluctuations in North Island, New Zealand (39 Degrees S)." *Quaternary Science Reviews* 132 (January): 40–56. https://doi.org/10.1016/j.quascirev.2015.11.004.
Eaves, Shaun R, Gisela Winckler, Joerg M Schaefer, Marcus J Vandergoes, Brent V Alloway, Andrew N Mackintosh, Dougal B Townsend, Matthew T Ryan, and Xun Li. 2015. "A Test of the Cosmogenic 3He Production Rate in the Southwest Pacific (39S)." *Journal of Quaternary Science* 30: 9.
Farley, K A, B P Kohn, and B Pillans. 2002. "The Effects of Secular Disequilibrium on (U-Th)/He Systematics and Dating of Quaternary Volcanic Zircon and Apatite." *Earth and Planetary Science Letters* 201: 117–25.
Farley, K. A., and D. F. Stockli. 2002. "(U-Th)/He Dating of Phosphates: Apatite, Monazite, and Xenotime." *Reviews in Mineralogy and Geochemistry* 48 (1): 559–77. https://doi.org/10.2138/rmg.2002.48.15.
Farley, K.A. 2018. "Helium Diffusion Parameters of Hematite from a Single-Diffusion-Domain Crystal." *Geochimica et Cosmochimica Acta* 231 (June): 117–29. https://doi.org/10.1016/j.gca.2018.04.005.
Farley, K.A., J. Libarkin, S. Mukhopadhyay, and W. Amidon. 2006. "Cosmogenic and Nucleogenic 3He in Apatite, Titanite, and Zircon." *Earth and Planetary Science Letters* 248 (1–2): 451–61. https://doi.org/10.1016/j.epsl.2006.06.008.
Fenton, Cassandra R., and Samuel Niedermann. 2014. "Surface Exposure Dating of Young Basalts (1-200ka) in

the San Francisco Volcanic Field (Arizona, USA) Using Cosmogenic 3He and 21Ne." *Quaternary Geochronology* 19: 87–105. https://doi.org/10.1016/j.quageo.2012.10.003.
Fenton, Cassandra R., Samuel Niedermann, Tibor Dunai, and Steven A. Binnie. 2019. "The SPICE Project: Production Rates of Cosmogenic 21Ne, 10Be, and 14C in Quartz from the 72 Ka SP Basalt Flow, Arizona, USAu." *Quaternary Geochronology* 54 (October): 101019. https://doi.org/10.1016/j.quageo.2019.101019.
Ferrier, K. L., J. T. Perron, S. Mukhopadhyay, M. Rosener, J. D. Stock, K. L. Huppert, and M. Slosberg. 2013. "Covariation of Climate and Long-Term Erosion Rates across a Steep Rainfall Gradient on the Hawaiian Island of Kaua'i." *Geological Society of America Bulletin* 125 (7–8): 1146–63. https://doi.org/10.1130/B30726.1.
Fisher, D. 1972. "Cosmogenic Rare Gas Production Rates in Chondritic Meteorites." *Earth and Planetary Science Letters* 16 (3): 391–95. https://doi.org/10.1016/0012-821X(72)90157-4.
Fleck, Robert J., and Andrew T. Calvert. 2014. "Modified Expression for Bulb-Tracer Depletion-Effect on Argon Dating Standards." *Geochemistry, Geophysics, Geosystems* 15 (4): 1657–62. https://doi.org/10.1002/2013GC005205.
Foeken, Jurgen P.T., Finlay M. Stuart, and Darren F. Mark. 2012. "Long-Term Low Latitude Cosmogenic 3He Production Rate Determined from a 126ka Basalt from Fogo, Cape Verdes." *Earth and Planetary Science Letters* 359–360: 14–25. https://doi.org/10.1016/j.epsl.2012.10.005.
Gayer, E., R. Pik, J. Lavé, C. France-Lanord, D. Bourlès, and B. Marty. 2004. "Cosmogenic 3He in Himalayan Garnets Indicating an Altitude Dependence of the 3He/10Be Production Ratio." *Earth and Planetary Science Letters* 229 (1–2): 91–104. https://doi.org/10.1016/j.epsl.2004.10.009.
Gayer, Eric, Sujoy Mukhopadhyay, and Brendan J. Meade. 2008. "Spatial Variability of Erosion Rates Inferred from the Frequency Distribution of Cosmogenic 3He in Olivines from Hawaiian River Sediments." *Earth and Planetary Science Letters* 266 (3–4): 303–15. https://doi.org/10.1016/j.epsl.2007.11.019.
Goehring, Brent M., Mark D. Kurz, Greg Balco, Joerg M. Schaefer, Joseph Licciardi, and Nathaniel Lifton. 2010. "A Reevaluation of in Situ Cosmogenic 3He Production Rates." *Quaternary Geochronology* 5 (4): 410–18. https://doi.org/10.1016/j.quageo.2010.03.001.
Gosse, John C., and Fred M. Phillips. 2001. "Terrestrial in Situ Cosmogenic Nuclides: Theory and Application." *Quaternary Science Reviews* 20 (14): 1475–1560. https://doi.org/10.1016/S0277-3791(00)00171-2.
Granger, D.E. 2006. "A Review of Burial Dating Methods with 26Al and 10Be." In *In Situ–Produced Cosmogenic Nuclides and Quantifi Cation of Geological Processes*, edited by L. Siame, D.L. Bourlès, and E.T. Brown, 1–16. Geological Society of America Special Paper 415.
Heineke, Caroline, Samuel Niedermann, Ralf Hetzel, and Cüneyt Akal. 2016. "Surface Exposure Dating of Holocene Basalt Flows and Cinder Cones in the Kula Volcanic Field (Western Turkey) Using Cosmogenic 3He and 10Be." *Quaternary Geochronology* 34 (August): 81–91. https://doi.org/10.1016/j.quageo.2016.04.004.
Hess, V.F. 1912. "Observations of Penetrating Radiation during Seven Free Balloon Flights." *Phys. Zeit.* 13: 1084–91.
Hidy, Alan J., John C. Gosse, Paul Sanborn, and Duane G. Froese. 2018. "Age-Erosion Constraints on an Early Pleistocene Paleosol in Yukon, Canada, with Profiles of 10Be and 26Al: Evidence for a Significant Loess Cover Effect on Cosmogenic Nuclide Production Rates." *CATENA* 165 (June): 260–71. https://doi.org/10.1016/j.catena.2018.02.009.
Hilton, D.R., K. Hammerschmidt, S. Teufel, and H. Friedrichsen. 1993. "Helium Isotope Characteristics of Andean Geothermal Fluids and Lavas." *Earth and Planetary Science Letters* 120 (3–4): 265–82. https://doi.org/10.1016/0012-821X(93)90244-4.
Hippe, K., S. Ivy-Ochs, F. Kober, J. Zasadni, R. Wieler, L. Wacker, P. W. Kubik, and C. Schlüchter. 2014. "Chronology of Lateglacial Ice Flow Reorganization and Deglaciation in the Gotthard Pass Area, Central Swiss Alps, Based on Cosmogenic10Be and in Situ14C." *Quaternary Geochronology* 19: 14–26. https://doi.org/10.1016/j.quageo.2013.03.003.
Hoffman, John H., and Alfred O. Nier. 1993. "Atmospheric Helium Isotopic Ratio." *Geophysical Research Letters* 20 (2): 121–23. https://doi.org/10.1029/93GL00112.
Hofmann, Florian, Emily H. G. Cooperdock, A. Joshua West, Dominic Hildebrandt, Kathrin Strößner, and Kenneth A. Farley. 2021. "Exposure Dating of Detrital Magnetite Using 3He Enabled by MicroCT and Calibration of the Cosmogenic 3He Production Rate in Magnetite." Preprint. Cosmogenic nuclide dating. https://doi.org/10.5194/gchron-2021-10.
Ivy-Ochs, S, P. W. Kubik, J. Masarik, R. Wieler, L. Bruno, and C. Schluechter. 1998. "Preliminary Results on the Use of Pyroxene for 10Be Surface Exposure Dating." *Schweizerische Mineralogische Und Petrographische Mitteilungen* 78: 375–82.
Kasbohm, Jennifer, and Blair Schoene. 2018. "Rapid Eruption of the Columbia River Flood Basalt and Correlation with the Mid-Miocene Climate Optimum." *Science Advances* 4 (9): eaat8223.

https://doi.org/10.1126/sciadv.aat8223.
Kelly, Meredith A., Thomas V. Lowell, Patrick J. Applegate, Fred M. Phillips, Joerg M. Schaefer, Colby A. Smith, Hanul Kim, Katherine C. Leonard, and Adam M. Hudson. 2015. "A Locally Calibrated, Late Glacial \textlesssup\textgreater10\textless/Sup\textgreaterBe Production Rate from a Low-Latitude, High-Altitude Site in the Peruvian Andes." *Quaternary Geochronology* 26 (1): 70–85. https://doi.org/10.1016/j.quageo.2013.10.007.
Klein, J., R. Middleton, and Hongqing Tang. 1982. "Modifications of an FN Tandem for Quantitative 10Be Measurement." *Nuclear Instruments and Methods in Physics Research* 193 (3): 601–16. https://doi.org/10.1016/0029-554X(82)90258-0.
Kober, F., S. Ivy-Ochs, I. Leya, H. Baur, T. Magna, R. Wieler, and P. W. Kubik. 2005. "In Situ Cosmogenic 10Be and 21Ne in Sanidine and in Situ Cosmogenic 3He in Fe-Ti-Oxide Minerals." *Earth and Planetary Science Letters* 236 (1–2): 404–18. https://doi.org/10.1016/j.epsl.2005.05.020.
Kober, F., S. Ivy-Ochs, F. Schlunegger, H. Baur, P. W. Kubik, and R. Wieler. 2007. "Denudation Rates and a Topography-Driven Rainfall Threshold in Northern Chile: Multiple Cosmogenic Nuclide Data and Sediment Yield Budgets." *Geomorphology* 83 (1–2): 97–120. https://doi.org/10.1016/j.geomorph.2006.06.029.
Kurz, M., D. Colodner, T.W. Trull, R.B. Moore, and K. O'Brien. 1990. "Cosmic Ray Exposure Dating with in Situ Produced Cosmogenic 3He: Results from Young Hawaiian Lava Flows." *Earth and Planetary Science Letters* 97: 177–89.
Kurz, Mark D. 1986a. "In-Situ Production of Cosmogenic Terrestrial Helium and Some Applications to Geochronology." *Geochimica et Cosmochimica Acta* 50 (12): 2855–62.
———. 1986b. "Cosmogenic Helium in a Terrestrial Igneous Rock." *Nature* 320 (6061): 435–39. https://doi.org/10.1038/320435a0.
Lal, D. 1958. "Investigations of Nuclear Interactions Produced by Cosmic Rays." PhD Thesis, Bombay University.
Lal, D. 1987. "Production of 3He in Terrestrial Rocks." *Chemical Geology: Isotope Geoscience Section* 66: 89–98.
Lal, D. 1989. "An Important Source Of4He (And3He) in Diamonds." *Earth and Planetary Science Letters* 96 (1–2): 1–7. https://doi.org/10.1016/0012-821X(89)90118-0.
———. 1991. "Cosmic Ray Labeling of Erosion Surfaces: In Situ Nuclide Production Rates and Erosion Models." *Earth and Planetary Science Letters* 104 (2–4): 424–39. https://doi.org/10.1016/0012-821X(91)90220-C.
Lal, D., and B. Peters. 1967. "Cosmic Ray Produced Radioactivity on the Earth." In *Handbuch Der Physik*, Sitte, K., 551-612. Berlin: Springer.
Larsen, I.J., K.A. Farley, M.P. Lamb, and C.J. Pritchard. 2021. "Empirical Evidence for Cosmogenic 3He Production by Muons." *Earth and Planetary Science Letters*, February, 116825. https://doi.org/10.1016/j.epsl.2021.116825.
Larsen, Isaac J., Kenneth A. Farley, and Michael P. Lamb. 2019. "Cosmogenic 3He Production Rate in Ilmenite and the Redistribution of Spallation 3He in Fine-Grained Minerals." *Geochimica et Cosmochimica Acta* 265 (November): 19–31. https://doi.org/10.1016/j.gca.2019.08.025.
Lebatard, Anne Elisabeth, M. Cihat Alçiçek, Pierre Rochette, Samir Khatib, Amélie Vialet, Nicolas Boulbes, Didier L. Bourlès, et al. 2014. "Dating the Homo Erectus Bearing Travertine from Kocabaş (Denizli, Turkey) at at Least 1.1 Ma." *Earth and Planetary Science Letters* 390: 8–18. https://doi.org/10.1016/j.epsl.2013.12.031.
Licciardi, J, M Kurz, and J Curtice. 2006. "Cosmogenic 3He Production Rates from Holocene Lava Flows in Iceland." *Earth and Planetary Science Letters* 246 (3–4): 251–64. https://doi.org/10.1016/j.epsl.2006.03.016.
Licciardi, J.M., C.L. Denoncourt, and R.C. Finkel. 2008. "Cosmogenic 36Cl Production Rates from Ca Spallation in Iceland." *Earth and Planetary Science Letters* 267 (1–2): 365–77. https://doi.org/10.1016/j.epsl.2007.11.036.
Licciardi, J.M, M.D Kurz, P.U Clark, and E.J Brook. 1999. "Calibration of Cosmogenic 3He Production Rates from Holocene Lava Flows in Oregon, USA, and Effects of the Earth's Magnetic Field." *Earth and Planetary Science Letters* 172 (3–4): 261–71. https://doi.org/10.1016/S0012-821X(99)00204-6.
Lifton, Nathaniel, Tatsuhiko Sato, and Tibor J. Dunai. 2014. "Scaling in Situ Cosmogenic Nuclide Production Rates Using Analytical Approximations to Atmospheric Cosmic-Ray Fluxes." *Earth and Planetary Science Letters* 386 (January): 149–60. https://doi.org/10.1016/j.epsl.2013.10.052.
Litherland, A E. 1980. "Ultrasensitive Mass Spectrometry with Accelerators." *Annual Review of Nuclear and Particle Science* 30 (1): 437–73. https://doi.org/10.1146/annurev.ns.30.120180.002253.
Litty, Camille, Julien Charreau, Pierre-Henri Blard, Raphael Pik, and Sébastien Nomade. 2021. "Spatial Variability of Quaternary Denudation Rates across a Volcanic Ocean Island (Santo Antão, Cape Verde) from Cosmogenic 3He." *Geomorphology* 375 (February): 107557.

https://doi.org/10.1016/j.geomorph.2020.107557.
Luna, Lisa V., Bodo Bookhagen, Samuel Niedermann, Georg Rugel, Andreas Scharf, and Silke Merchel. 2018. "Glacial Chronology and Production Rate Cross-Calibration of Five Cosmogenic Nuclide and Mineral Systems from the Southern Central Andean Plateau." *Earth and Planetary Science Letters* 500 (October): 242–53. https://doi.org/10.1016/j.epsl.2018.07.034.
Lupker, Maarten, Pierre Henri Blard, Jérôme Lavé, Christian France-Lanord, Laetitia Leanni, Nicolas Puchol, Julien Charreau, and Didier Bourlès. 2012. "10Be-Derived Himalayan Denudation Rates and Sediment Budgets in the Ganga Basin." *Earth and Planetary Science Letters* 333–334: 146–56. https://doi.org/10.1016/j.epsl.2012.04.020.
Lupton, John, and David Graham. 1991. "Comment on 'A Ten-Year Decrease in the Atmospheric Helium Isotope Ratio Possibly Caused by Human Activity', by Y. Sano et Al." *Geophysical Research Letters* 18 (3): 482–85. https://doi.org/10.1029/91GL00493.
Mabry, Jennifer C., Tefang Lan, Christine Boucher, Peter G. Burnard, Matthias S. Brennwald, Ray Langenfelds, and Bernard Marty. 2015. "No Evidence for Change of the Atmospheric Helium Isotope Composition since 1978 from Re-Analysis of the Cape Grim Air Archive." *Earth and Planetary Science Letters* 428 (October): 134–38. https://doi.org/10.1016/j.epsl.2015.07.035.
Mabry, Jennifer, Tefang Lan, Pete Burnard, and Bernard Marty. 2013. "High-Precision Helium Isotope Measurements in Air." *J. Anal. At. Spectrom.* 28 (12): 1903–10. https://doi.org/10.1039/C3JA50155H.
Mamyrin, B. A., G. S. Anufriev, I. N. Kamenskii, and I. N. Tolstikhin. 1970. "Determination of the Isotopic Composition of Atmospheric Helium." *Geochemical International* 7: 498–505.
Marchetti, David W., Allen L. Stork, D. Kip Solomon, Thure E. Cerling, and Wil Mace. 2020. "Cosmogenic 3He Exposure Ages of Basaltic Flows from Miller Knoll, Panguitch Lake, Utah: Using the Alternative Isochron Approach to Overcome Low-Gas Crushes." *Quaternary Geochronology* 55 (February): 101035. https://doi.org/10.1016/j.quageo.2019.101035.
Margerison, H.R., W.M. Phillips, F.M. Stuart, and D.E. Sugden. 2005. "Cosmogenic 3He Concentrations in Ancient Flood Deposits from the Coombs Hills, Northern Dry Valleys, East Antarctica: Interpreting Exposure Ages and Erosion Rates." *Earth and Planetary Science Letters* 230 (1–2): 163–75. https://doi.org/10.1016/j.epsl.2004.11.007.
Marrero, Shasta M., Fred M. Phillips, Brian Borchers, Nathaniel Lifton, Robert Aumer, and Greg Balco. 2016. "Cosmogenic Nuclide Systematics and the CRONUScalc Program." *Quaternary Geochronology* 31: 160–87. https://doi.org/10.1016/j.quageo.2015.09.005.
Martin, L. C.P., P.-H. Blard, G. Balco, J. Lavé, R. Delunel, N. Lifton, and V. Laurent. 2017. "The CREp Program and the ICE-D Production Rate Calibration Database: A Fully Parameterizable and Updated Online Tool to Compute Cosmic-Ray Exposure Ages." *Quaternary Geochronology* 38: 25–49. https://doi.org/10.1016/j.quageo.2016.11.006.
Martin, L.C.P., P.-H. Blard, J. Lavé, R. Braucher, M. Lupker, T. Condom, J. Charreau, V. Mariotti, and E. Davy. 2015. "In Situ Cosmogenic 10Be Production Rate in the High Tropical Andes." *Quaternary Geochronology* 30 (March 2016): 54–68. https://doi.org/10.1016/j.quageo.2015.06.012.
Martin, L.C.P., P.-H. Blard, J. Lavé, V. Jomelli, J. Charreau, T. Condom, M. Lupker, et al. 2020. "Antarctic-like Temperature Variations in the Tropical Andes Recorded by Glaciers and Lakes during the Last Deglaciation." *Quaternary Science Reviews* 247 (November): 106542. https://doi.org/10.1016/j.quascirev.2020.106542.
Martin, Léo C. P., Pierre-Henri Blard, Jérôme Lavé, Thomas Condom, Mélody Prémaillon, Vincent Jomelli, Daniel Brunstein, et al. 2018. "Lake Tauca Highstand (Heinrich Stadial 1a) Driven by a Southward Shift of the Bolivian High." *Science Advances* 4 (8): eaar2514. https://doi.org/10.1126/sciadv.aar2514.
Marty, B., and A. Jambon. 1987. "C3He in Volatile Fluxes from the Solid Earth: Implications for Carbon Geodynamics." *Earth and Planetary Science Letters* 83 (1–4): 16–26. https://doi.org/10.1016/0012-821X(87)90047-1.
Matsumoto, Takuya, Jun-Ichi Matsuda, Igor Yatsevich, and Minoru Ozima. 2010. "Noble Gas Mass Spectrometry with a Compressor Driven Recycling System for Improved Sensitivity." *GEOCHEMICAL JOURNAL* 44 (3): 167–72. https://doi.org/10.2343/geochemj.1.0055.
Medynski, S., R. Pik, P. Burnard, S. Dumont, R. Grandin, A. Williams, P.-H. Blard, et al. 2016. "Magmatic Cycles Pace Tectonic and Morphological Expression of Rifting (Afar Depression, Ethiopia)." *Earth and Planetary Science Letters* 446: 77–88. https://doi.org/10.1016/j.epsl.2016.04.014.
Megrue, G. H. 1967. "Isotopic Analysis of Rare Gases with a Laser Microprobe." *Science* 157 (3796): 1555–56. https://doi.org/10.1126/science.157.3796.1555.
———. 1971. "Distribution and Origin of Helium, Neon, and Argon Isotopes in Apollo 12 Samples Measured by in Situ Analysis with a Laser-Probe Mass Spectrometer." *Journal of Geophysical Research* 76 (20): 4956–68. https://doi.org/10.1029/JB076i020p04956.
Min, Kyoungwon, Peter W. Reiners, John a. Wolff, Roland Mundil, and R. Lee Winters. 2006. "(U–Th)/He Dating

of Volcanic Phenocrysts with High-U–Th Inclusions, Jemez Volcanic Field, New Mexico." *Chemical Geology* 227 (3–4): 223–35. https://doi.org/10.1016/j.chemgeo.2005.10.006.

Muscheler, Raimund, Jürg Beer, Peter W. Kubik, and H.-A. Synal. 2005. "Geomagnetic Field Intensity during the Last 60,000 Years Based on 10Be and 36Cl from the Summit Ice Cores and 14C." *Quaternary Science Reviews* 24 (16–17): 1849–60. https://doi.org/10.1016/j.quascirev.2005.01.012.

Nesterenok, A. V., and O. V. Yakubovich. 2016. "Production of 3He in Rocks by Reactions Induced by Particles of the Nuclear-Active and Muon Components of Cosmic Rays: Geological and Petrological Implications." *Petrology* 24 (1): 21–34. https://doi.org/10.1134/S0869591116010057.

Niedermann, S. 2002. "Cosmic-Ray-Produced Noble Gases in Terrestrial Rocks: Dating Tools for Surface Processes." *Reviews in Mineralogy and Geochemistry* 47 (1): 731–84. https://doi.org/10.2138/rmg.2002.47.16.

Nishiizumi, K., J. Klein, R. Middleton, and H. Craig. 1990. "Cosmogenic 10Be, 26Al and 3He in Olivine from Maui Lavas." *Earth and Planetary Science Letters* 98 (3–4): 263–66. https://doi.org/10.1016/0012-821X(90)90028-V.

Pacini, Domenico, translated, commented by Michela De Maria, and Alessandro De Angelis. 1911. "Penetrating Radiation on the Sea." *ArXiv:1101.3015 [Astro-Ph, Physics:Physics]*. http://arxiv.org/abs/1101.3015.

Parman, S. W. 2007. "Helium Isotopic Evidence for Episodic Mantle Melting and Crustal Growth." *Nature* 446 (7138): 900–903. https://doi.org/10.1038/nature05691.

Pigati, Jeffrey S, Nathaniel A Lifton, A J Timothy Jull, and Jay Quade. 2010. "A Simplified in Situ Cosmogenic ^{14}C Extraction System." *Radiocarbon* 52 (3): 1236–43. https://doi.org/10.1017/S0033822200046324.

Protin, Marie, Pierre Henri Blard, Yves Marrocchi, and François Mathon. 2016. "Irreversible Adsorption of Atmospheric Helium on Olivine: A Lobster Pot Analogy." *Geochimica et Cosmochimica Acta* 179: 76–88. https://doi.org/10.1016/j.gca.2016.01.032.

Puchol, Nicolas, Pierre Henri Blard, Raphaël Pik, Bouchaïb Tibari, and Jérôme Lavé. 2017. "Variability of Magmatic and Cosmogenic3He in Ethiopian River Sands of Detrital Pyroxenes: Impact on Denudation Rate Determinations." *Chemical Geology* 448: 13–25. https://doi.org/10.1016/j.chemgeo.2016.10.033.

Raisbeck, G.M., F. Yiou, D. Bourlès, J. Lestringuez, and D. Deboffle. 1987. "Measurements of 10Be and 26Al with a Tandetron AMS Facility." *Nuclear Instruments and Methods in Physics Research Section B: Beam Interactions with Materials and Atoms* 29 (1–2): 22–26. https://doi.org/10.1016/0168-583X(87)90196-0.

Ramalho, Ricardo S., Gisela Winckler, José Madeira, George R. Helffrich, Ana Hipólito, Rui Quartau, Katherine Adena, and Joerg M. Schaefer. 2015. "Hazard Potential of Volcanic Flank Collapses Raised by New Megatsunami Evidence." *Science Advances* 1 (9): e1500456. https://doi.org/10.1126/sciadv.1500456.

Ritz, J. F., A. Avagyan, M. Mkrtchyan, H. Nazari, P. H. Blard, A. Karakhanian, H. Philip, et al. 2016. "Active Tectonics within the NW and SE Extensions of the Pambak-Sevan-Syunik Fault: Implications for the Present Geodynamics of Armenia." *Quaternary International* 395: 61–78. https://doi.org/10.1016/j.quaint.2015.05.021.

Sano, Yuji, Yukiko Furukawa, and Naoto Takahata. 2010. "Atmospheric Helium Isotope Ratio: Possible Temporal and Spatial Variations." *Geochimica et Cosmochimica Acta* 74 (17): 4893–4901. https://doi.org/10.1016/j.gca.2010.06.003.

Sano, Yuji, Taichi Tokutake, and Naoto Takahata. 2008. "Accurate Measurement of Atmospheric Helium Isotopes." *Analytical Sciences : The International Journal of the Japan Society for Analytical Chemistry* 24 (4): 521–25. https://doi.org/10.2116/analsci.24.521.

Sartégou, Amandine, Pierre-Henri Blard, Régis Braucher, Didier L. Bourlès, Patrick Sorriaux, Laurent Zimmermann, Alexis Laffitte, et al. 2020. "Late Cenozoic Evolution of the Ariège River Valley (Pyrenees) Constrained by Cosmogenic 26Al/10Be and 10Be/21Ne Dating of Cave Sediments." *Geomorphology* 371 (December): 107441. https://doi.org/10.1016/j.geomorph.2020.107441.

Scarsi, Paolo. 2000. "Fractional Extraction of Helium by Crushing of Olivine and Clinopyroxene Phenocrysts: Effects on the 3He/4He Measured Ratio." *Geochimica et Cosmochimica Acta* 64 (21): 3751–62. https://doi.org/10.1016/S0016-7037(00)00419-1.

Schaefer, Joerg M., Gisela Winckler, Pierre-Henri Blard, Greg Balco, David L. Shuster, Ronny Friedrich, A.J.T. Jull, Rainer Wieler, and Christian Schluechter. 2016. "Performance of CRONUS-P – A Pyroxene Reference Material for Helium Isotope Analysis." *Quaternary Geochronology* 31 (February): 237–39. https://doi.org/10.1016/j.quageo.2014.07.006.

Schiffer, Markus, Alexander Stolz, Damián Alejandro López, Richard Spanier, Susan Herb, Claus Müller-Gatermann, Stefan Heinze, et al. 2020. "Method Developments for Accelerator Mass Spectrometry at CologneAMS, 53Mn/3He Burial Dating and Ultra-Small 14CO2 Samples." *Global and Planetary Change* 184 (January): 103053. https://doi.org/10.1016/j.gloplacha.2019.103053.

Schimmelpfennig, Irene, Lucilla Benedetti, Robert Finkel, Raphaël Pik, Pierre Henri Blard, Didier Bourlès, Pete Burnard, and Alice Williams. 2009. "Sources of In-Situ 36Cl in Basaltic Rocks. Implications for Calibration of Production Rates." *Quaternary Geochronology* 4 (6): 441–61.

https://doi.org/10.1016/j.quageo.2009.06.003.
Schimmelpfennig, Irene, Alice Williams, Raphaël Pik, Pete Burnard, Samuel Niedermann, Robert Finkel, Björn Schneider, and Lucilla Benedetti. 2011. "Inter-Comparison of Cosmogenic in-Situ 3He, 21Ne and 36Cl at Low Latitude along an Altitude Transect on the SE Slope of Kilimanjaro Volcano (3°S, Tanzania)." *Quaternary Geochronology* 6 (5): 425–36. https://doi.org/10.1016/j.quageo.2011.05.002.
Shuster, David L, Kenneth a Farley, Janet M Sisterson, and Donald S Burnett. 2004. "Quantifying the Diffusion Kinetics and Spatial Distributions of Radiogenic 4He in Minerals Containing Proton-Induced 3He." *Earth and Planetary Science Letters* 217 (1–2): 19–32. https://doi.org/10.1016/S0012-821X(03)00594-6.
Shuster, David L., Kenneth A. Farley, Paulo M. Vasconcelos, Greg Balco, Hevelyn S. Monteiro, Kathryn Waltenberg, and John O. Stone. 2012. "Cosmogenic 3He in Hematite and Goethite from Brazilian 'Canga' Duricrust Demonstrates the Extreme Stability of These Surfaces." *Earth and Planetary Science Letters* 329–330 (May): 41–50. https://doi.org/10.1016/j.epsl.2012.02.017.
Stone, J. O. 2000. "Air Pressure and Cosmogenic Isotope Production." *Journal of Geophysical Research-Solid Earth* 105 (B10): 23753–59. https://doi.org/10.1029/2000JB900181.
Tremblay, Marissa M., David L. Shuster, and Greg Balco. 2014. "Diffusion Kinetics of 3He and 21Ne in Quartz and Implications for Cosmogenic Noble Gas Paleothermometry." *Geochimica et Cosmochimica Acta* 142: 186–204. https://doi.org/10.1016/j.gca.2014.08.010.
Trull, T.W., M.D. Kurz, and W.J. Jenkins. 1991. "Diffusion of Cosmogenic3He in Olivine and Quartz: Implications for Surface Exposure Dating." *Earth and Planetary Science Letters* 103 (1–4): 241–56. https://doi.org/10.1016/0012-821X(91)90164-D.
Uppala, S. M., P. W. Kallberg, A. J. Simmons, U. Andrae, V. D. Bechtold, M. Fiorino, J. K. Gibson, et al. 2005. "The ERA-40 Re-Analysis." *Quarterly Journal of the Royal Meteorological Society* 131 (612): 2961–3012. https://doi.org/10.1256/qj.04.176.
Vasconcelos, Paulo M., Kenneth A. Farley, John Stone, Thiago Piacentini, and L. Keith Fifield. 2019. "Stranded Landscapes in the Humid Tropics: Earth's Oldest Land Surfaces." *Earth and Planetary Science Letters* 519 (August): 152–64. https://doi.org/10.1016/j.epsl.2019.04.014.
Vermeesch, Pieter. 2018. "IsoplotR: A Free and Open Toolbox for Geochronology." *Geoscience Frontiers* 9 (5): 1479–93. https://doi.org/10.1016/j.gsf.2018.04.001.
Vermeesch, Pieter, Greg Balco, Pierre-Henri Blard, Tibor J. Dunai, Florian Kober, Samuel Niedermann, David L. Shuster, et al. 2015. "Interlaboratory Comparison of Cosmogenic 21 Ne in Quartz." *Quaternary Geochronology* 26 (February): 20–28. https://doi.org/10.1016/j.quageo.2012.11.009.
Williams, A.J., F.M. Stuart, S.J. Day, and W.M. Phillips. 2005. "Using Pyroxene Microphenocrysts to Determine Cosmogenic 3He Concentrations in Old Volcanic Rocks: An Example of Landscape Development in Central Gran Canaria." *Quaternary Science Reviews* 24 (1–2): 211–22. https://doi.org/10.1016/j.quascirev.2004.07.004.
Wittmann, H., and F. von Blanckenburg. 2009. "Cosmogenic Nuclide Budgeting of Floodplain Sediment Transfer." *Geomorphology* 109 (3–4): 246–56. https://doi.org/10.1016/j.geomorph.2009.03.006.
Wolf, R.A, K.A Farley, and D.M Kass. 1998b. "Modeling of the Temperature Sensitivity of the Apatite (U–Th)/He Thermochronometer." *Chemical Geology* 148 (1–2): 105–14. https://doi.org/10.1016/S0009-2541(98)00024-2.
Wood, Bernard J., Jonathan D. Blundy, and J.Andrew C. Robinson. 1999. "The Role of Clinopyroxene in Generating U-Series Disequilibrium during Mantle Melting." *Geochimica et Cosmochimica Acta* 63 (10): 1613–20. https://doi.org/10.1016/S0016-7037(98)00302-0.
Yokochi, Reika, Bernard Marty, Raphaël Pik, and Pete Burnard. 2005. "High 3 He/ 4 He Ratios in Peridotite Xenoliths from SW Japan Revisited: Evidence for Cosmogenic 3 He Released by Vacuum Crushing." *Geochemistry, Geophysics, Geosystems* 6 (1): n/a-n/a. https://doi.org/10.1029/2004GC000836.
York, D. 1966. "Least-Squares Fitting of a Straight Line." *Canadian Journal of Physics* 44: 1079–86.
Zerathe, Swann, Pierre-Henri Blard, Régis Braucher, Didier Bourlès, Laurence Audin, Julien Carcaillet, Fabrizio Delgado, Carlos Benavente, Georges Aumaître, and Karim Keddadouche. 2017. "Toward the Feldspar Alternative for Cosmogenic 10Be Applications." *Quaternary Geochronology* 41 (August): 83–96. https://doi.org/10.1016/j.quageo.2017.06.004.
Ziegler, James F., M.D. Ziegler, and J.P. Biersack. 2010. "SRIM – The Stopping and Range of Ions in Matter (2010)." *Nuclear Instruments and Methods in Physics Research Section B: Beam Interactions with Materials and Atoms* 268 (11–12): 1818–23. https://doi.org/10.1016/j.nimb.2010.02.091.
Ziegler, J.F. 1977. *Helium: Stopping Powers and Ranges in All Elemental Matter*. Pergamon Press.
Zimmermann, Laurent, Guillaume Avice, Pierre-Henri Blard, Bernard Marty, Evelyn Füri, and Peter G. Burnard. 2018. "A New All-Metal Induction Furnace for Noble Gas Extraction." *Chemical Geology* 480 (March): 86–92. https://doi.org/10.1016/j.chemgeo.2017.09.018.
Zimmermann, Laurent, and David Bekaert. 2020. "Analyse des gaz rares par spectrométrie de masse statique - Théorie et instrumentation," 30.

2023